

**TIMING AND KINEMATICS OF THE DUKE RIVER FAULT;
INSIGHTS INTO THE EVOLUTION OF THE INSULAR
TERRANE, SOUTHWEST YUKON**

by

ROSE NATALIE COBBETT

A THESIS SUBMITTED IN PARTIAL FULFILLMENT OF
THE REQUIREMENTS FOR THE DEGREE OF

MASTER OF SCIENCE

in

THE FACULTY OF GRADUATE STUDIES

(Geology)

THE UNIVERSITY OF BRITISH COLUMBIA

(Vancouver)

October 2011

© Rose Natalie Cobbett, 2011

ABSTRACT

The Duke River fault is a terrane-bounding structure that separates the Alexander terrane from Wrangellia in southwest Yukon. Detailed geological mapping and sampling of six key areas along the fault were completed in order to determine the history of movement on the fault. In these areas, the Duke River fault juxtaposes pervasively foliated and folded greenschist facies rocks of the Alexander terrane against low-grade, less deformed Wrangellian rocks. Multiple lines of evidence indicate the Alexander terrane has been thrust over Wrangellia. $^{40}\text{Ar}/^{39}\text{Ar}$ ages from muscovite grains, which are interpreted to have grown during faulting or have been reset by motions along the Duke River fault, range in age from 82-104 Ma, suggesting that movement along the fault is at least as old as Cretaceous. This mid-to Late Cretaceous event along the Duke River fault is overprinted by brittle deformation that affects rocks as young as Miocene to Pliocene in age and suggests that fault movement has occurred as recently as the Pliocene.

TABLE OF CONTENTS

Abstract	ii
Table of Contents	iii
List of Tables	vi
List of Figures	vii
Acknowledgements	ix
 1: Introduction	 1
1.1 Previous Work	3
1.2 Duke River Fault Definitions	4
1.3 Objectives of Thesis	4
 2: Regional Geology and Tectonic Overview	 6
2.1 Regional Geology of Wrangellia	6
2.1.1 Stratigraphy	6
2.1.2 Intrusive Rocks	8
2.1.3 Structure and Metamorphism within Wrangellia	9
2.2 Regional Geology of the Alexander Terrane	10
2.2.1 Stratigraphy	10
2.2.2 Intrusive Rocks	11
2.2.3 Structure and Metamorphism within the Alexander Terrane	11
2.3 Overlap Assemblages of Wrangellia and Alexander Terrane	12
2.4 Regional Tectonic Overview	12
2.4.1 Early Paleozoic Evolution of the Alexander Terrane	13
2.4.2 Middle to Late Paleozoic Evolution of Wrangellia and the Alexander Terrane	16
2.4.3 A Model for the Early Mesozoic History of Wrangellia and the Alexander Terrane.	17
2.4.4 A Model for the Middle Mesozoic History of Wrangellia and the Alexander Terrane.	19
2.4.5 Middle to Late Mesozoic Collision of Insular Superterrane with North America.	20
2.4.6 Summary	20
 3: Structural and Lithologic Character of the Duke River Fault	 20
3.1 Squaw Creek	20
3.1.1 Stratigraphy of Foot Wall	26
3.1.2 Stratigraphy of Hanging Wall	26
3.1.3 Stratigraphy of the Imbricate Zone	29

3.1.4	Structure of the Foot Wall	29
3.1.5	Structure of the Hanging Wall	31
3.1.6	Structure within the Imbricate Zone	31
3.1.7	Discussion.....	33
3.2	Silver Creek	36
3.2.1	Stratigraphy of Foot Wall.....	36
3.2.2	Stratigraphy of Hanging Wall	38
3.2.3	Stratigraphy of the Imbricate Zone	38
3.2.4	Structure of Foot Wall	40
3.2.5	Structure of Hanging Wall	40
3.2.6	Structure of the Imbricate Zone.....	40
3.2.7	Discussion.....	45
3.3	Jessie Creek	46
3.3.1	Stratigraphy of the Foot Wall.....	46
3.3.2	Stratigraphy of the Hanging Wall	46
3.3.3	Stratigraphy of the Imbricate Zone	46
3.3.4	Structure of the Foot Wall	49
3.3.5	Structure of the Hanging Wall	49
3.3.6	Structure of Imbricate Zone.....	51
3.3.7	Discussion.....	53
3.4	Bullion Creek	54
3.4.1	Stratigraphy of Foot Wall.....	54
3.4.2	Stratigraphy of Hanging Wall	54
3.4.3	Stratigraphy of the Imbricate Zone	56
3.4.4	Structure of the Foot Wall	56
3.4.5	Structure of the Hanging Wall	59
3.4.6	Structure of the Imbricate Zone.....	59
3.4.7	Discussion.....	61
3.5	Hoge Creek.....	62
3.5.1	Stratigraphy of Foot Wall.....	62
3.5.2	Stratigraphy of Hanging Wall	64
3.5.3	Stratigraphy of the Imbricate Zone	64
3.5.4	Structure of the Foot Wall	64
3.5.5	Structure of the Hanging Wall	67
3.5.6	Structure of the Imbricate Zone.....	67
3.5.7	Discussion.....	69
3.6	Klutlan Glacier	70
3.6.1	Stratigraphy of the Foot Wall.....	70
3.6.2	Stratigraphy of the Hanging Wall	70
3.6.3	Structure of the Foot Wall	74
3.6.4	Structure of the Hanging Wall	74
3.6.5	Discussion.....	77
4:	Timing of Deformation Along the Duke River Fault.....	78
4.1	Methodology	78
4.1.1	U-Pb LA-ICPMS Pacific Centre for Geochronology Research - UBC.....	78
4.1.2	U-Pb TIMS – Boise State University Geochronology Laboratory.....	79
4.1.3	⁴⁰ Ar/ ³⁹ Ar	81
4.1.3.1	Pacific Centre for Isotope and Geochemical Research - UBC.....	81

4.1.3.2 Geological Survey of Canada - Ottawa.....	83
4.2 U-Pb Results.....	85
4.3 ⁴⁰ Ar/ ³⁹ Ar Results.....	87
4.4 Discussion	90
4.4.1 Significance of Permian Ages Along the Duke River Fault	90
4.4.2 Cretaceous Movements Along the Duke River Fault	90
4.4.3 Miocene to Pliocene Movement on the Duke River Fault	92
4.4.4 Summary.....	92
5: Discussion and Conclusions.....	94
5.1 Timing and Kinematics of the Duke River Fault.....	94
5.1.1 Cretaceous Motion of the Duke River Fault	94
5.1.2 Miocene to Pliocene Reactivation of the Duke River Fault	95
5.2 Pre-Tertiary Tectonic Framework of the Northern Cordillera	97
5.3 The Role of the Duke River Fault in Northern Cordilleran Tectonics	97
5.4 Conclusions and Future Work	98
Reference List	100
Appendices.....	106
Appendix I – U-Pb LA-ICPMS Data	106
Appendix II – U-Pb TIMS Data.....	108
Appendix III – ⁴⁰ Ar/ ³⁹ Ar Data	110
Appendix III – Geologic Maps	125

LIST OF TABLES

Table 4.1 $^{40}\text{Ar}/^{39}\text{Ar}$ ages from samples collected within the Duke River fault imbricate zone.....	82
---	----

LIST OF FIGURES

Figure 1.1: Terrane map of Alaska, Yukon Territory and British Columbia showing the location of the Duke River fault.....	2
Figure 2.1: Simplified stratigraphic columns for the Alexander terrane and Wrangellia including overlap assemblages.....	7
Figure 2.2: Simplified geologic map of Canadian and Alaskan Cordillera outlining the limits of the St. Elias Subterrane and Craig Subterrane.....	14
Figure 2.3: Regional cross section through the Alexander terrane and Wrangellia from Palaeozoic through Late Triassic.....	15
Figure 2.4: Regional cross section through the Alexander terrane and Wrangellia from Jurassic to Cretaceous.....	18
Figure 3.1: Location of mapped areas along the Duke River fault.....	23
Figure 3.2: Geologic map along the Duke River fault near Squaw Creek.....	24
Figure 3.3: Legend for all of the geologic maps along the Duke River fault.....	25
Figure 3.4: Geologic cross section through the Squaw Creek area.....	27
Figure 3.5: Photographs of outcrops Squaw Creek area.....	28
Figure 3.6: Stereonets showing structures measured near Squaw Creek.....	29
Figure 3.7: Photographs and photo micro-graphs of outcrops near the Squaw Creek area.....	32
Figure 3.8 Photographs of outcrops from within the Duke River fault imbricate zone near Squaw Creek.....	34
Figure 3.9: Geologic map along the Duke River fault near Silver Creek.....	37
Figure 3.10: Geological cross section A-A' through the Silver Creek map area and photograph of mapped ridge.....	39
Figure 3.11: Stereonets showing structures measured near Silver Creek.....	41
Figure 3.12: Photographs and photo micro-graphs of outcrops near the Silver Creek area.....	42
Figure 3.13: Photographs of outcrops taken near the Silver Creek area.....	44
Figure 3.14: Geologic map along the Duke River fault near Jessie Creek.....	47
Figure 3.15: Photographs and photo micro-graphs of outcrops near the Jessie Creek area.....	48
Figure 3.16: Geologic cross section A-A' through the Jessie Creek map area.....	50

Figure 3.17: Stereonets showing structures measured near Jessie Creek.....	52
Figure 3.18: Geologic map along the Duke River fault near Bullion Creek.....	55
Figure 3.19: Geologic cross section A-A' through the Bullion Creek map area.....	57
Figure 3.20: Stereonets showing structures measured near Bullion Creek.....	58
Figure 3.21: Photographs and photo micro-graphs of outcrops near the Bullion Creek area.....	60
Figure 3.22: Geologic map of the Duke River fault near Hoge Creek.....	63
Figure 3.23: Photographs and photo micro-graphs of outcrops near the Hoge Creek area.....	65
Figure 3.24: Geologic cross sections A-A' and B-B' through the Hoge Creek area.....	66
Figure 3.25: Stereonets showing structures measured near Hoge Creek.....	68
Figure 3.26: Geologic map of the Duke River fault near Klutlan Glacier.....	71
Figure 3.27: Geologic cross section A-A' through the Klutlan Glacier area.....	72
Figure 3.28: Photographs and photo micro-graphs of outcrops near the Klutlan Glacier area.....	73
Figure 3.29: Stereonets showing structures measured near Klutlan Glacier.....	75
Figure 4.1: U-Pb zircon ages for samples collected near the Duke River fault.....	86
Figure 4.2: $^{40}\text{Ar}/^{39}\text{Ar}$ ages from samples collected within the Duke River fault imbricate zone.....	88
Figure 4.3: Photo micro-graphs of samples that were dated using $^{40}\text{Ar}/^{39}\text{Ar}$ methods....	89
Figure 4.4: Photograph of folded Wrangell Volcanics capping the Duke River fault.....	93
Figure 5.1: Maps of northern Canadian and Alaskan Cordillera.....	96

ACKNOWLEDGEMENTS

First and foremost I thank Steve Israel, who designed this project and took full responsibility in making sure I had everything I needed not only complete the project, but to do a thorough job of it. I could not have asked for a better supervisor and mentor over the last few years and I feel blessed to have had the opportunity to learn from, and work beside Steve. He has provided me with the skills and attitude to have a successful and meaningful career in geology no matter which sector I decide to enter.

I owe a lot of thanks to my two other thesis supervisors, Cees Van Staal, and Jim Mortensen and Lori Kennedy. Cees's expertise in structural geology and field observations has pushed me to a higher level of understanding than I would have achieved without his involvement. Jim and Lori's commitment to answering questions and getting edits back to me whenever I needed them has allowed me to get through UBC in a timely fashion. Jim has also spent late nights in the geochronology lab dating samples for me.

I would also like to thank Nancy Joyce for dating some of my samples. Research geologists at the Yukon Geological Survey, including Maurice Colpron, Don Murphy and Lee Pigage, have each contributed by giving me expert advice in map making, and regional and structural geology. I would also like to thank the rest of the staff at the YGS for making it a fun place to work and play.

Lastly, I would like to thank my field assistants, Catherine, Shawn, Kristy, Syd and Jenny, who without complaint followed me up, down, around and through some of the toughest country I've ever been in. Without their efforts I would not have been able to get such a complete look at the Duke River fault.

1: INTRODUCTION

The northern Cordillera in western Canada and Alaska is composed of a number of terranes that accreted to the North American continental margin during late Paleozoic to early Mesozoic time (Figure 1.1; Monger and Price, 1979; Coney et al., 1980; Gabrielse and Yorath, 1991; Gabrielse et al., 2011). Terranes are defined as discrete, unrelated, fault bounded crustal entities that evolved away from the North American continental margin (Coney et al., 1980). The Canadian Cordillera is interpreted to be made up of several large terranes, based on detailed bedrock mapping, geochronology, geochemistry, isotopic and paleomagnetic analyses. (Colpron et al., 2007). These terranes include the middle to late Paleozoic Yukon-Tanana terrane; late Paleozoic to early Mesozoic Stikinia and Quesnellia; Middle Devonian to Early Triassic Slide Mountain and Cache Creek terranes; Neoproterozoic to Triassic Alexander terrane and middle and late Paleozoic to Upper Triassic Wrangellia. Two of the largest and least studied terranes in the Cordillera are Wrangellia and the Alexander terrane. In western Canada and southeast Alaska these two terranes together make up the Insular Superterrane (Monger et al., 1982; Wheeler et al., 1991; van der Heyden, 1992;).

Exactly how Wrangellia was amalgamated with the Alexander terrane and the tectonic evolution of the Insular Superterrane prior to and after its accretion to the North American margin, are poorly understood. Gardner et al. (1988) reported that a Pennsylvanian aged pluton intrudes both the Alexander terrane and Wrangellia, indicating that these two terranes were amalgamated prior to Pennsylvanian time. However the late Paleozoic through late Mesozoic stratigraphies of these terranes are markedly different, and only in the latest Cenozoic are there firm geologic ties between the two terranes. In southwest Yukon the boundary between Wrangellia and the Alexander terrane is defined by the Duke River fault (Muller, 1967; Campbell and Dodds, 1991) (Fig. 1.1). As the only post

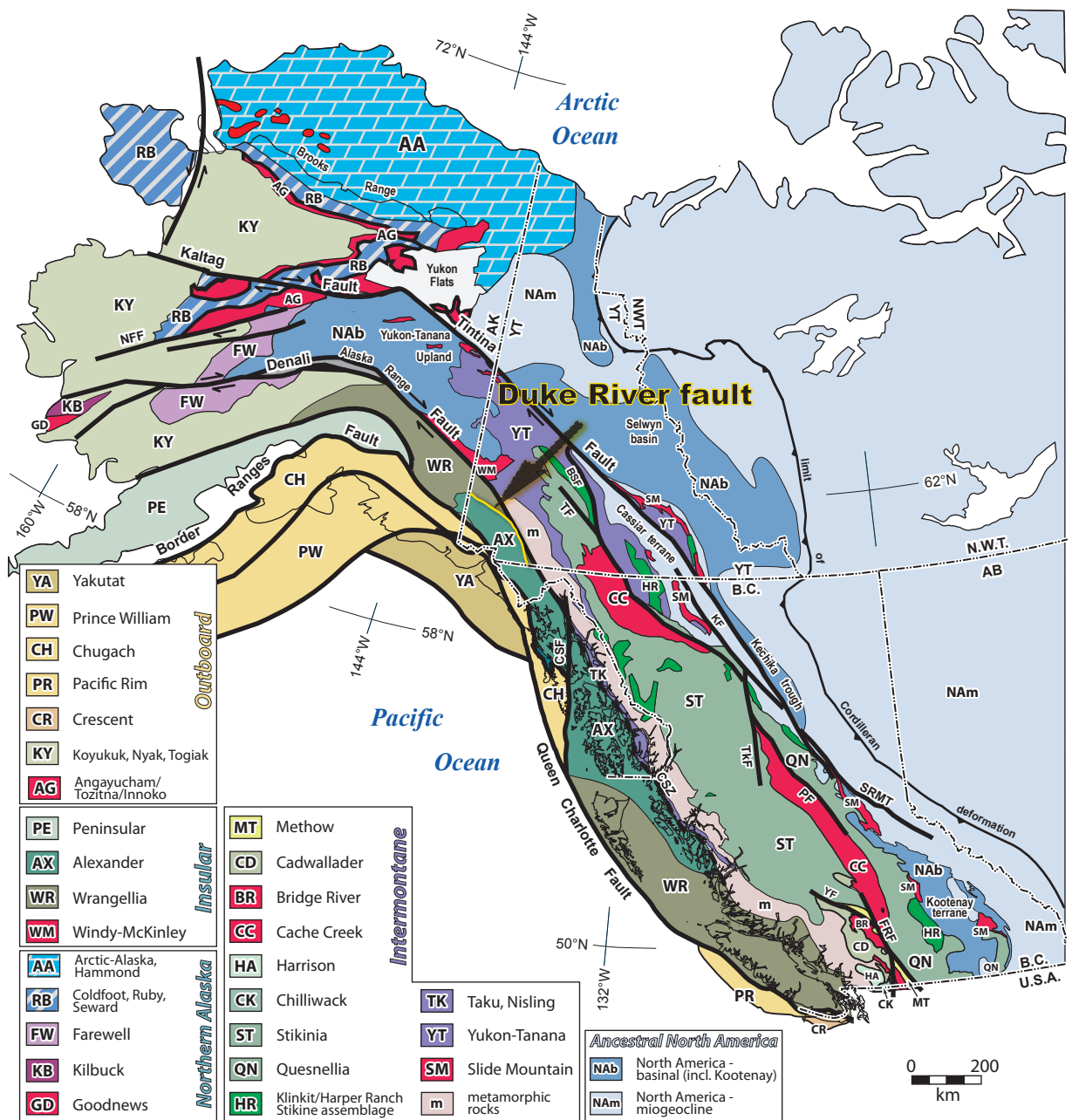


Figure 1.1: Terrane map of Alaska, Yukon Territory and British Columbia showing the location of the Duke River fault in southwest Yukon. *Modified from Colpron et al., 2007.*

Paleozoic contact currently known, the Duke River fault provides an excellent opportunity to study the geologic relationships between the two terranes. The Duke River fault is exposed over much of its strike-length in southwest Yukon allowing for detailed study of the nature and timing of this terrane bounding structure.

1.1 Previous Work

The Duke River fault in southwest Yukon was first recognized by Muller (1967) as a moderate to steeply northwest dipping thrust fault which separates Devonian and Mississippian rock units from structurally underlying Permian to early Tertiary units. Work by MacKevett and Jones (1975) interpreted the Duke River fault as part of a megathrust that placed Wrangellia westward over the Alexander terrane. Read and Monger (1976) mapped the Duke River fault as a steeply dipping structure that was in part, covered by undeformed conglomerates of Oligocene age, and interpreted the fault to be a splay off the Denali fault (Fig. 1.1) that accommodated mainly strike slip movement. Dodds and Campbell (1992) suggested the Duke River fault is a post-Triassic dextral strike slip fault that has accommodated major displacements. Mapping by the British Columbia Geological Survey in northwest British Columbia (Mihalynuk et al., 1993) indicates that both high-angle and moderately southwest dipping, thrust faults make up an imbricate zone that defines the Duke River fault. Detailed study of Tertiary sedimentary rocks in southwest Yukon suggests that basins formed as a result of secondary thrust and normal fault splays off a dominantly strike-slip Duke River fault (Ridgeway and Decelles, 1993).

In 2004, the Yukon Geological Survey initiated a multi-year mapping project that focused on re-mapping parts of the southwest Yukon. The aim of the project was to remap the Paleozoic and younger rocks of Wrangellia and reassess the mineral potential of the area. This provided the logistical support for a detailed study of the Duke River fault that complimented the revised regional map being constructed by the Yukon Geological Survey.

1.2 Duke River Fault Definitions

For the purpose of this thesis, the Duke River fault imbricate zone is a high strain zone composed of an imbricately deformed area that separates the Alexander terrane from Wrangellia. Specifically, the Duke River fault (*sensu stricto*) has been defined in this thesis as the leading edge of deformation within this high strain zone and marks the exact boundary between the Alexander terrane and Wrangellia. The Duke River fault imbricate zone comprises a 200 to more than 1000 m wide zone of ductile deformation within the Alexander terrane, formed as a result of movement related to the Duke River fault itself. Clearly overprinting the ductile deformation within the imbricate zone are localized zones of intense brittle deformation forming gouge zones. It was not possible to examine the southwestern boundary of this imbricate zone in some places due to the nature of the mountainous terrane.

1.3 Objectives of Thesis

The objectives of this study are: 1) to determine the timing and kinematics of movement along the Duke River fault; 2) to investigate the relationships between the Duke River fault and other major faults that have affected the Canadian and Alaskan portions of the Cordillera; and 3) to establish a pre-Tertiary tectonic framework for the outboard margin of the Cordillera in western Canada and southeast Alaska.

In order to meet these objectives two seasons of bedrock geological mapping and sample collection were carried out at six locations along the Duke River fault in southwest Yukon. Geological maps produced from the data collected are used to form the basis for understanding the stratigraphy of Wrangellia and the Alexander terrane in the vicinity of the Duke River fault as well as to examine fault related structures within the imbricate zone. Petrographic analysis of microstructures and mineralogy were performed on samples taken from within and near the Duke River fault imbricate zone to aid in determining the kinematics of the Duke River fault

motion and gain insights into the metamorphic conditions experienced by rocks on either side of the fault. Lastly, samples were collected and dated using $^{40}\text{Ar}/^{39}\text{Ar}$ and U-Pb geochronological techniques in an attempt to constrain the timing of deformation within the Duke River imbricate zone.

Six 1:10,000 scale maps are presented in this thesis, together with cross sections, lower hemisphere equal area projections of structural data, and descriptions of the stratigraphy, metamorphic grade and structure of the Alexander terrane and Wrangellia. A description of the strain gradient across the imbricate zone, deformation mechanisms that were active during movement along the fault and overprinting relationships are presented for each mapped area. Structures and lithological units are correlated between mapped areas where possible.

2: REGIONAL GEOLOGY AND TECTONIC OVERVIEW

2.1 Regional Geology of Wrangellia

2.1.1 Stratigraphy

Wrangellia is the larger of the two Insular terranes and is found from central Alaska to southern British Columbia (Fig. 1.1). Wrangellia is characterized by Paleozoic rock units of island arc affinity that are overlain by a thick package of Mesozoic flood basalts and sedimentary rocks (Fig 2.1). The Skolai Group is the oldest succession of layered rocks in Wrangellia. In southwest Yukon the Skolai Group consists of Mississippian to Permian volcanic and volcanoclastic rocks of the Station Creek Formation and Permian sedimentary rocks of the Hasen Creek Formation (Smith and MacKevett, 1970; Read and Monger, 1976; Israel et al., 2007; Israel and Cobbett, 2008). The Station Creek Formation includes a lower package of mafic to intermediate, plagioclase and pyroxene phyric flows and an upper package of volcanoclastic rocks that range from coarse breccias to fine tuffs (Read and Monger, 1976; Israel et al., 2007; Israel and Cobbett, 2008). The Hasen Creek Formation gradationally overlies the Station Creek Formation and consists of minor chert, black shale, siltstone, sandstone, turbidites, minor conglomerate and limestone. The age of the Station Creek Formation is at least as old as Early Mississippian based on a 351 Ma U-Pb zircon age from crystal tuff near the base (S. Israel, pers. comm., 2010). The age of the Hasen Creek Formation is Early Permian based on fossils from limestone (Smith and MacKevett, 1970; Read and Monger, 1976).

Middle Triassic *doenella*-bearing siltstones unconformably overlie the Hasen Creek Formation, and are locally preserved in graben-like structures (Israel et al., 2007; Israel and Cobbett, 2008). Basal conglomerates of the Late Triassic Nikolai formation generally overlie these siltstones, and are themselves overlain by a

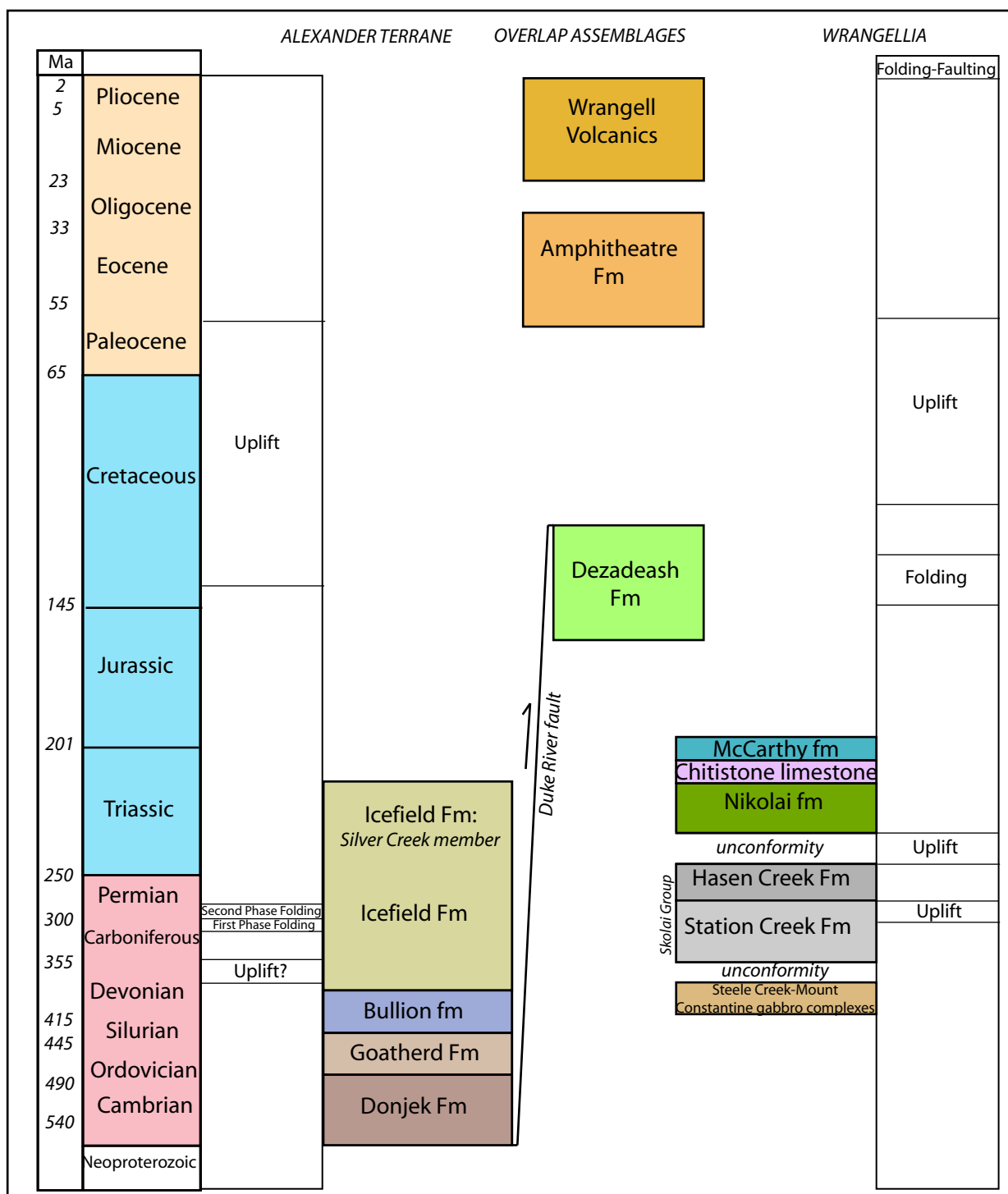


Figure 2.1: Simplified stratigraphic sections for the Alexander terrane and Wrangellia including overlap assemblages. Approximate timing of uplift and folding that affected the Alexander terrane and Wrangellia.

package of amygdaloidal basalt flows that locally are up to 3000 m thick (Read and Monger, 1976). Locally, thin-bedded, limestone and green and maroon shale are interbedded with the basalt flows near the top of the formation. Basalts of the Nikolai formation are interpreted to be part of a large igneous province that is a product of a mantle plume (Greene et al., 2008). Upper Triassic Chitistone limestone is locally interbedded with the Nikolai formation but generally disconformably overlies it (Read and Monger, 1976; Israel and Cobbett, 2008). Gypsum is locally present at the base of the Chitistone limestone and varies in thickness from metre-scale deposits to accumulations up to several hundreds of metres thick (MacKevett, 1971; Read and Monger, 1976; Israel et al., 2006). Calcareous and carbonaceous sedimentary rocks of the McCarthy formation conformably overlie the Chitistone limestone (Read and Monger, 1976; Israel and Cobbett, 2008).

2.1.2 Intrusive Rocks

Coarse-grained, pyroxene-bearing gabbros of the Late Devonian Steele Creek – Mount Constantine gabbro complexes are the oldest rocks that have been identified thus far in Wrangellia in southwest Yukon (Fig. 2.1; Campbell and Dodds, 1992). Sedimentary rocks of the Hasen Creek Formation locally sit unconformably on top of the gabbros (Read and Monger, 1976). Bodies of Late Triassic gabbro, peridotite and minor dunite of the Kluane Mafic-Ultramafic Complex intrude Palaeozoic rocks and have been inferred to be part of the plutonic roots of the Late Triassic Nikolai formation basalts (Hulbert, 1997). Plutons of medium- to coarse-grained granodiorite to tonalite of Late Triassic age locally intrude the Palaeozoic rocks (Israel and Cobbett, 2008). Medium- to coarse-grained diorite to granodiorite of the Early Cretaceous Kluane Ranges suite is the most abundant intrusive rocks in the area. Small bodies of medium-grained hornblende-pyroxene gabbro and biotite-hornblende diorite that have been assigned to the Pyroxenite Creek Ultramafic unit are similar to intrusions of the Kluane Mafic-Ultramafic Complex, but must be younger because of their intrusive relationship with Jurassic to Cretaceous rocks.

The youngest identified intrusive rocks belong to the Tkope and the Wrangell igneous suites, which comprise Oligocene plutonic rocks and Miocene plutonic and volcanic rocks, respectively (Read and Monger, 1976; Campbell and Dodds, 1992).

2.1.3 Structure and Metamorphism within Wrangellia

The dominant structures in Wrangellia in southwest Yukon are northwest trending and are the result of several phases of deformation beginning as early as pre-Middle Triassic time and continuing until the present day (Read and Monger, 1976; Power, 1988; Israel and Cobbett, 2008). A pre-Middle Triassic compressional event has been inferred on the basis of upright, shallowly plunging, tightly folded Palaeozoic strata overlain by relatively undeformed Triassic strata, the absence of Early Triassic rocks and an unconformable contact between Triassic and Paleozoic stratigraphic units (Read and Monger, 1976; Israel and Cobbett, 2007; 2008). A second, post-Triassic, pre-Late Cretaceous contractional event is recorded by well documented regionally extensive, upright, northeast verging, tight to isoclinal folds and accompanying northeast- and southwest-verging thrust faults (Read and Monger, 1976; Israel and van Zeyl, 2005; Israel and Cobbett, 2007). Finally, Wrangellian rocks units are deformed by latest Cretaceous to Eocene strike-slip and associated second-order faults. This includes at least 400 km of right-lateral movement along the Denali fault and associated structures as well as possible strike-slip movement along the Duke River fault (Read and Monger, 1976; Lowey, 1998; Israel and van Zeyl, 2005; Israel and Cobbett, 2008). Many of the Cretaceous and older structures were reactivated during this time.

Wrangellia has been metamorphosed to prehnite-pumpellyite grade. Evidence for this includes the presence of pumpellyite-filled amygdules in Nikolai basalts. Locally, usually around high strain zones, the metamorphic grade increases to lower greenschist facies. All phases of structures are preserved in Wrangellia except near large faults such as the Denali fault in southwest Yukon, where they are obliterated.

2.2 Regional Geology of the Alexander Terrane

2.2.1 Stratigraphy

The Alexander terrane is exposed in eastern and southeast Alaska, southwest Yukon and parts of northwest British Columbia (Fig. 1.1). It includes intrusive, volcanic and sedimentary rocks that range in age from Neoproterozoic to Late Triassic (Fig. 2.1; Gehrels and Saleeby, 1987).

New studies from Alaska and southwest Yukon suggest that the Alexander terrane as defined by Gehrels and Saleeby (1987) in southeast Alaska differs from Alexander terrane exposed in southwest Yukon, which are now termed the St. Elias Alexander or St. Elias subterrane (Figure 2.2; Beranek et al., 2011; S. Karl pers. comm., 2010). This paper only discusses the Alexander terrane rocks in southwest Yukon and northwestern most British Columbia (termed the St. Elias Subterrane by Beranek et al., 2011) and does not consider the originally defined portions of the Alexander terrane exposed in southeast Alaska and British Columbia.

Very little geological work has been completed on rocks of the Alexander terrane in Yukon, other than the regional scale mapping by Wheeler (1963), Read and Monger (1976), and Campbell and Dodds (1992), mostly because a large percentage of the terrane is covered by glacial ice. Furthermore, much of the area that is not ice-covered is exposed in very remote, extremely rugged parts of the Saint Elias Mountains, which hinders detailed investigations. The Alexander terrane in Yukon is composed of successions of siliciclastic, carbonate and volcanic rocks of a variety of ages. The descriptions below are mainly from Campbell and Dodds (1992) with more detailed observations from Beranek et al., (2011).

The oldest exposed rocks belong to the Cambrian to Ordovician Donjek Formation, which consists of sandstone and metabasalt and minor carbonate rocks. The Lower Ordovician to Devonian Goatherd Formation, which comprises dominantly carbonate and clastic rocks, overlies the Donjek Formation. A similar

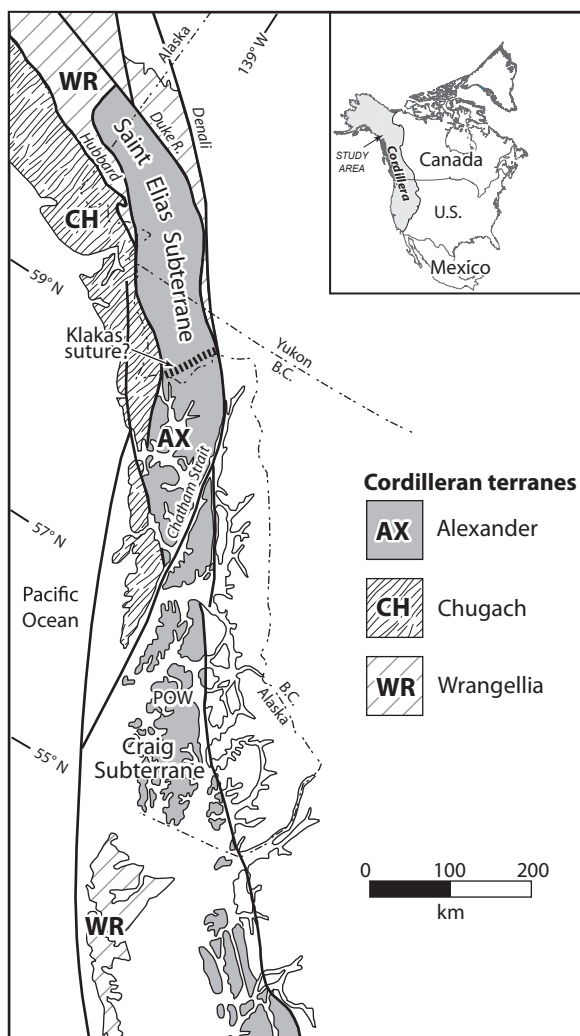


Figure 2.2 Simplified geologic map of Canadian and Alaskan Cordillera outlining the limits of the Saint Elias Subterrane and the Craig Subterrane. (Berenak et.al., 2011)

package of carbonate and clastic rocks of Silurian to Devonian age make up the Bullion formation and is exposed throughout southwest Yukon. The youngest package of layered rocks in the St. Elias Alexander terrane belongs to the Devonian to Upper Triassic Icefield Formation; this package also consists of siliciclastic, carbonate and volcanic rocks.

2.2.2 Intrusive Rocks

Three main plutonic suites intrude St. Elias Alexander terrane. Previous to this study, the oldest igneous rocks known to intrude the Alexander terrane were assigned to the Icefield Ranges Suite, which consists of Pennsylvanian to Permian biotite-hornblende syenite, quartz monzodiorite and diorite. Rocks of this suite include the stitching pluton of Gardner et al., (1988). The Saint Elias Suite consists of bodies of Late Jurassic to Early Cretaceous, non-porphyritic to porphyritic (K-feldspar), biotite-hornblende granodiorite that are widespread throughout the Alexander terrane in southwest Yukon. The youngest plutonic suite that intrudes the Alexander terrane in southwest Yukon is relatively fresh and undeformed hornblende +/- biotite granodiorite to porphyritic (K-feldspar) hornblende granodiorite of the Miocene Wrangell Suite..

Voluminous gabbro bodies of suspected Late Devonian age are observed to intrude the Goatherd and Bullion formations near the Duke River fault in southwest Yukon. The significance of these gabbros is not yet fully understood.

2.2.3 Structure and Metamorphism within the Alexander terrane

A northwest-southeast structural trend is present throughout the terrane and comprises folds and associated metamorphic fabrics (Dodds and Campbell, 1992). Two generations of regional-scale folds are interpreted to be at least Pennsylvanian in age as plutons assigned to the Icefield Ranges Suite cross cut refolded folds in carbonates belonging to the Donjek Formation (Read and Monger, 1976; Gardner et al., 1988; Dodds and Campbell, 1992). These folds are closed to isoclinal and are subsequently deformed by later open to closed folds most similar

to type three interference patterns. Several phases of faulting deform Alexander terrane rocks in southwest Yukon. These include thrust faults of uncertain age, steeply dipping strike-slip faults that are interpreted to be related to the Denali fault, and normal faults that have been interpreted to be post Oligocene in age (Dodds and Campbell, 1992).

Rocks of the Alexander terrane rocks have been metamorphosed to greenschist facies conditions, as indicated by the presence of greenschist (chlorite/actinolite schists) and strongly chloritized and epidotized metabasalt units (Read and Monger, 1976; Dodds and Campbell, 1992).

2.3 Overlap Assemblages of Wrangellia and Alexander Terrane

Several stratigraphic sequences overlie both the Alexander terrane and Wrangellia (Fig 2.1). The oldest of these comprises Upper Jurassic to Lower Cretaceous turbidites of the Dezadeash Formation. The Dezadeash Formation is one of several stratigraphic packages of similar age that were deposited in basins that developed between the Insular and Intermontane superterranes during middle Mesozoic time (Smith and MacKevett, 1970; Read and Monger, 1976; McLelland et al., 1992; van der Heyden, 1992). Terrestrial clastic sedimentary rocks of the Oligocene Amphitheatre Formation also overlie both the Alexander terrane and Wrangellia and were deposited in syntectonic basins developed along the Duke River and Denali fault systems (Read and Monger, 1976; Ridgeway et al., 2002). Miocene to Pliocene and (?) younger volcanic rocks of the Wrangell volcanic formation are widely exposed extensively throughout southwest Yukon. These mainly comprise mafic to intermediate volcanic flows, breccias and tuffs.

2.4 Regional Tectonic Overview

Our current understanding of the Paleozoic and Mesozoic tectonic evolution of the Cordilleran margin in the northern Cordillera in northwest British Columbia, southwest Yukon and southeast Alaska is still fragmentary. A regional tectonic

overview of southwest Yukon is presented based on present understanding of how various elements of the northern Cordillera evolved in Paleozoic and early and late Mesozoic time. An understanding of the pre-Duke River fault tectonic and stratigraphic relationships between Wrangellia and the Alexander terrane are crucial to the understanding of the nature of the Duke River fault and the fault's role in the further evolution of the Insular terranes.

2.4.1 Early Paleozoic Evolution of the Alexander Terrane

The Alexander terrane in Yukon and northwest British Columbia differs significantly from the classic description of the Alexander terrane in southeast Alaska (Gehrels and Saleeby, 1987). In this thesis the term St. Elias subterrane is used to distinguish the rocks in southwest Yukon and northwest British Columbia from Alexander terrane in southeast Alaska (Craig subterrane) (Fig. 2.2). This difference was first noted and described by Dodds and Campbell (1992) and more recently by S. Karl (pers. comm., 2009) and Beranek et al. (2011). These workers outlined a markedly different geological Early Paleozoic evolution for the St. Elias subterrane, compared to the Craig subterrane of southeast Alaska during the Early Paleozoic.

Donjek formation mafic magmatism and spatially related, coeval sedimentary rocks that are intercalated with the volcanic rocks, suggest deposition in a shallow marine rift environment (Beranek et al., 2010). The age and distribution patterns of detrital zircons from sandstones from the Donjek Formation match those present in regions of northern Baltica (e.g. Timanides) (Fig. 2.3a). Beranek et al. (2011) explain the age similarities by suggesting that the Late Cambrian to Early Ordovician St. Elias subterrane was linked to or part of Baltica at that time. Van Staal et al. (2010) suggest that the Donjek-Goathead pair forms part of a rift to drift sequence that records rifting of a sliver of the margin of Baltica, followed by the formation of a passive margin and isolation of this terrane from Baltica.

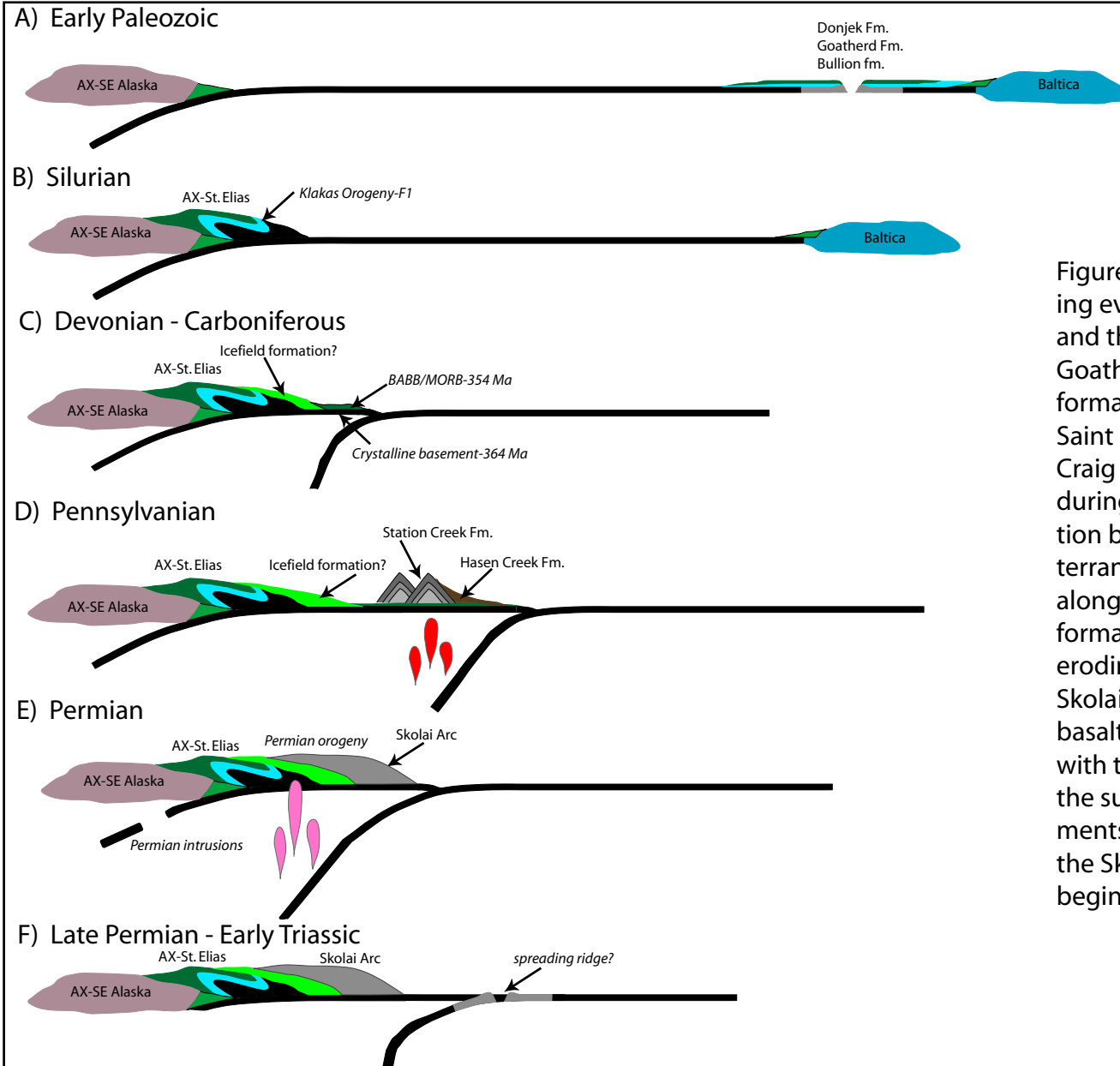


Figure 2.3 Schematic cross sections showing evolution of the Saint Elias Subterrane and the Skolai Arc. A) Donjek Formation, Goathead Formation and the Bullion formation formed near Baltica. B) The Saint Elias Subterrane collides with the Craig Subterrane (Southeast Alaska) during the Klakas Orogeny. C) Subduction begins outboard of the Alexander terrane and an oceanic arc develops along with a back arc basin. The Icefield formation is deposited from sediment eroding off the Alexander terrane. D) The Skolai Arc is built on back arc basin basalts. E) The Skolai Arc is amalgamated with the Alexander terrane. Melts from the subducting slab intrude the basements of both the Alexander terrane and the Skolai Arc. F) A spreading ridge begins to be subducted.

2.4.2 Middle to Late Paleozoic Evolution of Wrangellia and the Alexander Terrane

A well-documented Silurian age orogenic event, termed the Klakas orogeny, is described in the Alexander terrane in southeast Alaska and is inferred to have also affected Alexander terrane in southwest Yukon (Gehrels et al., 1983; Dodds and Campbell, 1992). The Klakas orogeny has recently been interpreted as the result of the collision between the Craig subterrane and the St. Elias subterrane (Fig. 2.3b; Van Staal et al., 2010). If this is the case, it is likely that the Klakas orogeny is the mechanism that is responsible for the formation of early regional folds observed in southwest Yukon (Van Staal et al., 2010). Van Staal et al. (2010) suggest that the refolding of the early folds may be the result of a collision between the Skolai Arc and the Alexander terrane, followed by an arc-polarity reversal.

Paleozoic Wrangellia comprises the Skolai Arc, an oceanic arc that is floored by basalts that have a back arc basin (BABB) to mid-ocean ridge basalt (MORB) geochemical signature (Israel and Cobbett, 2008). The Skolai Arc comprises mafic to intermediate volcanic and overlying volcanoclastic rocks of the Early Mississippian to Permian Station Creek Formation, that are in turn overlain by Early Permian sedimentary rocks of the Hasen Creek Formation (Smith and MacKevett, 1970; Read, 1976; Read and Monger, 1976; Israel et al., 2007; Israel and Cobbett, 2008). A back arc basin between the Alexander terrane and the Skolai Arc would account for the geochemical signature of the basalts at the base of the Skolai Arc (Fig. 2.3c). The Hasen Creek sediments could have been deposited in a forearc basin that flanked the oceanic arc (Fig. 2.3d). Devonian age gabbros are unconformably overlain by the Hasen Creek formation near Mount Steele in southwest Yukon (Israel, pers. comm, 2011). These gabbros may be the crystalline basement to the BABB/MORB volcanic units that occur at the base of the Skolai Arc and are also unconformably overlain by Hasen Creek strata on the fore-arc basin side of the arc (Fig. 2.3d).

The Icefield Formation in the Alexander terrane comprises Devonian to Triassic pelitic, carbonate and volcanic rocks that are interpreted to have been

deposited on top of the Bullion formation. The Icefield Formation could represent detritus eroded from the Alexander terrane and shed into the back arc basin (Fig. 2.3c-d).

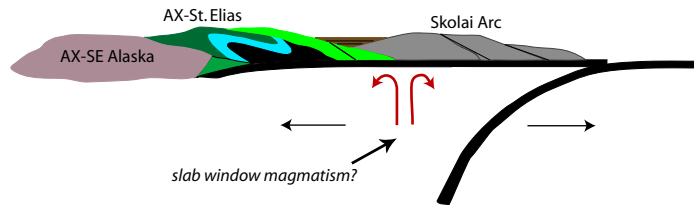
2.4.3 A Model for the Early Mesozoic History of Wrangellia and the Alexander Terrane.

Wrangellia is characterized by a thick sequence of Late Triassic flood basalts and overlying carbonate and sedimentary rocks that lie unconformably above the Skolai Arc (Read and Monger, 1976). Mafic rock units of similar age and composition to the Nikolai formation occur in the Alexander terrane in northwest British Columbia where they are referred to as the Tats Volcanic Complex. The Nikolai flood basalts have been interpreted to be part of a large igneous province derived from a mantle plume (Greene et al., 2008). Doming and heating of the overlying lithosphere by a rising plume beneath the amalgamated Alexander terrane and Wrangellia could have initiated a rift that separated the two terranes in Triassic time. Upper Triassic basalts from the Windy Craggy deposit in northwest British Columbia (part of Tats Volcanic Complex) have compositions consistent with eruption in a back arc basin setting (Peter and Scott, 1999). There is little evidence of a magmatic arc of Late Triassic age preserved in the Alexander terrane or Wrangellia.

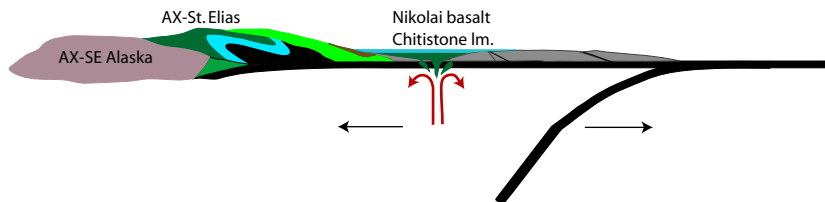
An alternative scenario may be subduction of an oceanic ridge, resulting in slab-window magmatism (van Staal et al., 2010). In such a scenario rising asthenospheric mantle would have thinned the crust beneath the amalgamated Wrangellia and Alexander terranes and eventually led to the eruption of flood basalts (Fig. 2.3f, 2.4a-b), represented by both the Nikolai basalts in Wrangellia and the Tats Volcanic Complex in the Alexander terrane (MacIntyre, 1984). In addition, subduction of a ridge could cause subduction-related arc magmatism of the Skolai Arc to cease (Van Staal et al., 2010).

The Silver Creek member of the Icefield Formation is a package of volcanoclastic rocks, conglomerate, sandstone and locally fossiliferous limestone

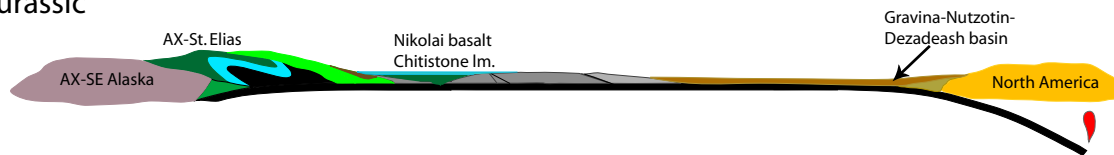
A) Triassic



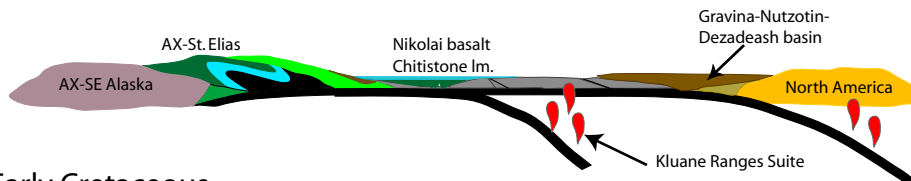
B) Late Triassic



C) Jurassic



D) Late Jurassic - Early Cretaceous



E) Early Cretaceous

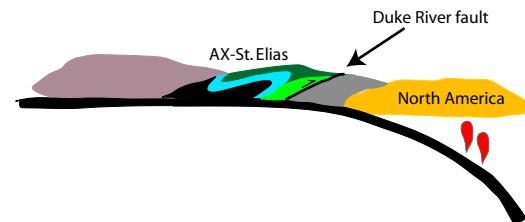


Figure 2.4. Regional cross section through Wrangellia and the Alexander terrane from Jurassic to Cretaceous time. A) Slab window magmatism heats up the crust and causes uplift and crustal thinning that initiates rifting of Wrangellia and the Alexander terrane. B) Eruption of the Nikolai basalts on top of the Skolai Arc. C) Subduction of oceanic crust beneath North America is initiated and the deposition of the Gravina-Nutzotin and Dezadeash packages begins. D) The Coast Plutonic Complex begins forming as partial melts from the subducting oceanic crust intrude North America. Partial melts from a subduction zone that initiated beneath Wrangellia forms the Kluane Ranges Suite. E) Closure of the Gravina-Nutzotin and Dezadeash basins and the rift basin between Wrangellia and the Alexander terrane leads to the accretion of the Inuslar Superterrane with North America. The Duke River fault is part of the suture zone between the Wrangellia and Alexander terrane.

that crop out west of Kluane Lake along the Duke River fault. Dodds and Campbell (1992) report a Triassic fossil collected from this member near Jessie Creek. If this succession of rocks is Triassic in age, it may represent infill into the rift basin that is described above.

2.4.4 A Model for the Middle Mesozoic History of Wrangellia and the Alexander Terrane.

A series of Jurassic to Cretaceous basinal assemblages have been mapped between the Insular terranes and the Intermontane terranes from northwest British Columbia to central Alaska (Eisbacher, 1976; Richter, 1976; MacKevett, 1978). The basins located in eastern and southeast Alaska (Gravina-Nutzotin formations) have been interpreted to have originally accumulated along the eastern margin of Wrangellia and the Alexander terrane in the Late Jurassic to Early Cretaceous (Berg et al., 1972). In Yukon the basin fill is represented by the Dezadeash Formation, which is mapped as overlying parts of Wrangellia (Eisbacher, 1976). The Gravina belt is interpreted to tie the Alexander terrane and Wrangellia to the North American margin by Upper Jurassic time. This interpretation is based upon detrital zircon ages from Gravina stratigraphy that match well-known igneous ages from the Alexander terrane as well as detrital zircon age signatures from Yukon Tanana and Stikine terranes (Figure 2.4c; Kapp and Gehrels, 1998). Trop and Ridgeway (2007) suggest a model in which east dipping (present coordinates) subduction was initiated in the Jurassic along the North American margin and detritus from the Yukon Tanana terrane and Stikinia (essentially the western margin at that time) was shed into the basin. The convergent margin at the edge of the North American margin possibly began as early as Middle Jurassic, generating the arc magmatism observed within the Coast Plutonic Complex (Fig. 2.4c-d; McClelland, 1992; Van der Heyden, 1992). Continued subduction eventually led to the collapse of the back-arc basin (Gravina basin) or a small internal seaway between the Intermontane (upper plate) and Insular Superterrane (McClelland and Mattinson, 2000). This would explain the emplacement of the Cretaceous age Kluane Ranges suite in Wrangellia

(Read and Monger, 1976) and could be the driving force that is closing the Triassic rift basin that is suggested to have developed between Wrangellia and the Alexander terrane. One interpretation of the Duke River fault is that it represents a suture zone that formed with the final closure of the Triassic basin (Fig. 2.4e). A problem with this model is that there is no evidence of the existence of oceanic crust between Wrangellia and the Alexander terrane unless the Triassic Tats group and possibly the Upper Triassic Nikolai basalts were interpreted to be oceanic crust.

2.4.5 Middle to Late Mesozoic Collision of Insular Superterrane with North America.

There is evidence of a regional mid-Cretaceous compressional event at ~ 110- 90 Ma that affected the entire North American margin, from northern Washington to south-central Alaska (Crawford et al., 1987; Saleeby et al., 1990; McClelland and Mattinson, 2000; Rusmore et al., 2000). West-verging thrust faults (south dipping in south-central Alaska) are observed at numerous localities along the western edge of the Coast Plutonic Complex, and record deformation that began by at least 110 Ma and ceased by 90 Ma (McClelland and Mattinson, 2000). Both east and northeast-verging thrust faults that were coeval with the later phase of the west-vergent thrust systems occur east of the Coast Plutonic Complex in northwest British Columbia (Rusmore and Woodsworth, 1991). This deformation is attributed to the final docking of the amalgamated Wrangellia and Alexander terranes with the North America margin and the inversion of the intervening Dezadeash and Gravina-Nutzontin basins (Trop and Ridgeway, 2007).

2.4.6 Summary

1) The Early Paleozoic rift related volcanic and sedimentary rocks that comprise part of the St. Elias subterrane have linkages to Baltica. A passive margin carbonate platform likely developed on this block after it rifted away from Baltica. 2) Early folding (regional phase one observed in southwest Yukon) in the St. Elias subterrane may be the result of collision with the Craig subterrane in the Silurian (Klakas Orogeny). 3) Back-arc basin development occurring in the latest Devonian to

Mississippian may explain the geochemical signature of the base of the Skolai Arc.

4) Late Pennsylvanian Skolai Arc rocks were deposited on top of back-arc basin basalt and closure of the back-arc basin during construction of the Skolai Arc leading to uplift and erosion of the arc rocks and an unconformity between Permian Wrangellian rocks and Devonian gabbros. 5) A Triassic rift basin may have developed in response to heat generated from a mantle plume or slab roll-back from an as-yet unrecognized subduction zone or the subduction of a ridge that accommodated slab window magmatism. 6) Late Jurassic to Early Cretaceous subduction resulted in the intrusion of voluminous Early Cretaceous Kluane Ranges suite into Wrangellia and the development of the Coast Plutonic Complex. 7) At this same time a basin that developed between Wrangellia and the North American craton in response to a transtensional plate margin (McClelland and Mattinson, 2000), accumulated the Jurassic to Cretaceous basinal rocks now present throughout the northern Cordillera (e.g., Nutzotin, Gravina, Dezadeash, Kahiltna). 8) A change from transtensional to orthogonal subduction and collision of the St. Elias subterrane with Wrangellia may have occurred in Early Cretaceous time with the suture represented by the Duke River fault in southwest Yukon. 7) The final docking of the amalgamated Wrangellia and Alexander terranes (Insular Superterrane) with the North American margin (Intermontane terranes) occurred in the Cretaceous resulting in the compressional structures observed along the northern Cordilleran margin from northwest Washington to southern Alaska.

3: STRUCURAL AND LITHOLOGIC CHARACTER OF THE DUKE RIVER FAULT

Detailed mapping of six exposures of the Duke River fault imbricate zone in southwest Yukon was completed in the summers of 2008 and 2009 to address the objectives of the study (Fig. 3.1). A 1:10,000 scale bedrock geology map was created for each of the areas in Figure 3.1 and are found in Appendix I. Generalized versions of these maps, together with geologic cross-sections, lower hemisphere equal area projections of structural data, and descriptions of stratigraphy, metamorphic grade and structures of the individual project areas are also presented below. The field observations are used to determine the geometry and kinematic evolution of the Duke River fault. Each of these areas is compared to one another in order to develop a three-dimensional picture of the Duke River fault and how dynamics of the fault changed with varying depths over the life of the structure.

In the following sections, each area describes and discusses the fault based on structural position. These include, the footwall, the imbricate and the hangingwall zones of the Duke River fault. In all cases, the footwall is comprised of Wrangellian rocks, while the hangingwall and imbricate zones include a variety of rocks assigned to the Alexander terrane.

3.1 Squaw Creek

The Duke River fault in the Squaw Creek area is exposed in a steep-sided canyon near the Yukon-British Columbia border (Fig. 3.1). The canyon extends for about six kilometres along a northwest trend, where it shallows out within the Tatshenshini River valley (3.2, 3.3). In the Squaw Creek canyon, the Duke River fault is a low angle ductile and brittle thrust fault that places older, higher metamorphic grade rocks of the Alexander terrane over Wrangellia. The width of the Duke River

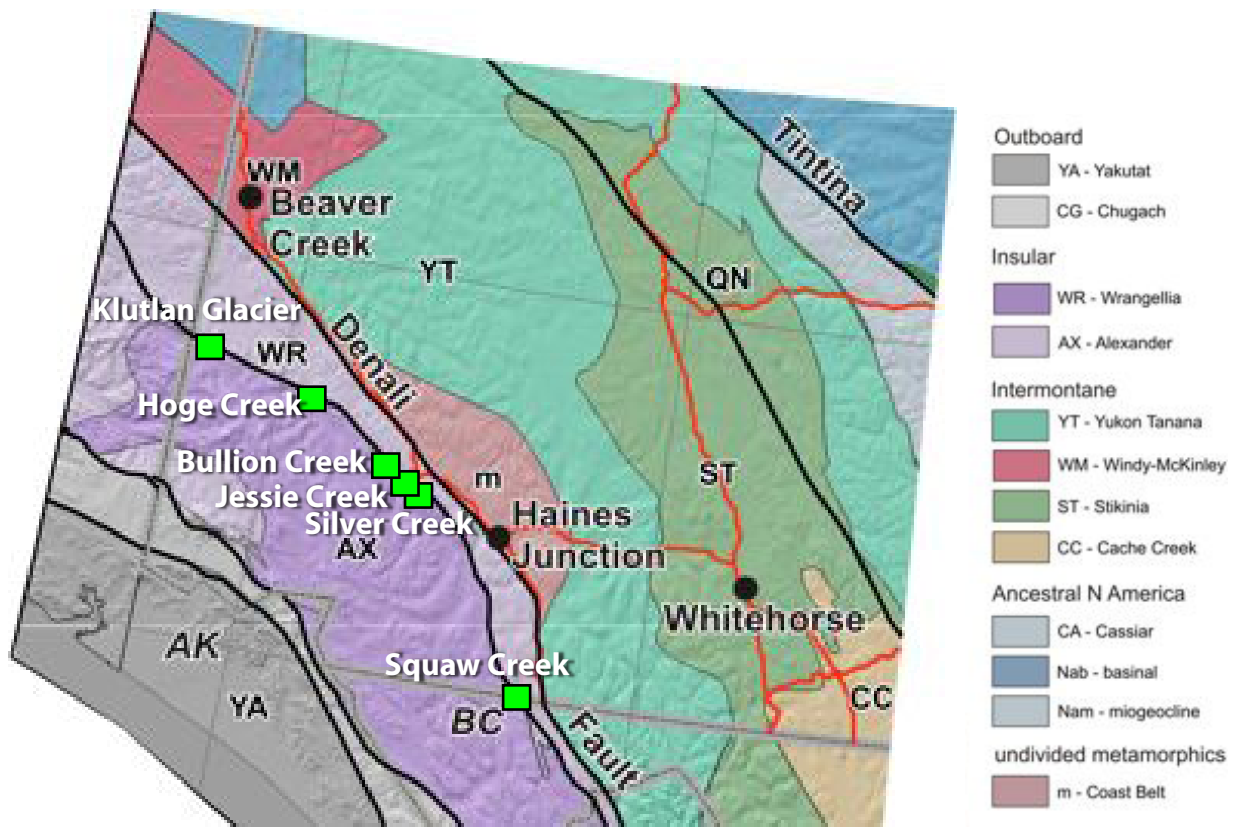


Figure 3.1. Location of mapped areas along the Duke River fault.

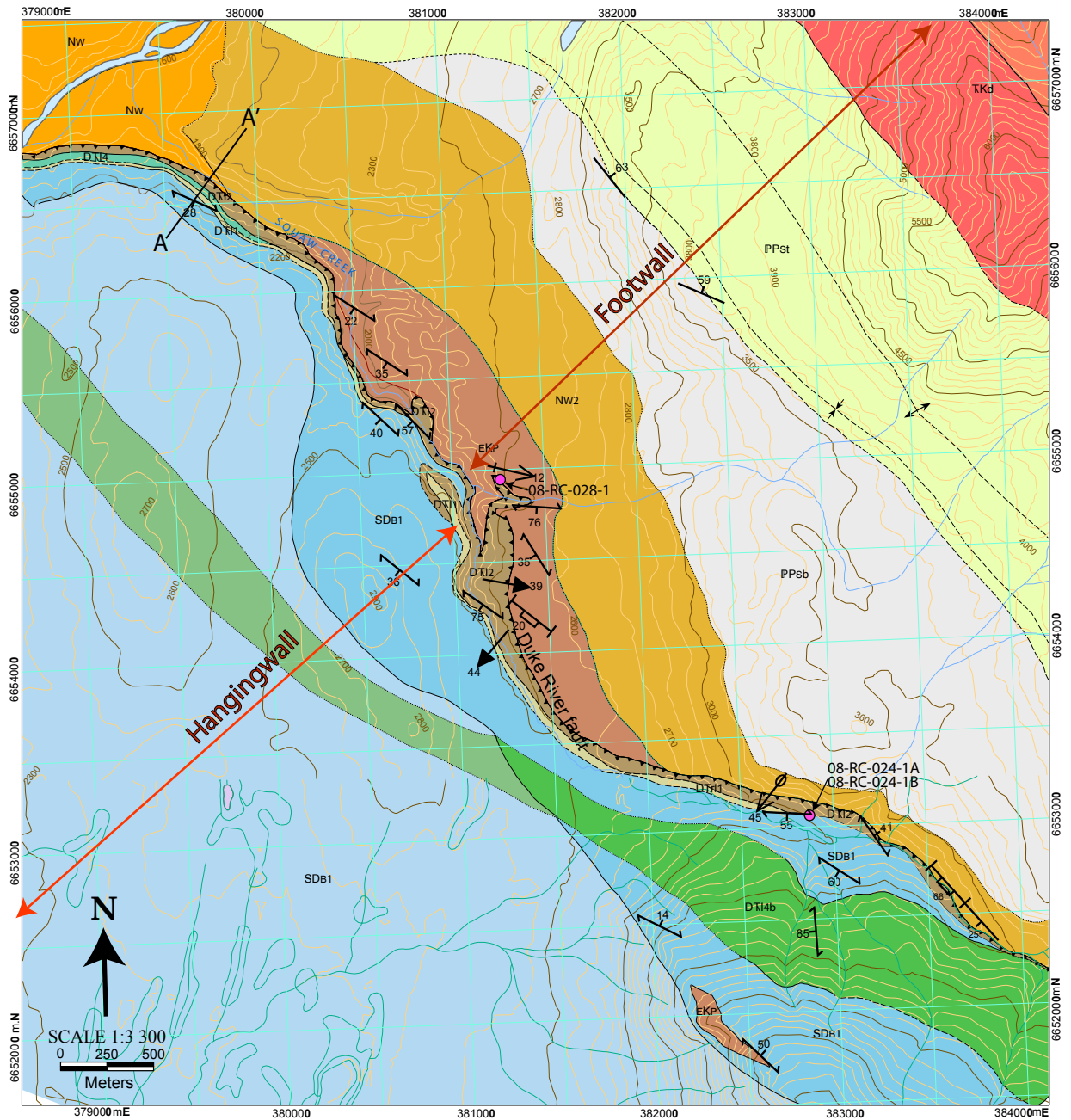


Figure 3.2 Bedrock geology map along the Duke River fault near Squaw Creek. Geological cross-section is shown in figure 3.4 and the legend for this map and all subsequent maps in figure 3.3.

MIOCENE

Wrangell Suite

MW	fine to medium-grained, feldspar-quartz porphyritic granite
-----------	---

EARLY CRETACEOUS

Pyroxenite Creek Ultramafic

EKP	medium-grained hornblende gabbro
EKP1	medium-grained hornblende pyroxene gabbro; dark green pyroxene gabbro to pyroxenite
EKK	fine to medium-grained hornblende-biotite granodiorite to quartz monzonite

TRIASSIC

TKd	medium to coarse-grained, unfoliated, salt and pepper appearance, hornblende +/- biotite diorite; quartz diorite; locally abundant dark grey, fine-grained gabbro
Tg	medium-grained hornblende gabbro
Tum	medium-grained hornblende gabbro

PERMIAN

Steele Creek Gabbro Complex

Psc	massive, locally foliated, grey-green hornblende pyroxene gabbro; minor medium-grained gabbro diabase; locally luecocatic gabbro
Psc	dark green to black, serpentinized ultramafic

MISSISSIPPIAN

MGr	fine to medium-grained granite
------------	--------------------------------

LAYERED ROCKS WRANGELLIA

Wrangell Volcanics

MIOCENE

NW	fine-grained, dark grey to black basalt
NW2	biege, fine-grained crystal lithic tuff

TRIASSIC

Chitstone limestone

uTC	grey massive limestone
------------	------------------------

Chitstone Gypsum

uTG	light grey to white, massive to laminated gypsum
------------	--

Nikolai formation

uTNV	dark green/maroon weathered and fresh, massive to locally foliated, amygdaloidal and vesicular basalt flows; rare pillows
-------------	---

PENNSYLVANIAN - PERMIAN

Skolai Group

Hasen Creek Formation

PHc	light to medium grey, massive to bedded limestone; dark grey, thin bedded siltstone; light grey to brown, calcareous, fossiliferous packstone; medium-grained litharenite sandstone; grades into a poorly bedded pebble conglomerate
PHc2	light grey, laminated to massive limestone
PHc3	green and maroon boulder conglomerate dominated by well-rounded clasts of gabbro and diorite; locally maroon volcanic breccia with a sandy matrix

Station Creek Formation

PPSo	green to purple medium to coarse-grained hornblende-pyroxene gabbro
PPst	dark grey to green, very fine-grained tuffaceous siltstones, sandstones and banded tuffs; dark green to black, medium-grained pyroxene gabbro
PPsb	dark green, fine-grained basalt; rare pillow basalts; pyroxene-phyric basalt breccia

ALEXANDER TERRANE

DEVONIAN TO TRIASSIC

Icefield assemblage

DTI1	light green, fine-grained feldspar quartz (?) schist to phyllite; very fine-grained phyllonite
DTI2	carbonaceous, calcareous feldspar muscovite quartz schist to phyllite; rare muscovite quartzite
DTI4	massive to thin-bedded limestone to calcareous siltstone
DTI4b	undifferentiated calcareous and carbonaceous siltstone; fine-medium-grained greenschist; banded limestone to marble
DTI5	white, foliated gypsum
DTI6	white to light grey, massive to banded marble
DTI6b	orange to biege, breccia made up of dominantly marble clasts and cemented by calcite

Icefield assemblage: Silver Creek member

DTI7	green and maroon, foliated conglomerate that grades upwards into maroon, medium-grained sandstone
DTI7b	grey to brown, coarse-grained lithic sandstone to pebble conglomerate dominated by chert and siltstone clasts
DTI8	dark grey to black, fine-grained, calcareous siltstone; brown to grey, thin-bedded chert; rare fossiliferous limestone dominated by crinoid stems

SILLURIAN TO DEVONIAN

Bullion Creek Limestone

SDB1	biege to grey fresh, orange weathered, thin-bedded to brecciated marble
SDB2	fine-grained, carbonaceous mica schist; fine to medium-grained greenschist; rare muscovite quartzite

ORDOVICIAN

Donjek formation

COD	grey, laminated marble
COD1	dark green, fine to medium-grained basalt; basalt breccia

SYMBOLS

geologic contacts (defined, approximate, inferred, covered).....	
fault; movement not known (defined, approximate, inferred, covered).....	
thrust fault (known, approximate, inferred).....	
fold axial trace (upright - anticline, syncline).....	
mapping limit.....	
bedding (tops known, inclined, vertical).....	
foliation (dominant, late).....	
stretching lineation.....	
mineral lineation.....	
fold axis (dominant phase).....	
crenulation lineation.....	
dyke, vein.....	
fault plane.....	
isotopic age locations (pink - ⁴⁰ Ar- ³⁹ Ar, yellow - U-Pb).....	
fossil location (red-this study, green-Wheeler 1953).....	
cross-section lines.....	

Figure 3.3. Legend for six geologic maps made along the Duke River fault trace, southwest Yukon

fault imbricate zone in this area is approximately 100-300 metres (Fig. 3.4). A cataclastic zone 10-20 metres in width overprints the ductile deformation.

3.1.1 Stratigraphy of Foot Wall

Footwall rocks in the Squaw Creek area include Wrangellian volcanic and volcanoclastic rocks, mafic to ultramafic intrusions and Miocene volcanics (Fig. 3.2). The most abundant rocks within the footwall of the Duke River fault belong to the Station Creek Formation. These include pyroxene-phyric basalt breccias overlain by green, very fine-grained banded tuffs that are interbedded with green, fine-medium-grained volcanoclastic sandstone (Fig. 3.5a). An altered diorite body, assigned to the Pyroxenite Creek Ultramafic suite, is inferred to intrude the basalt breccias, although no contact was examined in the field. The diorite is green, medium-grained and actinolite-bearing, contains minor amounts of epidote and has been strongly chloritized (Fig. 3.2). Miocene to Pliocene crystal tuff and basalt flows of the Wrangell Volcanic Formation unconformably overlie the Station Creek Formation and the diorite. The crystal tuffs are rhyolitic in composition, weather a beige colour and are characterized by quartz crystals up to 3 mm in a fine-grained matrix. Dark grey, fine-grained, amygdaloidal, magnetite-bearing basalt is inferred to overlie the crystal tuffs, although the contact between these two units was not examined. The basalts are common in the middle and upper portions of the Wrangell volcanics as mapped elsewhere in the southwest Yukon (Dodds and Campbell, 1992).

3.1.2 Stratigraphy of Hanging Wall

The hanging wall near Squaw Creek is composed of rocks belonging to the Alexander terrane. The best exposure of the lower (structural) section is found in a gully south of Squaw Creek where interlayered carbonate, meta-basalt and

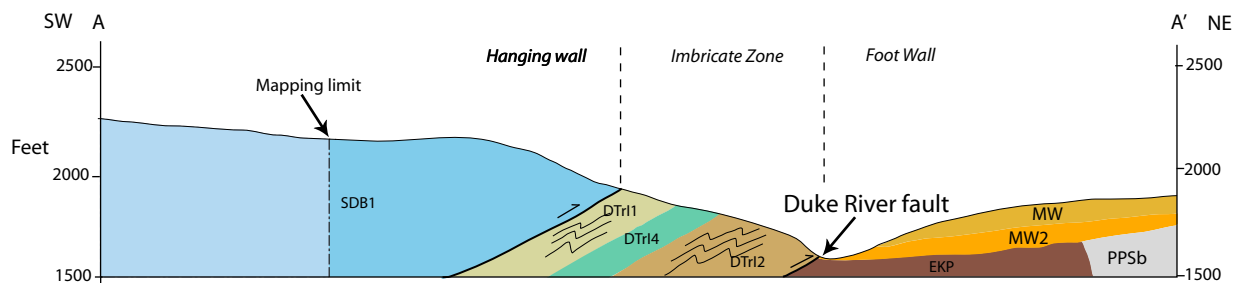


Figure 3.4. Geologic cross section through the Squaw Creek area. Vertically and horizontally exaggerated to show geologic detail around the Duke River fault. See figure 3.2 for location.



Figure 3.5 a) Pennsylvanian aged banded tuffs of the Station Creek Formation. b) Devonian marble of the Bullion formation cut by steeply dipping quartz veins.

calcareous siltstone crop out. A small ridge south of the gully is made up of blocky marble that are cut by a set of near vertical quartz veins ranging in width from 0.5 cm to 30 cm (Fig. 3.5b). This marble unit structurally overlies the carbonate, metabasalt and calcareous siltstone both of which have been assigned to the Silurian to Devonian Bullion formation. In the southwest corner of the map area, the carbonate is intruded by a green, medium-grained hornblende gabbro body of unknown age, but is here interpreted to be Triassic in age. The southern exposure of the Squaw Creek canyon is dominantly composed of Bullion formation marble that forms large, blocky outcrops above Squaw Creek (Fig. 3.2 & 3.4).

3.1.3 Stratigraphy of the Imbricate Zone

Between Wrangellia and Alexander terrane an imbricate zone characterized by strongly sheared and fractured rock separates the more intact hangingwall and footwall. The imbricate zone stratigraphy comprises an assemblage of foliated calcareous and carbonaceous siltstone; calcareous, fine-grained, muscovite-quartz-feldspar schist (82.8 – 104.6 Ma muscovite $^{40}\text{Ar}/^{39}\text{Ar}$ age, refer to chapter 4); carbonaceous quartz-muscovite schist; rare muscovite quartzite and greenschist that have been assigned to Devonian to Triassic Icefield Formation.

3.1.4 Structure of the Foot Wall

The Station Creek Formation basalt breccia and banded tuffs are deformed by open folds that plunge very shallowly to the northwest (Fig. 3.6a) and have been interpreted by Israel et al., (2008) to be part of the regional folding event that affected Wrangellia. Israel et al., (2008) clearly show these structures cut by a latest Triassic pluton, indicating the folding in the footwall cannot be attributed to the deformation along the Duke River fault, (see geochronology section for timing of movement).

Miocene crystal tuffs exposed near the Duke River fault (Fig. 3.2& 3.3) contain post lithification fabrics that include two closely spaced fracture sets that

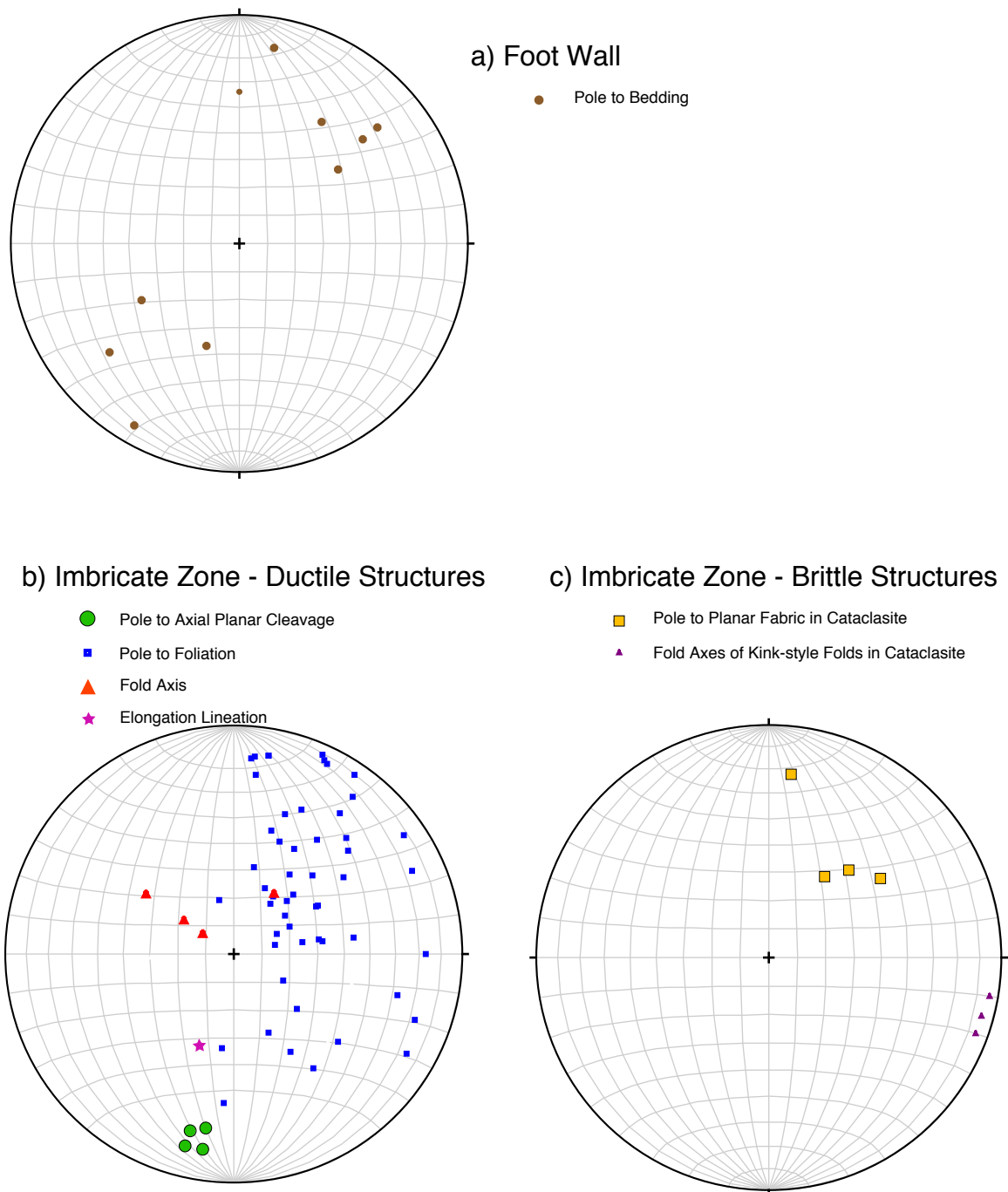


Figure 3.6 Structural data from the Squaw Creek area presented in equal area, lower hemisphere projection stereonet. a) Brown circles are poles to bedding taken several hundreds of metres away from the Duke River fault in the foot wall Station Creek Formation and show the effects of northwest-southeast trending regional folds in Wrangellia. b) Structural data from the imbricate zone of the Duke River fault near Squaw Creek. Blue squares are poles to foliations and red triangles are ductile fold axes. Green circles are poles to axial planar cleavages that are present in the hinges of ductile folds. Pink star is elongation lineation measured on main foliation (blue squares). c) Overprinting brittle fabrics from the imbricate zone of the Duke River fault near Squaw Creek. Orange squares are poles to planar fabric developed in fault gouge, purple triangles are kink-style fold axes that deform the fabric within the cataclasite.

dip steeply to the northeast and moderately to the east. The diorite that intrudes the Station Creek Formation exhibits a penetrative foliation that strikes southeast and dips steeply to the southwest and becomes less intense away from the fault (Fig 3.7a). The foliation is defined by aligned acicular grains of actinolite, elongate chlorite grains and dynamically recrystallized quartz that anastomose between larger blocky amphibole grains (Fig. 3.7b). The actinolite and chlorite crystals have grown during foliation development- i.e., metamorphism is syn-deformation. The quartz crystals were recrystallized during foliation development based on the observation of undulose extinction, and the development of sub-grain boundaries visible in the thin section.

3.1.5 Structure of the Hanging Wall

Foliations within the Alexander terrane rocks within the hangingwall of the Duke River fault strike northwest and dip to the southwest and northeast (Fig. 3.2). Based on the changes in the dip it is inferred that a regional west-northwest trending fold is present (Fig. 3.2). This is consistent with regional-scale structures mapped by Dodds and Campbell (1992). Outcrop-scale folding was not observed in the Alexander terrane rocks outside the imbricate zone of the Duke River fault.

The Triassic gabbro body ranges in the degree of deformation from undeformed to deformed by closely spaced brittle fractures with unknown orientations.

3.1.6 Structure within the Imbricate Zone

The main foliation within the imbricate zone strikes approximately southeast and dips moderately to the southwest; however, there is a large variation in orientation of this foliation within the zone (Fig. 3.6b). The main foliation is defined by muscovite layers within quartz-feldspar-muscovite schist. Elongation lineations, which are defined by elongated calcite and quartz are not common but are found on a few of the main foliation planes, plunge approximately 55° towards 200° (Fig. 3.6b; 3.7c).

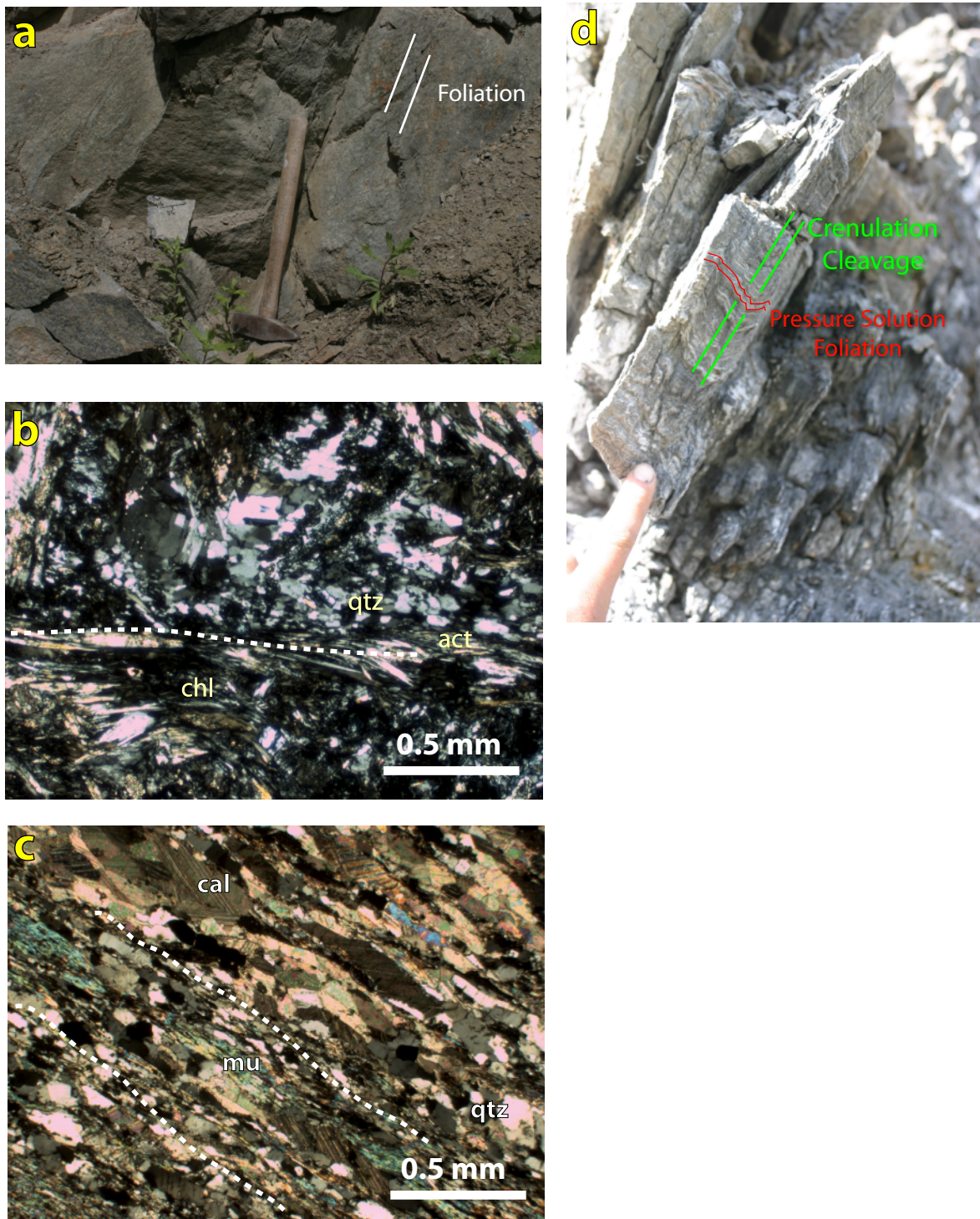


Figure 3.7. Photos of outcrops and thin sections from the hanging wall and imbricate zone in the Squaw Creek area. a) Foliated Early Cretaceous Pyroxenite Creek diorite. b) Photomicrograph of Pyroxenite Creek diorite in the foot wall showing aligned acicular actinolite (act) and chlorite (chl) grains and dynamically re-crystallized quartz (qtz) defining the foliation shown by dashed white line. c) Photo-micrograph of calcareous feldspar-quartz-muscovite (mu) schist from the imbricate zone. Thin section was cut parallel to elongation lineation defined by elongated grains of calcite (cal) and quartz (qtz). Foliation shown by dashed white lines. d) Early pressure solution fabrics overprinted by a pervasive crenulation cleavage in a calcareous, graphite-rich siltstone from the imbricate zone.

The main foliation in the imbricate zone itself is folded by tight, moderately to steeply plunging folds with an axial planar cleavage that strikes 280° and dips 70° (Fig. 3.6b). These folds are asymmetric and are characterized by thinned limbs and an approximately 45° interlimb angle. Within the siltstone of the Icefield Formation the main foliation is defined by quartz stringers and graphitic layers that have been locally deformed by a penetrative crenulation cleavage (Fig. 3.7d).

Brittle deformation overprints the ductile fabrics described above. A 10-20 m-wide, discrete cataclastic zone is observed within siltstone of the Icefield Formation. The cataclastic zone is composed of cohesionless fault gouge that comprises finely milled rock (dominantly quartz and feldspar) and clay deformed into a pervasive planar fabric that strikes 125° and dips approximately 30° towards the southwest (Fig. 3.7c, 3.8a). Locally within the Squaw Creek canyon, this planar fabric has been folded into tight, asymmetric, kink-style folds that have hinges plunging shallowly to the east (Fig 3.7c, 3.8b). No lineations or kinematic indicators (aside from the folding mentioned above) were found within the cataclastic zone. Bullion formation marble sits structurally above the cataclastic zone and remains relatively intact; however the marble has been cut by a number of quartz and calcite veins that form three dominant sets. Two of these sets are steeply dipping and range in thickness from 1-5 cm and a the third set is moderately dipping, closely spaced and are on average less than one cm thick (Fig. 3.8c).

3.1.7 Discussion

The data presented above indicates that the Duke River fault underwent a period of ductile deformation, which was overprinted by phase of brittle deformation. The earliest formed fabric within the siltstone unit (found only within the imbricate zone of the Duke River fault) is defined by the graphite layers and quartz stringers that is interpreted to have formed by pressure solution processes because it appears that the soluble material has been removed via pressure solution processes leaving layers of insoluble carbon and clay. In this case abundant fluids must have percolated through the imbricate zone during movement along the Duke

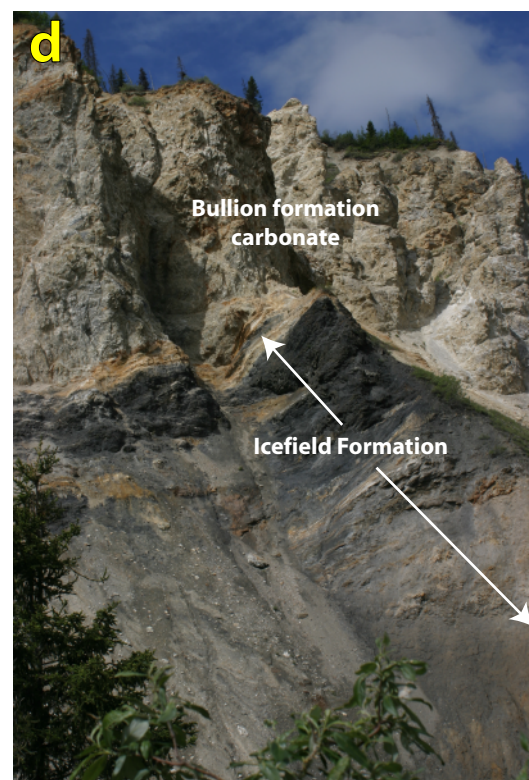


Figure 3.8. Photos of outcrops from the imbricate zone from the Squaw Creek area showing brittle overprinting deformation. a) Cataclastic zone composed of sand and silt sized milled rock and clay that has been deformed into a brittle planar fabric. b) Asymmetric folds that deform the brittle planar fabric in the cataclasite. c) Bullion formation marble cut by three sets of quartz veins. d) Icefield Formation deformed into cataclasite from its contact with the Bullion formation carbonate to the bottom of Squaw Creek canyon.

River fault. The pressure solution foliation has been crenulated to form a pervasive crenulation cleavage. The foliation within the quartz-feldspar-muscovite schist is interpreted to have formed by dislocation creep and dynamically recrystallized quartz. The main through-going foliation, asymmetric folds and associated axial planar cleavage developed within the quartz-feldspar schist are attributed to the early phase of ductile deformation along the Duke River fault. This early phase of Duke River fault deformation overprints the regional foliation and folds developed within the Alexander terrane. The basis for this interpretation is the difference in degree of deformation of intrusive rocks that are found outside the imbricate zone with those mapped within it. The Bullion Formation rocks in the hanging wall outside of the imbricate zone are intruded by a relatively undeformed gabbro that does not show evidence of being deformed by ductile deformation. In outcrop this gabbro body is strongly altered to chlorite and epidote and the degree of deformation ranges from undeformed to development of a closely spaced brittle fracture set. This brittle deformation is in contrast to a foliation developed within actinolite-bearing diorite observed at the footwall /imbricate zone contact of the fault. The foliation within the diorite is characterized actinolite, chlorite and recrystallized quartz.

Elongation lineations defined by elongated calcite and quartz that are found on the dominant foliation planes in the quartz-feldspar-muscovite schist are interpreted to be equivalent to the transport direction of early movements of the Duke River fault. The lineations plunge towards the south-southwest indicating movement along a north-northeast/south-southwest direction. The Duke River fault in its present configuration has older rocks of higher metamorphic grade structurally overlying younger rocks of lower metamorphic grade; therefore, it is here interpreted that the earlier, ductile phase of Duke River fault deformation is associated with thrusting that places the Alexander terrane over Wrangellia towards the north-northeast, along the elongation lineation axis.

In the Squaw Creek canyon there are good exposures of fault gouge that overprint and completely destroy any structures associated with the early ductile phase of deformation. The schistose rocks of the Icefield Formation localize the

brittle deformation and have been deformed into crushed rock and locally fault gouge (Fig. 3.8d).

Late, upper crustal movement along the Duke River fault is accommodated by the softer rocks of the Icefield Formation because these rocks are easily deformed compared to the blocky carbonate of the Bullion formation and the volcanics of the Station Creek Formation. Fracture sets within the Miocene tuffs appear to be associated with movement along the Duke River fault, as these features are not found away from the fault. The brittle features that overprint the imbricate zone suggests that there was a reactivation of the Duke River fault that occurred at shallow levels in the crust, above the brittle-ductile transition following the development of the ductile fabrics.

3.2 Silver Creek

The Silver Creek area lies roughly 130 km along strike to the northwest from the Squaw Creek area (Fig. 3.1). Here the Duke River fault imbricate zone is exposed across a steep sided ridge that runs nearly north-south. The Duke River fault itself, in the Silver Creek area, forms the leading edge of a 2000 metre wide zone of ductile deformation and is marked by the contact between Wrangellia and the Alexander terrane. Within the Duke River fault imbricate zone (zone of ductile deformation) the ductile deformation is overprinted by three moderately dipping brittle thrust faults.

3.2.1 Stratigraphy of Foot Wall

Exposure is very poor on the footwall (Wrangellia) side of the Duke River fault; however, the sparse outcrops in this area comprise black, very fine-grained chert and mudstone interbedded with grey limestone and local beds of fine-grained, green meta-volcanic rock (Fig. 3.9). Exposed to the northwest, is slightly altered and deformed basalt that is in contact with white marble. The age of these rocks is unknown but they are likely part of the Permian Hasen Creek Formation (Fig. 3.9).

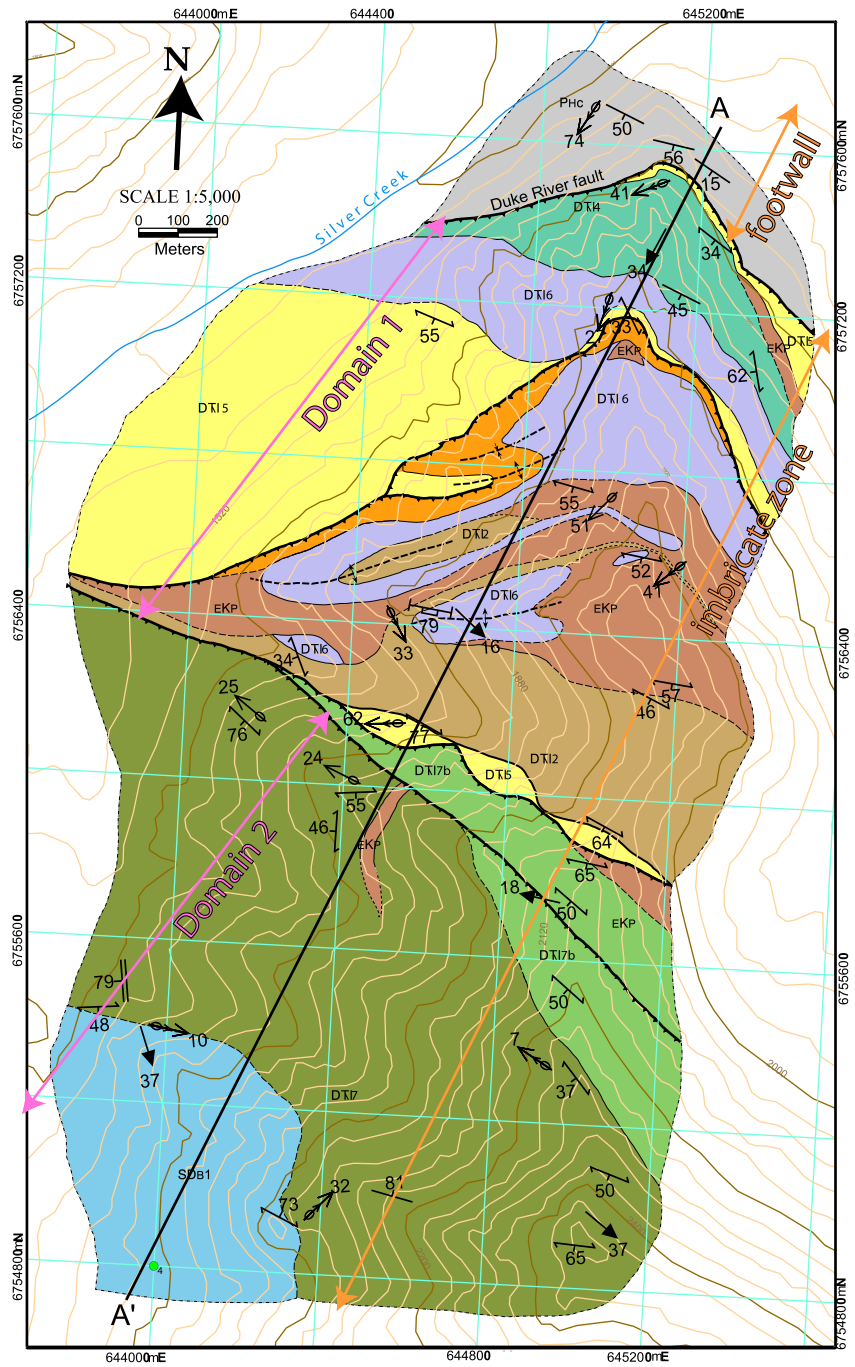


Figure 3.9 Geologic Map of the Duke River fault near Silver Creek.

3.2.2 Stratigraphy of Hanging Wall

The Alexander terrane outside the imbricate zone, near Silver Creek, was not examined during the course of this study due to extremely steep topography and the ice-covered nature of the mountains in this area. The regional map of southwest Yukon indicates that this area is underlain by rocks of the Icefield Formation and Bullion formation. These are intruded by ultramafic rocks of unknown affinity.

3.2.3 Stratigraphy of the Imbricate Zone

Rocks exposed in the imbricate zone of the Duke River fault belong to the Alexander terrane and can be divided into two assemblages. Adjacent to Hasen Creek Formation, gypsum, banded and massive marble, chert and carbonaceous shale are here included within the Icefield Formation (Fig. 3.4, 3.9 & 3.10). These rocks are intruded by hornblende gabbros that are likely part of the late Early Cretaceous Pyroxenite Creek Ultramafic suite (121.0 Ma whole rock $^{40}\text{Ar}/^{39}\text{Ar}$ age, refer to chapter 4).

Up structural section to the south-southwest, an assemblage of variably deformed gypsum, siltstone, conglomerate and volcanoclastic rocks are included within the Icefield Formation on the regional maps but are distinct from the typical description of the Icefield Formation. This assemblage is composed of volcanoclastic rocks that include foliated, green, very fine-grained banded tuff, as well as green, medium-grained, volcanoclastic sandstone, and maroon and green volcanic breccias and conglomerates. Also included within this assemblage is a grey, lithic conglomerate that is dominated by chert and mudstone clasts. Interbedded with the conglomerate is a black, fine-grained siltstone and white gypsum. In this thesis this assemblage and other packages that are grouped with it are assigned to the Silver Creek member of the Icefield Formation. This member has also been intruded by hornblende gabbros. The spatial extent of these gabbroic rocks is much less than in the gabbros observed in rocks structurally below the Silver Creek member described above.

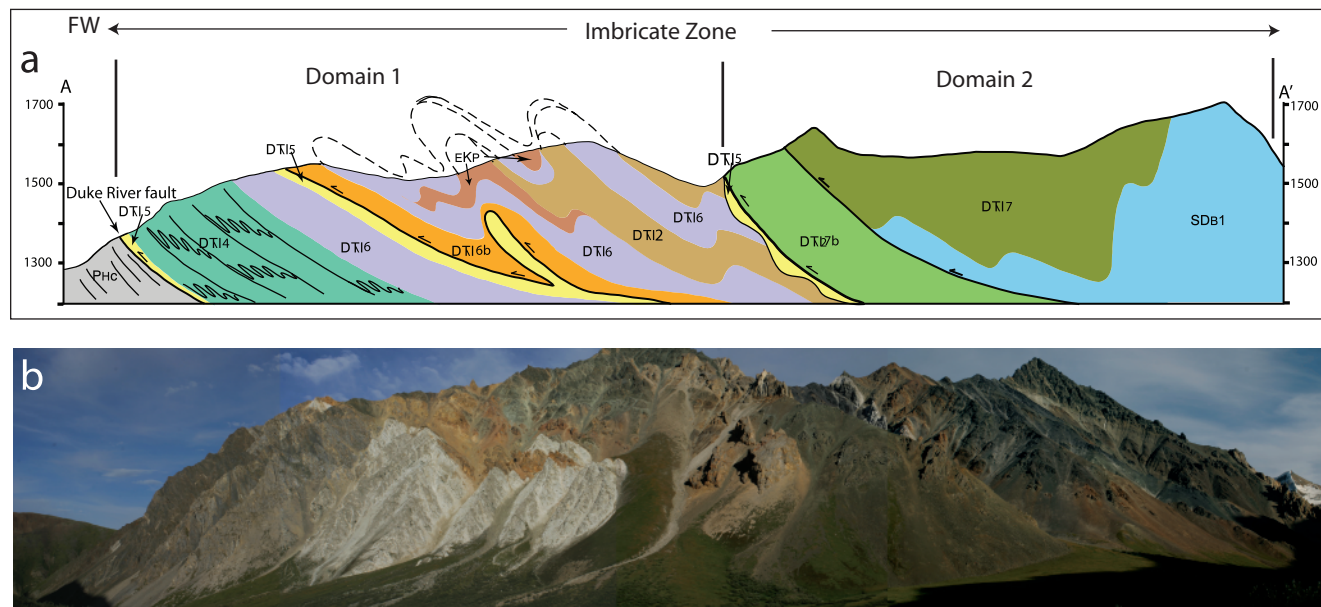


Figure 3.10. Geological cross section A-A' through the Silver Creek area. See figure 3.9 for location.

3.2.4 Structure of Foot Wall

Within the Hasen Creek Formation, bedding dips to the southwest (3.11a).

3.2.5 Structure of Hanging Wall

The regional map of the southwest Yukon for the area outside the imbricate zone at Silver Creek shows northwest-southeast trending faults that bound lithological units within the Alexander terrane. Regional scale, northwest-southwest trending folds are also present (Campbell and Dodds, 1991; Gordey and Makepeace, 2001).

3.2.6 Structure of the Imbricate Zone

The imbricate zone near Silver Creek is divided into two separate structural domains that coincide with the boundary between the Icefield Formation and the Silver Creek member. The structural domains are separated from each other by south-dipping faults that are localized within gypsum units and generally parallel the main foliation within the Duke River fault imbricate zone (Fig. 3.10).

The first domain (Domain 1) includes marble, gypsum, chert and siltstone that sit adjacent to Wrangellia but within the Duke River fault imbricate zone (separated from Wrangellia by the Duke River fault itself). Foliations within these rocks consistently strike $\sim 115^\circ$ and dip 42° SW (Fig. 3.11b). In addition, locally two phases of folding can be seen in the rocks in Domain 1. The two phases are well preserved in an outcrop of chert where small, early folds are preserved between foliation planes that are subsequently deformed by open to tight folds (Fig. 3.12a,b). This later phase of folding is manifest into tight to isoclinal folds in the marble and gypsum unit. The earlier phase of folding is rarely preserved in the gypsum and marble. Gabbro bodies appear to be caught up in the isoclinal folding event but locally do not appear to be foliated.

The main foliation within Domain 1 is sub parallel to the Duke River fault and strikes approximately 115° and dip moderately to the south. Elongation lineations on the main foliation plane plunge moderately towards 252° and are defined by

a) Footwall

■ Poles to bedding

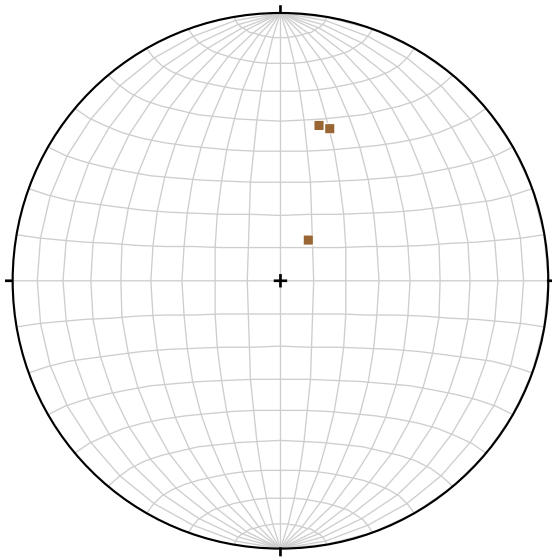
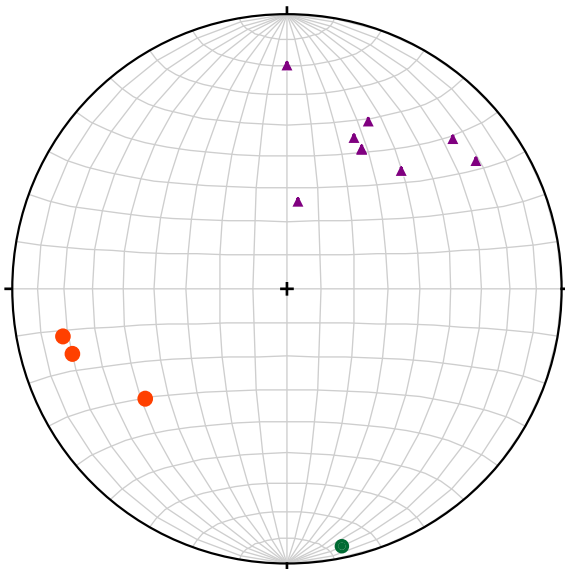


Figure 3.11 Structural data from the Silver Creek area presented on equal area, lower hemisphere stereonets. a) Brown circles are poles to bedding taken in the footwall of the Duke River fault in the Hasen Creek Formation. b) Purple triangles are poles to ductile foliations from within structural domain 1 of the imbricate zone. The green circles are elongation lineations and the red circle is a crenulation lineation from the Duke River fault. c) Blue squares are poles to ductile foliations within structural domain 2 of the imbricate zone. Green squares are poles to brittle foliations. Red stars are fold axes from asymmetric, kink-style folds.

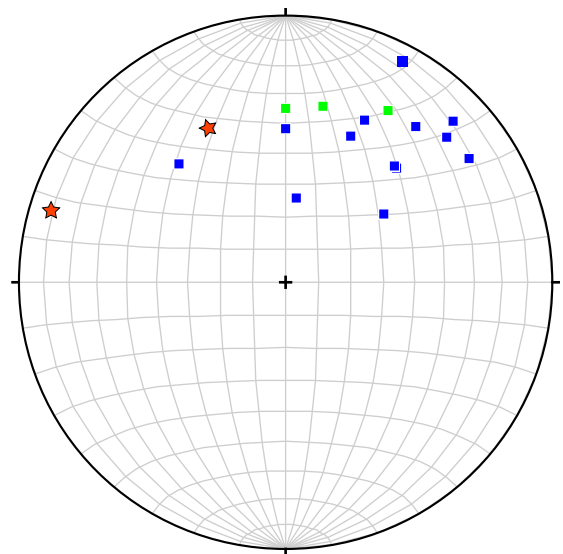
b) Imbricate Zone - Domain 1

▲ Poles to ductile foliations
● Crenulation lineation
● Stretching lineations



a) Imbricate Zone - Domain 2

■ Poles to ductile foliations
■ Poles to brittle foliations
★ Fold axes of kink-style folds



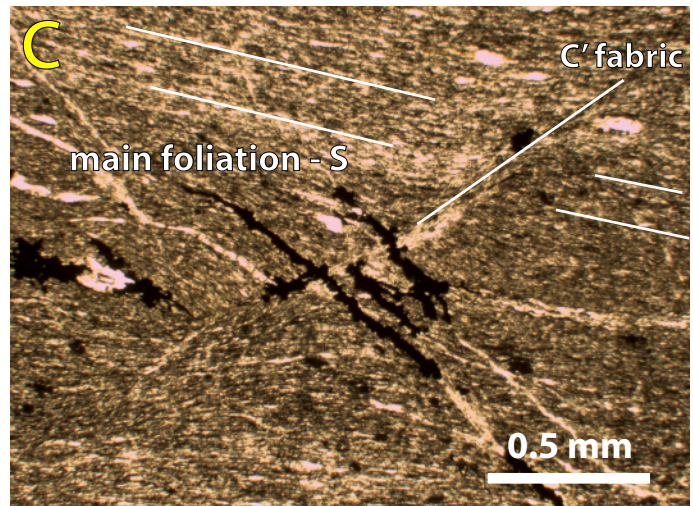


Figure 3.12. a) Early folds preserved within a layer of chert in structural domain 1 near Silver Creek area. White lines parallel early fold hinges. b) Openly folded cherts in structural domain 1 near Silver Creek. The open folds re-fold the folds in photograph 3.12a. c) Shear band (C'-S fabric) in fine-grained limestone found along the Duke River fault. d) Brecciated marble found along a thrust fault that dissects the Icefield Formation (structural domain 1).

elongate calcite crystals (Fig. 3.11b). This elongation direction was confirmed by a second thin section that was cut at an angle of 50° from the elongation lineation in question and perpendicular to the main foliation. The thin section cut parallel to the elongation lineation shows elongated calcite crystals (when compared to calcite crystals in the second thin section) and dextral shear bands (Fig. 3.12c). A thin layer of gypsum that separates crenulated marble of the Icefield Formation from Hasen Creek Formation rocks delineates the Duke River fault. The crenulations in the marble plunge very shallowly towards 168° (Fig. 3.11b). .

Sub-parallel to the Duke River fault, within Domain 1, the Icefield Formation rocks are dissected by a thrust fault that is defined by a folded gypsum unit of variable thickness that is in contact with a massive marble (Fig. 3.10). The marble is brecciated along its contact with the gypsum (Fig. 3.12d) and weathers a bright orange, which makes the fault easy to delineate in this area (Fig. 3.10).

Domain 2 is characterized by structures observed within the Silver Creek member, located structurally above Domain 1. Within Domain 2, a well-developed foliation strikes 110 – 135 degrees and dips moderately to the southwest and is best defined by flattened clasts within conglomerate (3.13a). No lineation was observed within Domain 2, and thin sections cut perpendicular to the main foliation do not show any evidence for stretching or asymmetric deformation fabrics. Within the volcanoclastic units, the foliation is defined by dynamically recrystallized quartz and chlorite.

The lower boundary of Domain 2 is a steeply, south-southwest dipping fault that places the Silver Creek member over rocks of the Icefield Formation (Fig. 3.9; 3.10). A gypsum layer found at this structural boundary is boudinaged on a scale of tens of meters. Juxtaposed against the boudinaged gypsum is a section of highly fractured to brecciated siltstone that is approximately 10 m wide. In addition, a foliation that is characterized by closely spaced brittle fractures overprints the earlier formed ductile foliation in the volcanoclastic units within Domain 2. This later foliation strikes easterly and dips moderately to the south (Fig. 3.11c). Asymmetric kink-style folds that have hinges that plunge steeply towards 330° deform the earlier foliation in the lithic conglomerate (Fig. 3.11c & 3.13b)



Figure 3.13 a) Conglomerate that has been assigned to the Silver Creek member of the Icefield Formation that has flattened clasts that define the ductile deformation. b) Kink-style folds overprint the ductile deformation defined by the flattened clasts in photo 3.13a.

3.2.7 Discussion

Isoclinal folds within structural Domain 1 in marble and gypsum and open folds within chert are interpreted to have formed during early movement along the Duke River fault. These early formed fabrics overprint regional deformation of the Alexander terrane. The long limbs of isoclinal folds are parallel to the Duke River fault suggesting they were formed within the imbricate zone during faulting. The folds are orientated in a favourable way to accommodate shortening within the imbricate zone. The variable deformed gabbro bodies within Domain 1 are interpreted to have intruded into the Duke River fault imbricate zone during movement along the Duke River fault and were subsequently folded by the movement. The elongation lineations observed within Domain 1 are interpreted to indicate the transport direction (i.e. northeast/southwest). The dextral shear bands that are seen in the thin section cut parallel to the elongation lineation indicate northeast directed thrusting of the Alexander over Wrangellia.

Within Domain 2 foliation is characterized by recrystallized quartz and chlorite and flattened clasts of mudstone and chert that is interpreted to be associated with movement along the Duke River fault. Foliation planes within these units are sub-parallel to the thrust faults within the imbricate zone and are the basis for this interpretation.

Within the Duke River fault imbricate zone, in the Silver Creek area, brittle deformation overprints the ductile fabrics. Brecciated marble found along a thrust fault within the imbricate zone indicates movement along the fault above the brittle-ductile transition. The thrust fault that separates Domain 1 from Domain 2, within the imbricate zone, is defined by boudinaged gypsum that parallels a 10 meter wide fault breccia zone that overprints the ductile foliation developed within the Silver Creek member of the Icefield Formation. This fault breccia is interpreted to have formed during reactivation of ductile faults within the Duke River fault imbricate zone.

3.3 Jessie Creek

The Jessie Creek map area lies a few kilometres to the northwest of Silver Creek (Fig. 3.1). At Jessie Creek, the Duke River fault imbricate zone is exposed in a narrow valley between steep-sided mountains of the Kluane Ranges (Fig. 3.14). In this area, the Duke River fault is the leading edge of deformation of an approximately 1500 metre wide zone of deformation (imbricate zone). Overprinting the ductile deformation at the leading edge of the imbricate zone is a brittle, steeply south-dipping reverse fault.

3.3.1 Stratigraphy of the Foot Wall

The footwall of the Duke River fault in the Jessie Creek area consists of rocks belonging to Wrangellia. These include dark grey to black siltstone and brown sandstone of the Permian Hasen Creek Formation unconformably overlain by light grey, thinly bedded carbonate of the Chitistone limestone.

3.3.2 Stratigraphy of the Hanging Wall

The hanging wall of the Duke River fault, includes grey, banded limestone interlayered with fine to medium-grained, dark green mafic volcanic rock composed of plagioclase, actinolite (that has been partly altered to chlorite), pyroxene and epidote (Fig. 3.14). These rocks are assigned to the Donjek Formation based on an Ordovician fossil age and the presence of the mafic volcanic rocks.

3.3.3 Stratigraphy of the Imbricate Zone

Within the imbricate zone, the rocks of the Alexander terrane consist of two distinct assemblages. The first assemblage forms the direct hanging wall to the Duke River fault (boundary between Wrangellia and Alexander terrane) and consists of Triassic (Campbell and Dodds; 1990) calcareous siltstone interbedded with ribbon chert and foliated, maroon and green volcanic conglomerate (Fig. 3.15a). Similar to the Bullion Creek area, this assemblage of rock is included in the Silver Creek member of the Icefield Formation. Rare exposures of fossiliferous

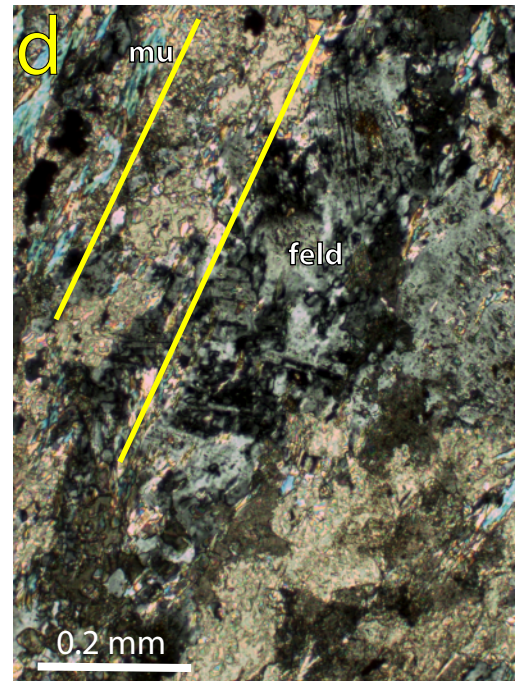
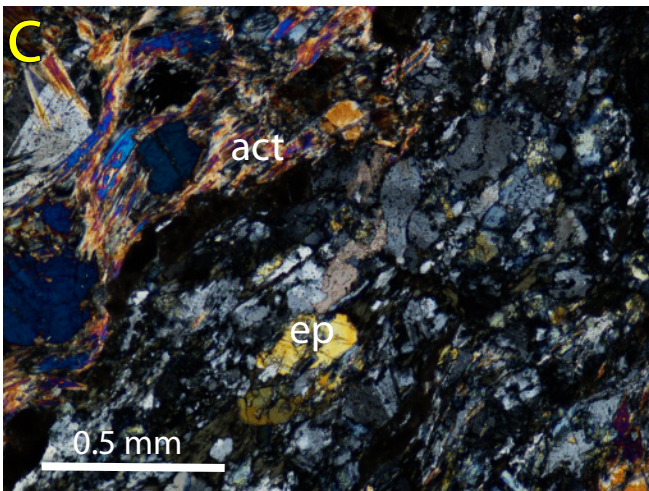


Figure 3.15. Photos from outcrops and thin section near Jessie Creek. a) Bedding within ribbon chert found within the Silver Creek member at Jessie Creek. b) Folded muscovite-bearing chert within domain 2 of the imbricate zone. c) Greenschist facies mineral assemblage from a gabbro that intrudes domain 1 rocks within the imbricate zone. Note the epidote (ep) and actinolite (act). d) Photo micro-graph of deformed, calcite altered ultramafic rock that intrudes domain 2 of the imbricate zone. Foliation planes (yellow lines) are defined by muscovite (mu) grains aligned between dynamically re-crystallized feldspar (feld).

carbonate are included in this package. The whole assemblage is intruded by gabbro and pyroxenite of probable Early Cretaceous age (Fig. 3.14).

A second assemblage of Alexander terrane rocks structurally overlies the Silver Creek member and consists of quartz-feldspar-chlorite phyllonite to schist, calcareous to carbonaceous, feldspar-muscovite-quartz schist (104.1 Ma muscovite $^{40}\text{Ar}/^{39}\text{Ar}$ age, refer to chapter 4), banded and massive marble and locally muscovite-bearing quartzite (Fig. 3.15b). These rocks have been assigned to the Icefield Formation proper and are intruded by hornblende-epidote gabbros and ultramafic rocks of probable Early Cretaceous age. Detailed examination of thin sections cut from the gabbro shows a plagioclase, hornblende, actinolite and epidote mineral assemblage (Fig. 3.15c).

3.3.4 Structure of the Foot Wall

The Chitistone limestone and Hasen Creek sedimentary rocks are tightly folded into east-plunging antiform within the Jessie Creek area (Fig. 3.4, 3.14 & 3.16). An unconformity between the Permian Hasen Creek the Upper Triassic Chitistone limestone may indicate the presence of a fault; however, this contact was not exposed. Normally flood basalts of the Nikolai Formation sit between the Hasen Creek Formation and the Chitistone limestone.

3.3.5 Structure of the Hanging Wall

As at Silver Creek, steep topography made examination of the structures within the hanging wall impossible. The regional map for the area outside the imbricate zone at Jessie Creek shows northwest-southeast trending faults that bound lithological units within the Alexander terrane (Campbell and Dodds, 1991). Regional scale, northwest-southwest trending folds are also shown deforming rocks of the Jessie Creek area.

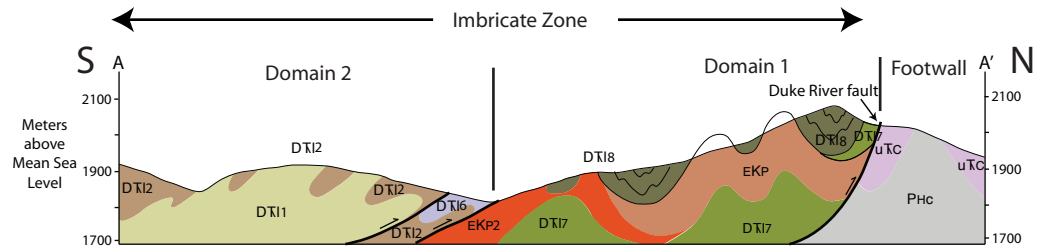


Figure 3.16. Geologic cross section A-A' of the Duke River fault in Jessie Creek map area. See figure 3.14 for location.

3.3.6 Structure of Imbricate Zone

The imbricate zone near Jessie Creek is separated into two structural domains that coincide with the two members of the Icefield Formation described in the hanging wall stratigraphy section above. The structural domains are separated from each other by a moderate, south-dipping fault (Fig. 3.16).

Domain 1 characterizes structures within chert, siltstone and conglomerate of the Silver Creek Icefield Formation. Ductile foliations within these rocks are best displayed in the conglomerates as flattened clasts and generally dip moderately to steeply northwest and southeast (Fig. 3.17a). The foliation is not observed in the chert; however, bedding in the chert has the same orientation as the foliation. The early phase foliation is tightly folded by west-southwest plunging folds that are subsequently deformed by a later phase of open, northwest plunging folds (Fig. 3.17a). Dome and basin fold interference patterns are developed where the hinges of these two folds intersect.

Domain 2 characterizes structures within schist, marble and quartzite of the Icefield Formation (Fig 3.16). Early stage ductile deformation is defined by a foliation characterized by planes of muscovite between dominantly dynamically recrystallized quartz in schist and quartzite and by muscovite grains and dynamically recrystallized feldspar in a deformed ultramafic rock (Fig. 3.15d). This foliation is the main layering seen in the marble. The early phase foliation strikes mainly to the east-southeast and dips moderately to the south and is deformed by shallow to moderately east-plunging tight to isoclinal folds (Fig. 3.17b). Within the long limb of the isoclinal folds, rarely preserved rootless isoclinal folds are evidence of an earlier phase of folding. A later, steeply plunging phase of folding, very openly deforms the isoclinal folds (Fig. 3.17b).

Overprinting the ductile structures described above is a broad zone composed of closely spaced fracture sets with discrete fault gouge zones within it. This zone separates structural Domain 1 from Domain 2. The volcanic conglomerate and the siltstone are both deformed into separate gouge zones composed of sub-rounded, pebble-sized clasts of siltstone and volcanic material in a clay matrix. Both

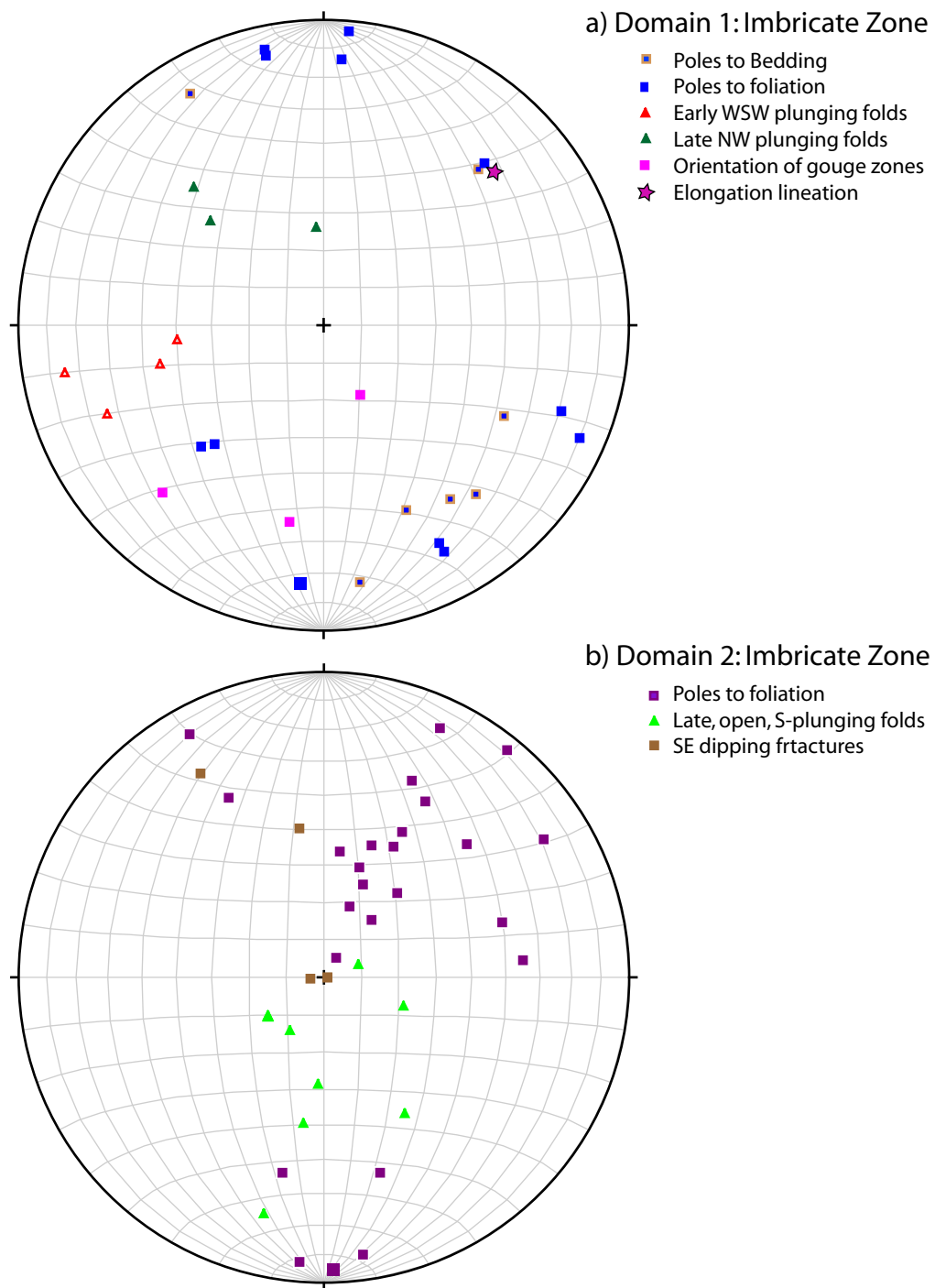


Figure 3.17 Structural data from the Jessie Creek area presented in equal area, lower hemisphere projection stereonet. a) Blue squares are poles to bedding in chert and poles to foliation in siltstone within domain 1 of the imbricate zone. Pink squares are poles to the strike and dip of gouge zones that separate domain 1 from domain 2. Red triangles are early, tight fold axes that fold the bedding and foliation. Dark green triangles are late, open, fold axes that deforms the early folds. b) Purple squares are poles to the dominant foliation within domain 2 of the imbricate zone. Brown squares are poles to fractures. Green triangles are fold axes from tight to isoclinal folds that deform the dominant foliation.

the gouge zones dip moderately steeply to the north and northeast (Fig. 3.17a) and are each approximately 1 meter wide. The fractures generally strike southeast and dip moderately to the southwest (Fig. 3.17b).

3.3.7 Discussion

Early phase foliation development within the schist and quartzite of Domain 1 is interpreted to be ductile in nature and formed by dislocation creep and dynamically recrystallized quartz. The development of the early foliation and the tight to isoclinal folds are interpreted to be a result of early stage movement along the Duke River fault. This deformation overprints regional deformation of the Alexander terrane, exhibited by the local preservation of rootless isoclinal folds between foliation planes. Ultramafic bodies that intrude schist within Domain 1 have developed a fabric defined by muscovite and dynamically recrystallized feldspar. Feldspar undergoes this type of deformation in the range 450 degrees (Price and Cosgrove, 1990) suggesting these bodies were deformed at this temperature and have undergone 10's of kilometres of uplift along the Duke River fault.

Within the Jessie Creek area brittle deformation overprints the early stage ductile fabrics. Gouge zones composed of fault breccia and clay overprint the ductile foliation developed within Domain 2 and are interpreted to be thrust faults that have been reactivated at higher levels in the crust. This indicates that the Duke River fault was reactivated at some time after the development of the early stage ductile deformation.

The overall orientation of the stratigraphy within the Duke River fault imbricate zone has implications for the amount of movement that has occurred along the Duke River fault. In the Silver Creek area the Silver Creek member is situated structurally above the Icefield Formation. This is in contrast to the Jessie Creek area where the Icefield Formation sits structurally above the Silver Creek member. One interpretation for this configuration is that significant shortening within the Duke River fault imbricate zone has stacked the Icefield Formation and

Silver Creek member stratigraphic package and erosion has exposed the current configuration.

3.4 Bullion Creek

The Duke River fault is exposed along the west side of Red Castle Ridge near Bullion Creek, near the south end of Kluane Lake and 15 km northwest of Jessie Creek (Fig. 3.18). In the Bullion Creek area, the Duke River fault is the leading edge of deformation within an imbricate zone that is at least 1500 metres wide. The imbricate zone is characterized by a broad zone of ductile deformation that is overprinted by discrete brittle, west dipping thrust faults with hanging walls comprised of openly folded silty marble and footwalls characterized by multiply folded schist.

3.4.1 Stratigraphy of Foot Wall

Dark green, locally amygdaloidal and rarely pillowed basalt of the Upper Triassic Nikolai Formation sits stratigraphically below light grey, banded limestone that belongs to the Upper Triassic Chitistone Limestone. In the south end of the map area a white gypsum unit crops out stratigraphically beneath the limestone and is interpreted to be a lower, discontinuous unit within the Chitistone limestone. The topographically highest points of Red Castle Ridge comprise reddish brown weathered, dark brown fresh, fine-grained basalt of the Miocene Wrangell volcanics. Ultramafic (pyroxenite) intrusives that grade into gabbro crop out in the northern part of the map area and have tentatively been assigned to the Kluane mafic-ultramafic complex (Fig. 3.18).

3.4.2 Stratigraphy of Hanging Wall

The Alexander terrane outside the imbricate zone, near Silver Creek, was not examined during the course of this study due to extremely steep topography and the ice-covered nature of the mountains. The regional map of southwest Yukon shows

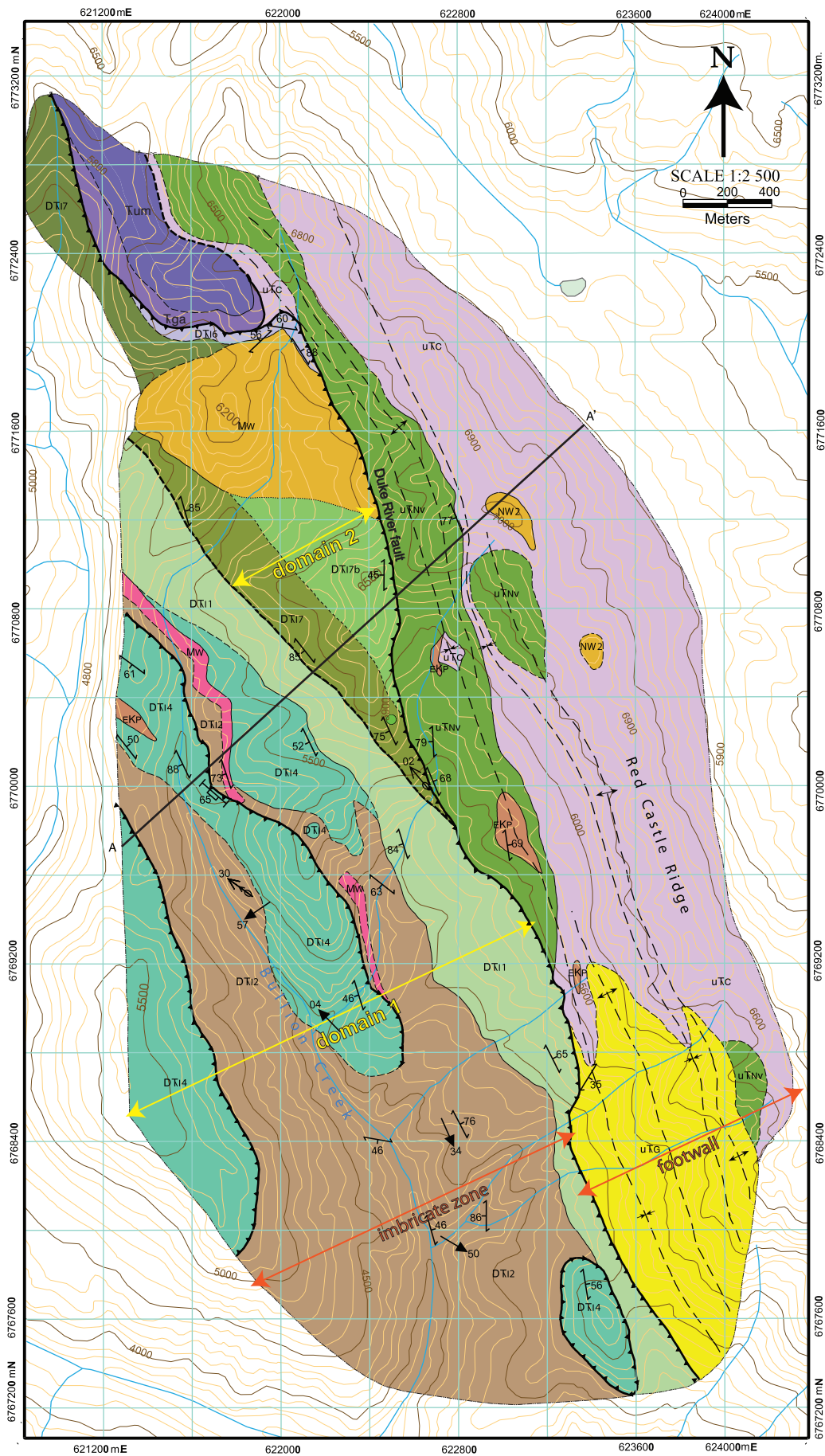


Figure 3.18
Geologic
map of the
Duke River
fault near
Bullion

the Icefield Formation and Bullion formation exposed in this area (Gordey and Makepeace, 2001).

3.4.3 Stratigraphy of the Imbricate Zone

The Alexander terrane rocks that comprise the imbricate zone of the Duke River fault near Bullion Creek and includes carbonaceous and calcareous, quartz-muscovite schist; calcareous, muscovite-feldspar-quartz schist and a calcareous, banded silty marble. This assemblage of rocks look similar to the Icefield Formation rocks mapped near Squaw Creek. These rocks are intruded by a series of quartz-feldspar porphyry dikes and small plutons that are interpreted as being part of the Miocene Wrangell Suite.

An assemblage of deformed green and maroon volcanic conglomerate that grade into volcanoclastic sandstone and then into fossiliferous, lithic sandstone and very fine-grained quartz and feldspar rich sandstone crops out between Wrangellian stratigraphy and the Icefield Formation (Fig. 3.18). This assemblage of rocks has been assigned to the Silver Creek member of the Icefield Formation based on its similarities to rocks mapped near Silver Creek (DTrl7). In the north central part of the map area a quartz-feldspar porphyritic tuff that has been assigned to the Miocene Wrangell volcanics unconformably overlies the Silver Creek member of the Icefield Formation.

3.4.4 Structure of the Foot Wall

The limestone, gypsum and basalt found within the Wrangellian footwall are openly to tightly folded into a series of upright antiforms and synforms that trend north-northwest (Fig. 3.18, 3.19 & 3.20a). The mafic-ultramafic body found in the hangingwall is in fault contact with the Chitistone limestone to the east and with the Icefield Formation to the west, along the Duke River fault (Fig. 3.18).

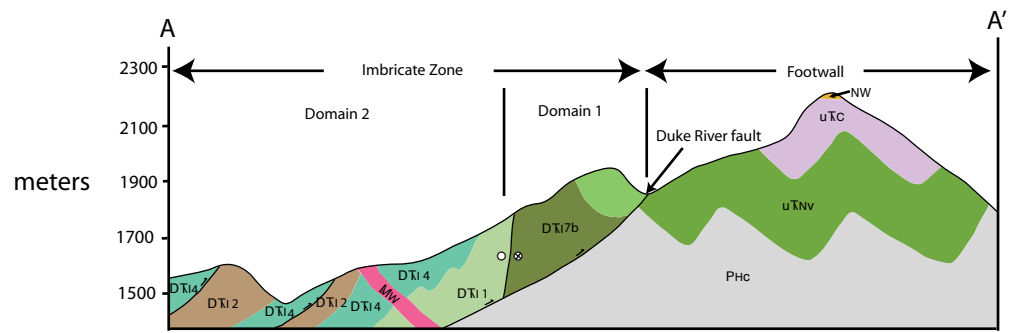


Figure 3.19 Geologic cross section A-A' of the Bullion Creek map area.

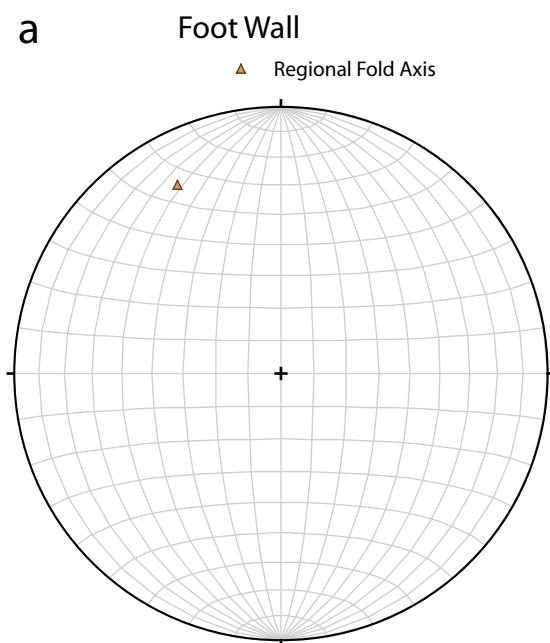
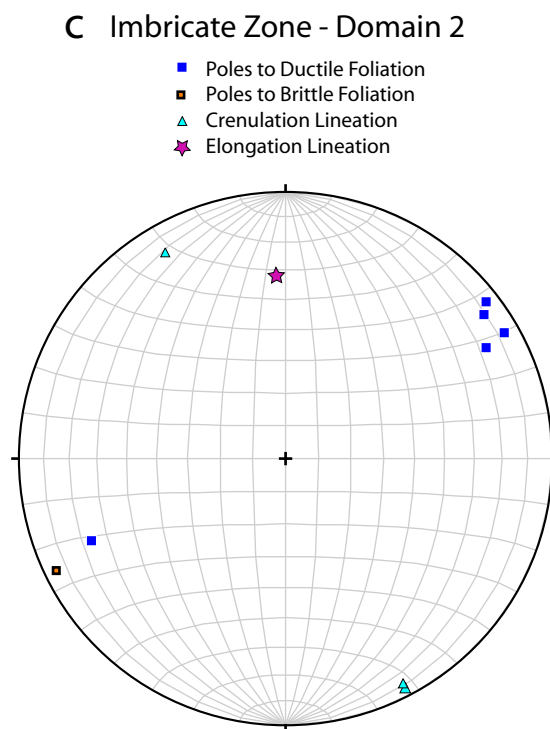
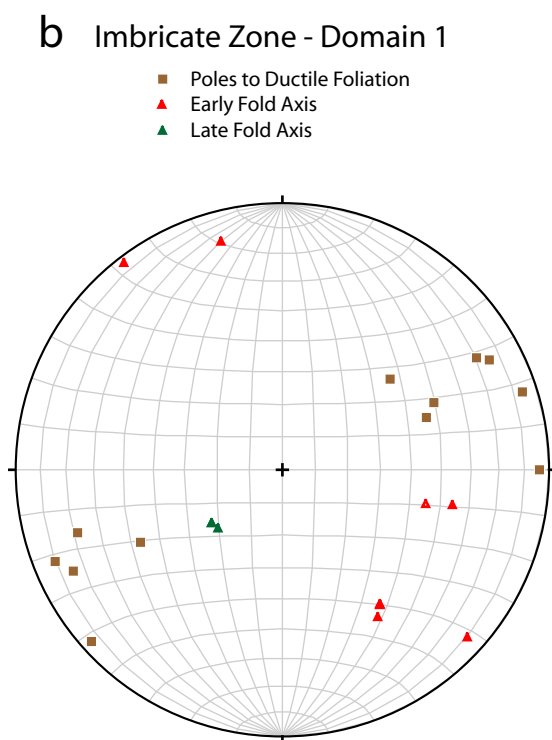


Figure 3.20. Structural Data from the Bullion Creek area presented on equal area, lower hemisphere stereonets. a) Brown triangle is the approximate orientation of the regional folds that deform the Upper Triassic rocks of Wrangellia that sit in the foot wall of the Duke River fault. b) Brown squares are poles to ductile foliations within domain 1 within the imbricate zone. Red triangles are fold axes of early, tight folds within domain 1. Green triangles are late, open fold axes that re-fold the tight folds. c) Blue squares are poles to ductile foliations within domain 2 within the imbricate zone. The yellow square is a pole to brittle foliation that occurs within a subsidiary fault within domain 2 of the imbricate zone. Light blue triangles are crenulation lineations within domain 2 of the imbricate zone. The pink star is an elongation lineation found near the Duke River fault and within domain 2 of the imbricate zone.



3.4.5 Structure of the Hanging Wall

The hanging wall rocks outside the imbricate zone were not examined during the course of this study. The regional map indicates that the Icefield Formation is in fault contact with the Bullion formation. Locally, the Bullion formation is folded into an overturned antiform (compilation map).

3.4.6 Structure of the Imbricate Zone

Within the imbricate zone the structure is split into two domains (similar to other areas along the Duke River fault) that coincide with the Icefield Formation (Domain 1) and the Silver Creek member of the Icefield Formation (Domain 2). The dominant fabric within Domain 1 is a ductile foliation that is defined by planes of muscovite between recrystallized quartz and feldspar grains (Fig. 3.21a). This foliation strikes generally south-southeast, dips between 45 and 80 degrees to the west-southwest and is tightly folded by folds that plunge shallowly to moderately to the southeast and northwest (Fig. 3.20b & 3.21b). A crenulation of the schist within Domain 1 is observed locally and only deformed micaceous layers within the schist. This lineation associated with the crenulation appears to be folded by the southwest to northeast plunging tight folds. The tight folds themselves are re-folded by a set of open folds that plunge moderately to steeply to the southwest (Fig. 3.20b).

Within Domain 2 a ductile foliation that is defined by flattened clasts within the green and maroon conglomerate strikes south-southeast and dips steeply to moderately to the southwest (Fig. 3.20c & 3.21c). The leading edge of the Duke River fault imbricate zone truncates this unit in the center of the map area (Fig. 3.18).

Overprinting the ductile deformation within Domain 1 are discrete brittle fault planes characterized by fault gouge composed of sub-angular, pebble-sized rock fragments in a silty matrix. The gouge zones sit directly underneath intact sections of silty marble (Fig. 3.19). These fault planes dip moderately to the south-southwest. The contact between domain 1 and 2 is a brittle fault that has a steep dip, strikes northwest and has a cataclastic zone up to 1.5 m wide (Fig 3.20c). The

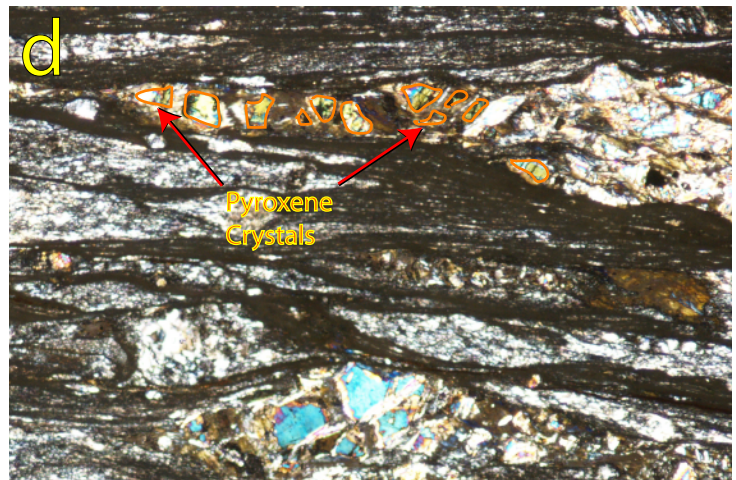
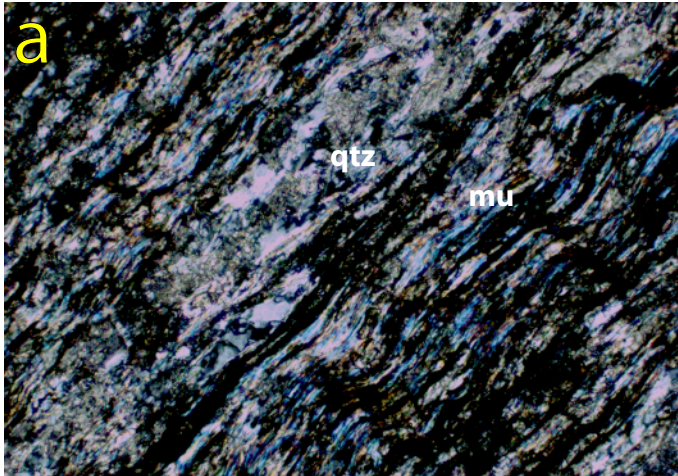


Figure 3.21. Photographs and micro-photographs from Bullion Creek. a) Ductile foliations defined by planes of muscovite between-bands of recrystallized quartz.b) Tight folds that deform the ductile deformation within Domain 1. White lines follow foliation plane. c) Ductile foliation within Domain 2 defined by flattened clasts in a conglomerate. White line shows-foliation plane. d) Pulled apart pyroxene crystals in a deformed volcanic rock found near the contact between domain 2 rocks and Wrangellia.

southern most extent of this structure deforms pyroxene-bearing basalt. A mineral lineation made up of stretched pyroxene grains within the basalt, trends towards the north-northwest with a shallow plunge. Examination of a thin section of this basalt; cut parallel to the lineation shows the pyroxene crystals that have been pulled apart along the trend of this lineation (Fig. 3.21d). Shear bands in outcrop, coupled with a near horizontal stretching lineation that trends northward (Fig. 3.20c), suggest a dextral strike slip motion across this subsidiary fault. The Duke River fault is interpreted to truncate the dextral strike slip fault because this fault cannot be traced into the south part of the map sheet.

In the north central part of the map area the Miocene crystal tuff is deformed along its contact with Nikolai basalts into fault gouge composed of dominantly clay with some sub-rounded quartz grains.

3.4.7 Discussion

Similar to both Silver Creek and Jessie Creek, in the Bullion Creek area the ductile foliation and the tight to isoclinal folding of this foliation are interpreted to be a result of early movement along the Duke River fault. This is based mainly on the similarities between the structures within the imbricate zone at Bullion Creek and those at Jessie Creek. In the Bullion Creek area, similar to Silver Creek and Jessie Creek the Alexander terrane stratigraphy, making up the imbricate zone, has been compressed between Wrangellia and the more distal rocks of the Alexander terrane. Shortening in these rocks was accommodated by folding and thrusting of the Icefield Formation rocks, specifically with competent silty marble units that have been thrust over softer schistose rocks of the Icefield Formation as shown in Figure 3.19. During this process the softer rocks of the footwalls to these discrete thrust faults have been crenulated and folded and the hanging wall is openly folded silty marble.

Later reactivation of the faults at a higher level in the crust formed discrete fault planes composed of fault gouge and cohesionless fault breccia. It has been

interpreted that this later movement also deformed the porphyritic crystal tuff into milled quartz clasts and clay gouge.

Evidence for strike slip faulting in this area includes a steeply dipping gouge zone coupled with nearly horizontal crenulation lineations and deformed basalt that has a shallowly dipping elongation lineation and dextral shear bands. Based on the brittle nature of the gouge zone, the strike slip fault probably occurred after the early ductile event but before the latest thrusting along the Duke River fault because it appears that the Duke River fault truncates the strike slip fault. The main piece of evidence for the truncation is that the steeply dipping gouge zone disappears in the southern part of the map sheet a short distance away from where this fault meets the Duke River fault itself (the leading edge of deformation within the imbricate zone).

3.5 Hoge Creek

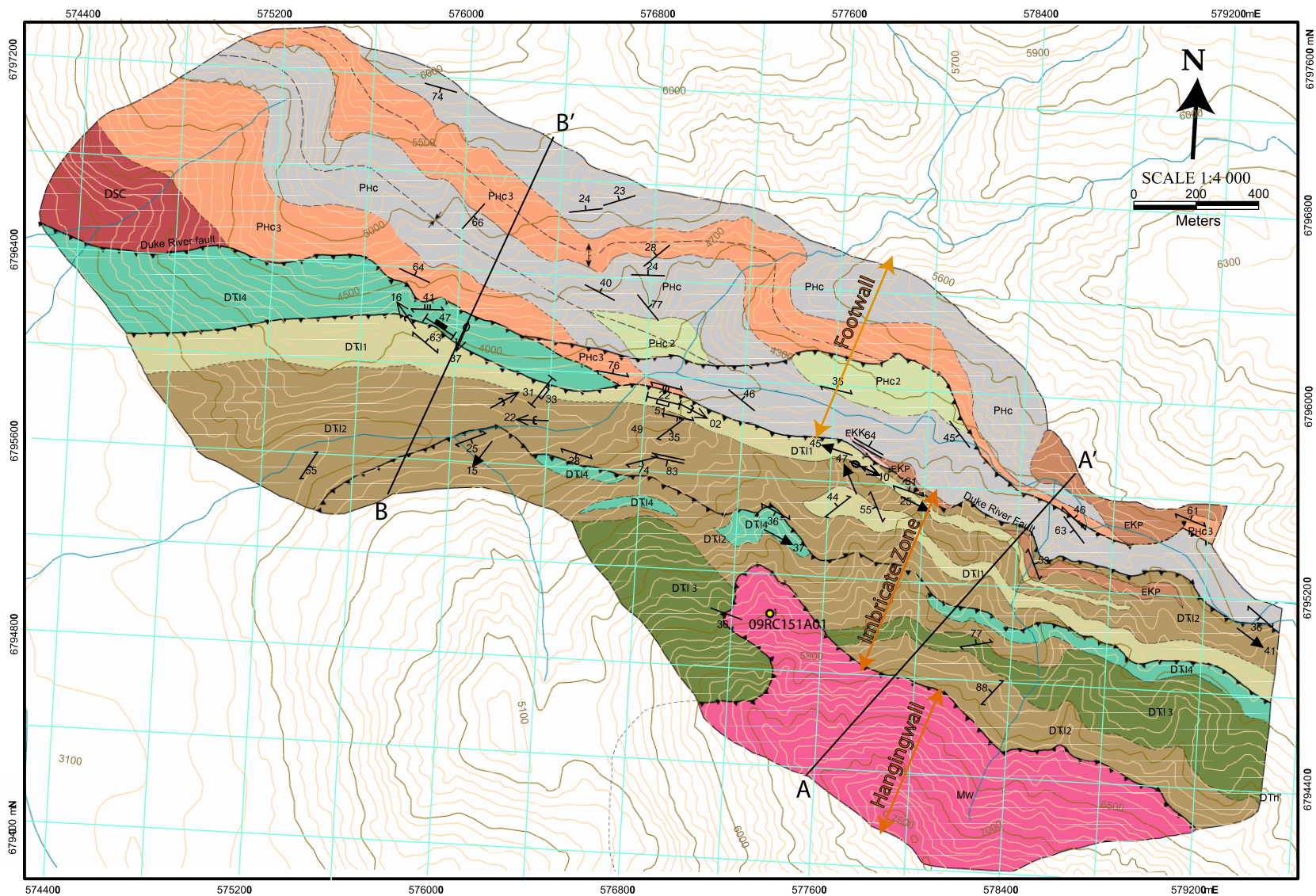
Approximately 45 km to the northwest of the Bullion Creek area, the Duke River fault is very well exposed in a steep valley occupied by Hoge Creek (Fig. 3.1). Between Bullion Creek and Hoge Creek, the Duke River fault has been interpreted to be covered by the Wrangell volcanics in some areas, and in other areas to cross cut the volcanics (Campbell and Dodds; 1990; Israel, 2004).

In the Hoge Creek area, the Duke River fault is the leading edge of a one kilometre wide imbricate zone of deformation that is bound to the south by a pluton assigned to the Wrangell suite and to the north by conglomerates of the Hasen Creek Formation (Fig. 3.22). Deformation within the imbricate zone is characterized by an early stage of ductile deformation, overprinted by discrete, brittle southwest dipping thrust faults.

3.5.1 Stratigraphy of Foot Wall

The footwall of the Duke River fault in the Hoge creek area is characterized by Wrangellia. The lowermost exposed part of Wrangellia in this area is a highly deformed gabbro that is only observed in the far western part of the map. This

Figure 3.22 Geologic Map of the Duke River fault near Hoge Creek.



gabbro is interpreted to be Devonian in age based on correlations with similar gabbro bodies that have been dated across the Donjek River from Hoge Creek (S. Israel pers. Comm. 2011). In the hangingwall of the Duke River fault in the Hoge Creek area, the gabbro is unconformably overlain by a cobble to boulder conglomerate of the Permian Hasen Creek Formation (Fig. 3.23a). The boulder conglomerate grades upward into a volcanic breccia that contains clasts up to one-centimetre in diameter in a sandy maroon matrix. This breccia grades upwards into a pebble conglomerate, then into a lithic sandstone, into a fossiliferous wackestone, and finally into a banded to massive marble (Fig. 3.24).

3.5.2 Stratigraphy of Hanging Wall

The Hanging wall of the Duke River fault is composed of beige, medium-grained hornblende-biotite diorite of the Miocene Wrangell suite (16 Ma U-Pb zircon age, refer to chapter 4). This diorite body is shown on regional maps to intrude the Icefield Formation; however, this relationship was not observed during this study (Campbell and Dodds, 1991).

3.5.3 Stratigraphy of the Imbricate Zone

All of the rocks within the imbricate zone are interpreted to belong to the Icefield Formation. The Icefield Formation in the Hoge Creek area is composed of massive, strongly deformed marble, very fine-grained mylonitic sandstone characterized by recrystallized feldspar and quartz that is interleaved with dark grey calcareous siltstone/shale, carbonaceous, calcareous, muscovite-feldspar-quartz schist and a grey, banded marble. Near the south end of the imbricate zone a section of volcanic breccia and plagioclase-phyric basalt flows is structurally sandwiched between sections of siltstone (Fig. 3.24).

3.5.4 Structure of the Foot Wall

The Devonian gabbro and Hasen Creek Formation rocks are deformed by upright, tight folds with hinges oriented northwest/southeast (Fig. 3.22). These

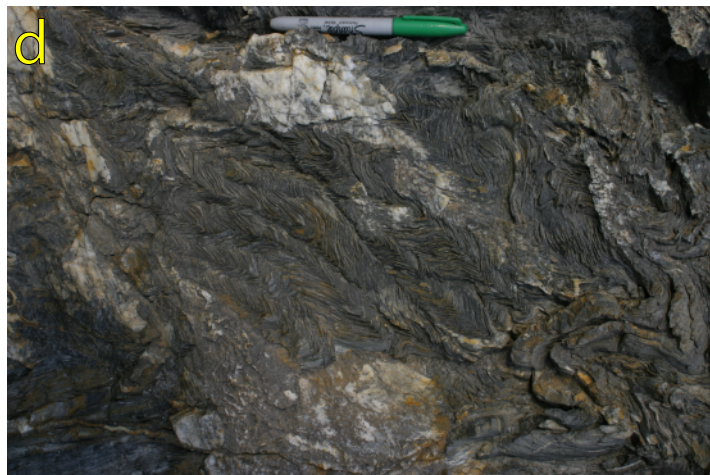
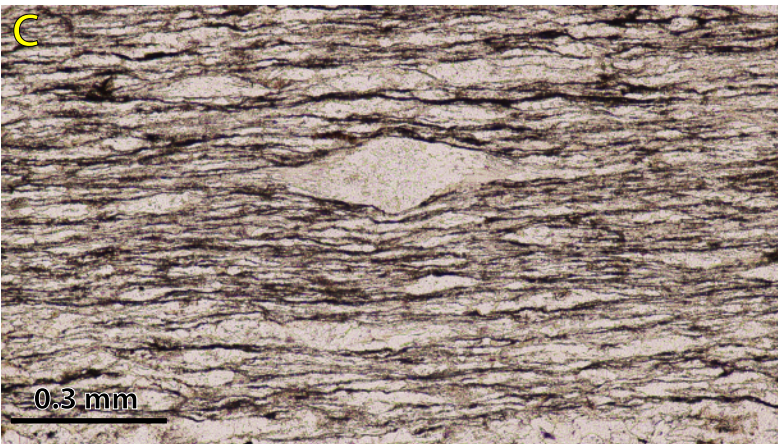


Figure 3.23. Photographs and phot micro-graphs taken near Hoge Creek. a) Boulder conglomerate at the base of the Hasen Creek Formation, dominantly made up of clasts of underlying gabbro and diorite. b) Wrangell suite diorite deformed and altered to clay gouge near the contact with the Icefield Formation. c) Photo-micrograph of calcareous siltstone composed of calcite and quartz between layers of insoluble minerals (dark material in photo). d) Icefield Formation schist folded into chevron style folds within the imbricate zone. e) South dipping gouge zone deforming the Icefield Formation within the imbricate zone.

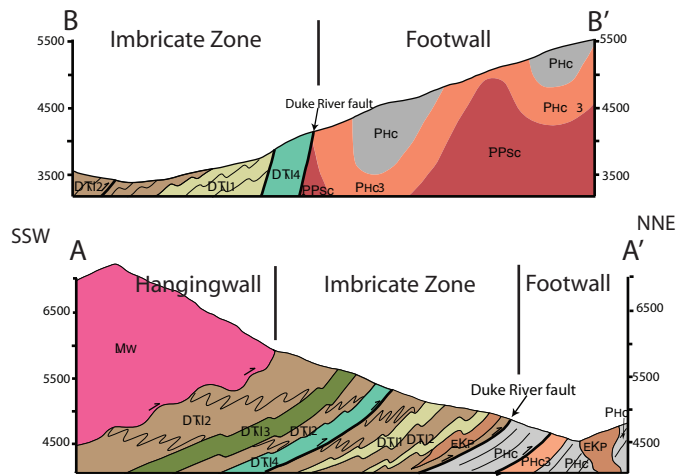


Figure 3.24. Geological cross sections A-A' and B-B' from the Hoge Creek area. See figure 3.22 for locations

folds are sub-parallel to the Hoge Creek synform, a large regional syncline found north of the Duke River fault (Read and Monger; 1976). One brittle fault structure deforms the volcanic breccia unit within the Hasen Creek succession into a cohesionless gouge zone that ranges in width from 1 to 5 metres and is composed of well-rounded pebble and sand sized clasts of volcanic material. A planar fabric defined by interlayered sandy sections between layers composed of dominantly pebble sized clasts, developed within the gouge zone, strikes southeast and dips moderately to the southwest (Fig. 3.25a).

3.5.5 Structure of the Hanging Wall

The tailing edge (southern boundary) of deformation with the imbricate zone is marked by the Wrangell suite pluton where it is deformed into gouge, composed of sub-rounded, sand sized grains of dominantly quartz in a clay matrix, near its contact with the Icefield Formation (Fig. 3.23b). Away from its contact with the Icefield Formation this body is undeformed.

3.5.6 Structure of the Imbricate Zone

An early phase of ductile foliation development within the imbricate zone strikes east-southeast and dips moderately southwest (Fig. 3.25b). Within the calcareous siltstone, this foliation is dominantly made up of calcite and quartz crystals between layers of clay and other dark, insoluble minerals (Fig. 3.23c), whereas within the schist the foliation is defined by feldspar crystals, dynamically recrystallized quartz and muscovite. Within the mylonite the ductile foliation is made up of very fine-grained, mildly elongated feldspar and quartz. This early phase foliation is tightly folded into chevron folds within the schist and folds with more rounded hinges within the other units (Fig. 3.23d & 3.25b).

Three brittle gouge zones overprint the early phase ductile foliation within the imbricate zone. At the upper portion of the imbricate zone, the contact between the Wrangell Suite diorite and the Icefield Formation is the brittle fault described in the Structure of the Hanging Wall section above (Fig. 3.23e). This gouge zone strikes

a) Foot Wall

- Poles to Bedding
- Poles to Brittle Foliation
- ▲ Fold Orientation

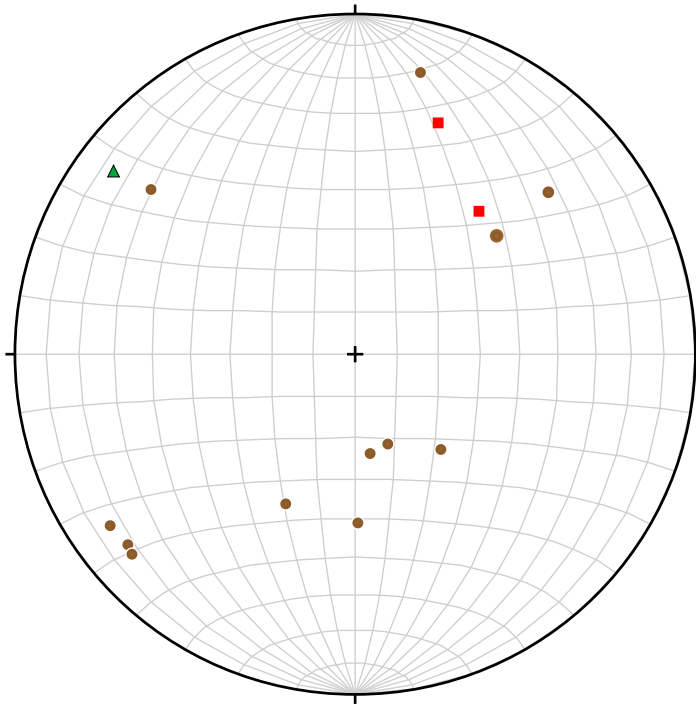
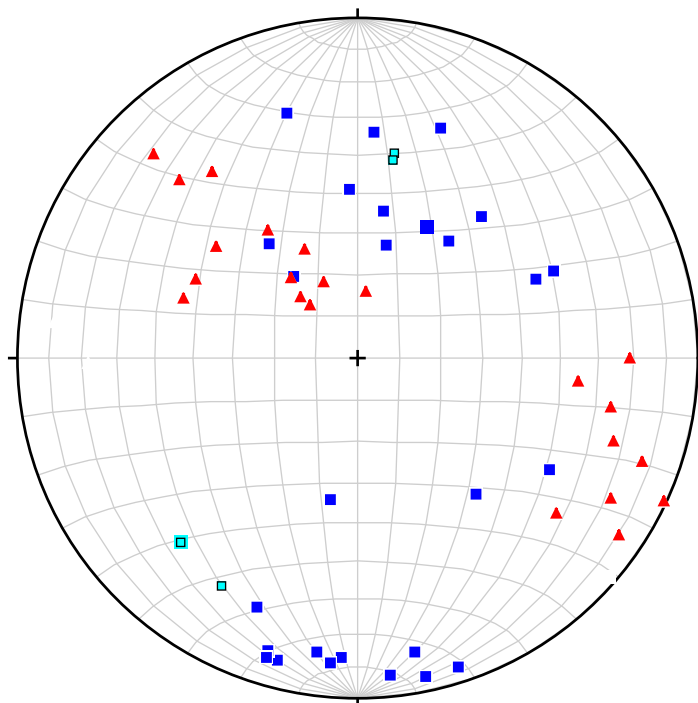


Figure 3.25. Structural data collected near Hoge Creek presented on equal area, lower hemisphere stereonets. a) Brown circles are poles to bedding in the foot wall Hasen Creek Formation. Red squares are poles to brittle foliations within a fault zone that deforms Hasen Creek rocks. The green triangle is an approximate orientation of the folds that deform the Hasen Creek rocks in the foot wall of the fault. b) Blue squares are poles to ductile foliations within the imbricate zone. Red triangles are fold axes for tight folds that deform the ductile foliation within the imbricate zone. Light blue squares are poles to the orientation of cataclastic zones that overprint the ductile deformation within the imbricate zone.

b) Imbricate Zone

- Poles to Ductile Foliations
- Poles to Brittle Faults
- ▲ Fold Axes



approximately 100 degrees ESE and dips moderately to the south and lacks any well-developed planar fabrics. At the structural bottom of the imbricate zone the leading edge of deformation is a gouge zone that separates Hasen Creek sandstone from Alexander terrane schist in the eastern end of the mapped area. The gouge is made up of clay and sub-angular, pebble-sized clasts of dominantly calcareous siltstone. Locally, near this zone a thick section of calcareous siltstone and schist are intruded by dikes that are folded, pulled apart and in places completely dismembered. In some locations the dikes cross cut the main foliation but are pulled apart parallel to the main foliations in other areas. In the west portion of the map, this same zone separates a marble unit from a mylonite, both likely belonging to the Alexander terrane. The zone strikes northwest and dips moderately to the southwest (Fig. 3.25b).

3.5.7 Discussion

Early phase foliation development within the schist and mylonite within the Icefield Formation is interpreted to be ductile in nature and formed by dislocation creep and dynamically recrystallized quartz. In specific the mylonite is interpreted to have formed through extensive grain size reduction in response to these processes being active over an extended period of time. The foliation within the calcareous schist is interpreted to have formed by pressure solution processes because it appears that the soluble material has been removed via pressure solution processes leaving layers of dark insoluble minerals and clay. This suggests that abundant fluids have percolated through the Duke River fault imbricate zone. The ductile foliation and tight folding of this fabric are interpreted to be a result of early movement along the Duke River fault. This interpretation is based mainly on similarities in structures within the imbricate zones near Bullion Creek and Jessie Creek.

Reactivation of the Duke River fault at higher crustal levels is indicated by the gouge zones that overprint the older ductile foliation and folding within the imbricate zone. Further, all minerals except quartz have altered to clay within the

structurally highest gouge zone suggesting abundant hot fluids have percolated through the fault zone when it was active at brittle levels in the crust.

The dikes that have been pulled apart and dismembered are interpreted to be syn to late syn-deformational because they cross cut the ductile foliation in some places and have been pulled apart parallel to the foliation in other places.

The scatter in the orientation of the tight folds suggests a later phase of folding refolds them. This could be related to a reactivation of the Duke River fault oblique to the early ductile movement.

From the Squaw Creek area to Hoge Creek and all areas in between the structures within the Duke River fault imbricate zone are comparable. There is no evidence that the fault has moved up or down section along strike.

3.6 Klutlan Glacier

The westernmost exposure of the Duke River fault in Yukon occurs along a ridge near the Klutlan Glacier, a few kilometres from the Alaska border (Fig. 3.1). In this area, the Duke River fault is a steep, south dipping reverse fault that has Station Creek and Hasen Creek rocks in the footwall and a Bullion Creek schist, quartzite and marble and a deformed gabbro in the hanging wall (3.26).

3.6.1 Stratigraphy of the Foot Wall

In the footwall of the Duke River fault in the Klutlan Glacier area, green, fine-grained, amygdaloidal basalt of the Station Creek Formation sits conformably below interbedded siltstone and sandstone of the Hasen Creek Formation (Fig. 3.27). The basalt is locally pillowed but mainly comprises massive flows (Fig. 3.28a). Amygdaloidal fine-grained, dark brown, basaltic dykes, likely related to the Wrangell volcanic rocks, intrude the Station Creek Formation (Fig. 3.26).

3.6.2 Stratigraphy of the Hanging Wall

In the hanging wall of the Duke River fault, the Alexander terrane consists of marble, carbonaceous and locally calcareous muscovite-feldspar-quartz schist

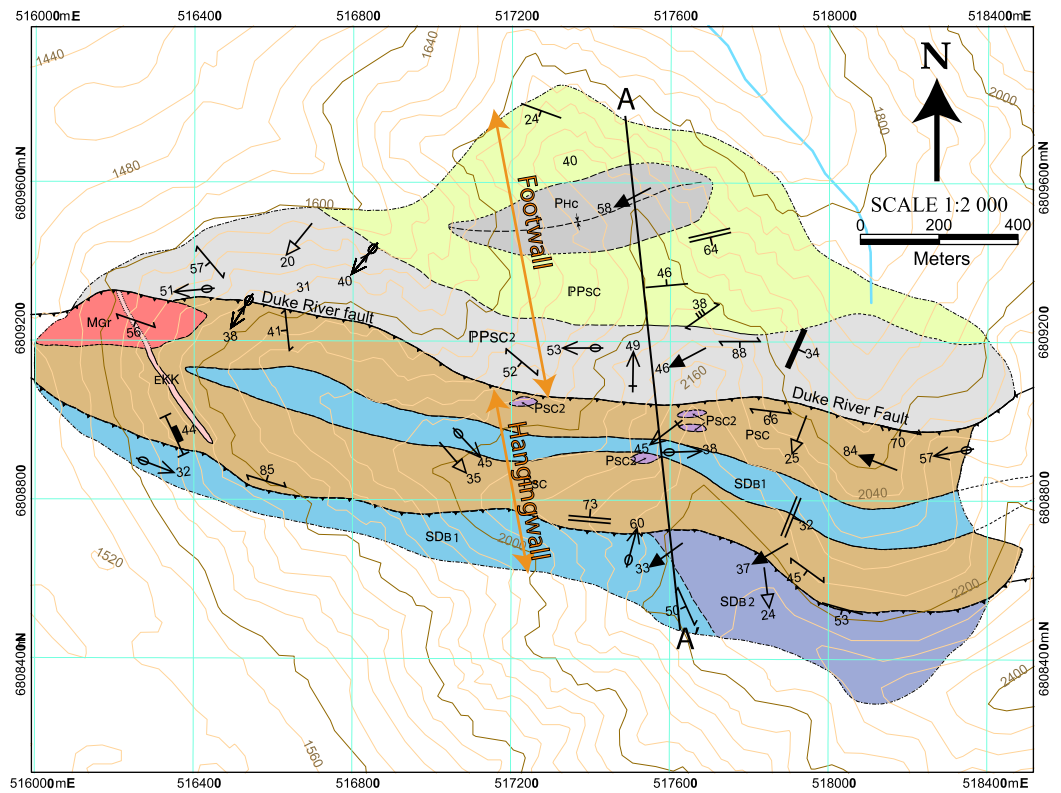


Figure 3.26 Geologic map of the Duke River fault near Klutlan Glacier.

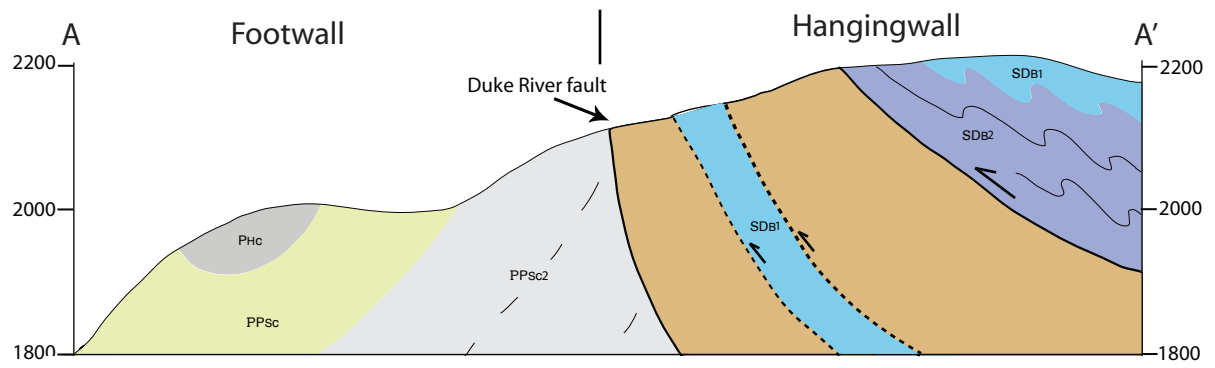


Figure 3.27. Geologic cross section A-A' of the Klutlan Glacier area. Vertically and horizontally exaggerated to show details. See figure 3.26 for location.

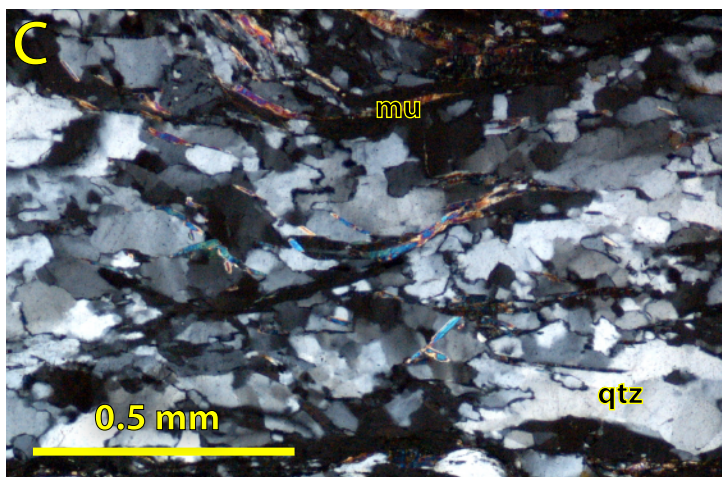


Figure 3.28. Photographs and photo micro-graphs of rocks from the Klutlan Glacier area. a) Pillow basalts from the Station Creek Formation in the foot wall of the Duke River fault. b) North verging folds in the Bullion formations in the hanging wall of the fault. c) Photo micro-graph showing dynamically re-crystallized quartz (qtz) between muscovite (mu) grains from a quartzite in the hanging wall. d) Crenulated quartzite from the Bullion formation. e) Brittle foliation in a granite defined by closely spaced fracture cleavage.

(267.5 Ma muscovite $^{40}\text{Ar}/^{39}\text{Ar}$ age, refer to chapter 4), greenschist and minor muscovite-bearing quartzite (256.8 Ma muscovite $^{40}\text{Ar}/^{39}\text{Ar}$ age, refer to chapter 4) of the Bullion formation. In structural contact with the Station Creek basalts and the Bullion Formation is a coarse-grained leuco-gabbro with pods of serpentinized ultramafics that crop out in the central map area (Fig. 3.26). The gabbro is composed mainly of plagioclase and pyroxene, and locally contains fuchsite. Secondary calcite alteration is prevalent throughout the rock. The gabbro is similar to other large intrusive bodies in the Alexander terrane, near the Duke River fault. It has been interpreted to be Devonian in age is correlated with the Steele Creek Gabbro Complex. A thin sliver of carbonaceous, mica schist occurs as a raft within the gabbro body; however, any evidence of an intrusive contact between the schist and the gabbro has been obscured by younger structures. Dark brown to black, fine-grained basaltic to dioritic dykes cut the gabbro and the Alexander terrane rocks and do not appear to have been deformed by the Duke River fault. These dykes are not observed crosscutting the Duke River fault and may be equivalent in age to the fine-grained dykes that intrude the Station Creek Formation rocks in the footwall of the Duke River fault. A pink, fine-medium grained granite intrudes into the gabbro and Bullion Creek schist and is faulted against the Station Creek basalts (Fig. 3.26)

3.6.3 Structure of the Foot Wall

Station Creek basalts are deformed into an upright syncline with thinly bedded sandstones and siltstones of Hasen Creek Formation in its core (Fig. 3.27). This synform trends east and its hinge line is sub-parallel to the Duke River fault (Fig. 3.29a).

3.6.4 Structure of the Hanging Wall

Immediately above the Duke River fault a leuco-gabbro in the hanging wall contains a ductile foliation that strikes to the east-southeast and dips moderately steeply to the south (Fig. 3.29b). This foliation is defined by dynamically recrystallized

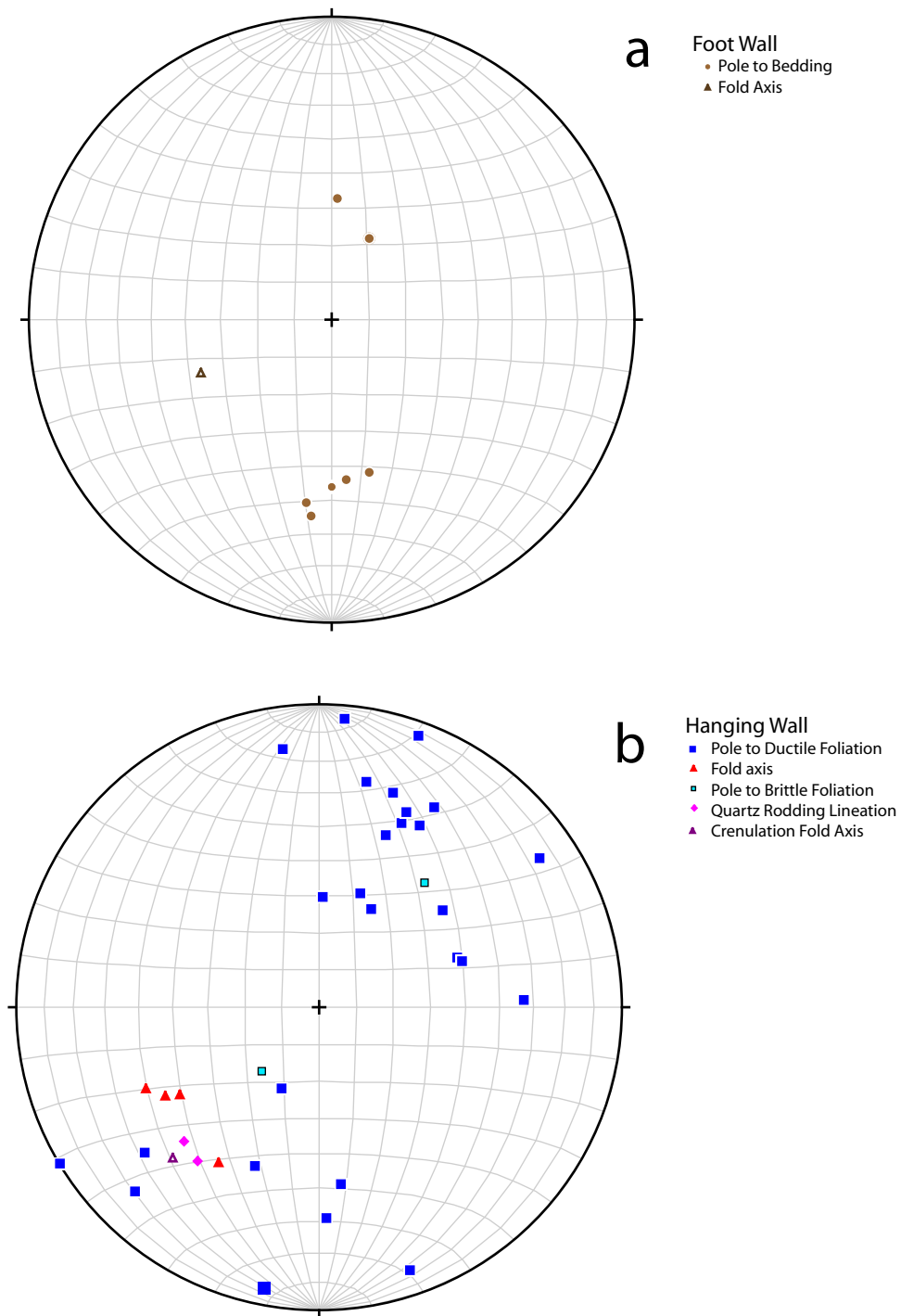


Figure 3.29 Structural data collected near Klutlan Glacier presented on equal area, lower hemisphere projection stereonet. a) Brown circles are poles to bedding measured in Hasen Creek rocks. Dark brown is the orientation of the fold axis that fold the Wrangellian rocks. b) Blue squares are poles to ductile foliations in the gabbro and the Bullion formation. Light blue squares are poles to brittle foliations measured within fault gouge. Red triangles are the orientations of folds that fold the ductile foliation. The purple triangle is the crenulation lineation within the quartzite. Pink diamonds are quartz rodding lineations.

feldspar between layers of calcite and fine-grained minerals such as clay, graphite and mica. Foliation within the sliver of schist within the gabbro strikes dominantly east-southeast and dips mainly to the south, although locally these structures dip moderately to the northeast (Fig. 3.26 & 3.29b). South of the gabbro an outcrop of marble is deformed by a foliation that strikes to the south-southeast and dips moderately to the west. This foliation is tightly folded into asymmetric folds that verge to the north (Fig. 3.28b). In contact with the marble is a quartzite with a ductile foliation defined by layers of dynamically recrystallized quartz grains and muscovite (Fig. 3.28c). This foliation is openly crenulated with crenulation lineations that plunge 33 degrees to the southwest (3.28d). Elongation lineations on the ductile foliation plane within the leuco-gabbro are defined by rodded quartz stringers plunge moderately to the south to southwest (Fig. 3.29b).

Near the Duke River fault, the granite in the hangingwall has been deformed by a closely spaced fracture cleavage (Fig. 3.28e). Overprinting the ductile fabrics within the Bullion formation and the gabbro is a gouge zone approximately 5-10 m-wide that occurs between the gabbro and the Bullion formation south of the Duke River fault. The gouge is composed of brecciated marble layers between layers of clay and sand sized grains of marble. A planar fabric defined by these layers in the gouge strikes southeast and dips moderately to the southwest. A similar gouge zone that separates the gabbro from the Bullion formation in the southwest corner of the map sheet strikes northwest and dips moderately to the northeast.

A purple, fine-grained intermediate dyke crosscuts most structural fabrics and shows minor, brittle offsets near the Duke River fault. This dyke cannot be traced across the contact between the foliated rocks of the Bullion formation and the Station Creek Formation, suggesting the Duke River fault truncates and/or offsets it. Exposure in this area is poor and the continuation of the dyke may be buried beneath colluvium on the north side of the fault.

3.6.5 Discussion

Provided the deformed gabbro is part of the Steele Creek Gabbro Complex it suggest the ductile fabrics are a result of movement along the Duke River fault as this gabbro is undeformed in other locations in southwest Yukon (S. Israel, Pers. Comm.; 2011). Shear bands observed in thin sections cut parallel to the elongation lineation on the foliation plane within the gabbro indicate dextral shear. This lineation is interpreted to represent the transport direction (south-southwest or north-northeast) along the Duke River fault and given that the fault places Devonian aged rocks over Permian rocks, it suggests the Alexander terrane has been thrust over Wrangellia towards the north-northeast. The dynamically recrystallized feldspar in the gabbro indicates it was deformed above 450 degrees Celsius (Price and Cosgrove, 1990) suggesting the gabbro may have moved 10's of kilometres vertically along this fault.

Reactivation of the fault at higher levels in the crust is suggested by overprinting brittle structures. These structures include the granite that is deformed into closely spaced fracture sets and gouge zones that follow the contact between the gabbro and the Bullion formation.

4: TIMING OF DEFORMATION ALONG THE DUKE RIVER FAULT

Samples were collected from within the imbricate zone and dated using a variety of geochronological techniques in order to constrain the timing of movement along the Duke River fault. Zircons from deformed intrusive bodies were analyzed using U-Pb laser and ID-TIMS techniques at the Pacific Centre for Geochronology Research (PCIGR) at the University of British Columbia (UBC) and the geochronology laboratory at Boise State University. Muscovite grains from foliated rock samples were analyzed using $^{40}\text{Ar}/^{39}\text{Ar}$ geochronology techniques at both the PCIGR at UBC and the Geological Survey of Canada. One sample of a hornblende gabbro was analyzed using $^{40}\text{Ar}/^{39}\text{Ar}$ at the Geological Survey of Canada.

4.1 Methodology

4.1.1 U-Pb LA-ICPMS Pacific Centre for Geochronology Research - UBC

U-Pb LA-ICPMS data presented in Appendix I were obtained using the following methodology. Zircons were separated from their host rocks using conventional mineral separation methods and sectioned in an epoxy grain mount along with grains of internationally accepted standard zircon (FC-1, a ~1100 Ma zircon standard), and brought to a very high polish. The grains were examined using a stage-mounted cathodoluminescence imaging unit that makes it possible to detect the presence of altered zones or inherited cores within the zircon. The highest quality portions of each grain, free of alteration, inclusion, or cores were selected for analysis. The surface of the mount was then washed for ~10 minutes with dilute nitric acid and rinsed in ultra clean water. Analyses were carried out using a New Wave 213nm Nd-YAG laser coupled to a Thermo Finnigan Element 2 high resolution ICP-MS. Ablation was done within a New Wave “Supercell” ablation chamber designed to achieve very high efficiency entrainment of aerosols into the

carrier gas. Helium was used as the carrier gas for all experiments and gas flow rates, together with other parameters such as torch position, were optimized prior to beginning a series of analyses. Typically a 25 micron spot with 60% laser power was used, and line scans rather than spot analyses were employed in order to avoid within-run elemental fractions. Each analysis consisted of a 7 second background measurement (laser off) followed by a ~28 second data acquisition period with the laser firing. A typical analytical session consisted of four analyses of the standard zircon, followed by four analyses of unknown zircons, two standard analyses, four unknown analyses, etc., and finally four standard analyses. Data were reduced using the GLITTER software package developed by the GEMOC group at Macquarrie University, which subtracts background measurements, propagate analytical errors, and calculates isotopic ratios and ages. This application generates a time-resolved record of each laser shot. Final interpreted ages for relatively young (Phanerozoic) zircons are based on a weighted average of the calculated $^{206}\text{Pb}/^{238}\text{U}$ ages for 20-25 individual analyses. Plotting of the analytical results employs ISOPLOT 3.00 software (Ludwig, 2003).

4.1.2 U-Pb TIMS – Boise State University Geochronology Laboratory

U-Pb TIMS data presented in Appendix II was produced using the following methodology. After conventional crushing and mineral separation, zircon was subjected to a modified version of the chemical abrasion method of Mattinson (2005), reflecting analysis of single grains. Zircon was placed in a muffle furnace at 900°C for 60 hours in quartz beakers. Single grains were then transferred to 3 ml Teflon PFA beakers and loaded into 300 ml Teflon PFA microcapsules. Fifteen microcapsules were placed in a large-capacity Parr vessel, and the crystals partially dissolved in 120 ml of 29 M HF for 12 hours at 180°C. The contents of each microcapsule were returned to 3 ml Teflon PFA beakers, the HF removed and the residual grains immersed in 3.5 M HNO_3 , ultrasonically cleaned for an hour, and fluxed on a hotplate at 80°C for an hour. The HNO_3 was removed and the grains were rinsed twice in ultrapure H_2O before being reloaded into the same 300 ml

Teflon PFA microcapsules (rinsed and fluxed in 6 M HCl during sonication and washing of the grains) and spiked with the EARTHTIME mixed ^{233}U - ^{235}U - ^{202}Pb - ^{205}Pb tracer solution. These chemically abraded grains were dissolved in Parr vessels in 120 ml of 29 M HF with a trace of 3.5 M HNO_3 at 220°C for 48 hours, dried to fluorides, and then re-dissolved in 6 M HCl at 180°C overnight. U and Pb were separated from the zircon matrix using an HCl-based anion-exchange chromatographic procedure (Krogh, 1973), eluted together and dried with 2 μl of 0.05 N H_3PO_4 .

Pb and U were loaded on a single outgassed Re filament in 5 μl of a silica-gel/phosphoric acid mixture (Gerstenberger and Haase, 1997), and U and Pb isotopic measurements made on a GV Isoprobe-T multicollector thermal ionization mass spectrometer equipped with an ion-counting Daly detector. Pb isotopes were measured by peak-jumping all isotopes on the Daly detector for 100 to 160 cycles, Pb mass fractionation was corrected using the known $^{202}\text{Pb}/^{205}\text{Pb}$ ratio of the ET2535 tracer solution. Transitory isobaric interferences due to high-molecular weight organics, particularly on ^{204}Pb and ^{207}Pb , disappeared within approximately 30 cycles, while ionization efficiency averaged 10^4 cps/pg of each Pb isotope. Linearity (to $\geq 1.4 \times 10^6$ cps) and the associated deadtime correction of the Daly detector were monitored by repeated analyses of NBS982, and have been constant since installation of the mass spectrometer. Uranium was analyzed as UO_2^+ ions in static Faraday mode on 10^{11} ohm resistors for 200 to 250 cycles, and corrected for isobaric interference of $^{233}\text{U}^{18}\text{O}^{16}\text{O}$ on $^{235}\text{U}^{16}\text{O}^{16}\text{O}$ with an $^{18}\text{O}/^{16}\text{O}$ of 0.00206. Ionization efficiency averaged 20 mV/ng of each U isotope. U mass fractionation was corrected using the known $^{233}\text{U}/^{235}\text{U}$ ratio of the ET2535 tracer solution.

U-Pb dates and uncertainties were calculated using the algorithms of Schmitz and Schoene (2007), a calibration of the ET2535 tracer solution (Condon et al., 2007) of $^{235}\text{U}/^{205}\text{Pb} = 100.206$, $^{233}\text{U}/^{235}\text{U} = 0.99464$, $^{202}\text{Pb}/^{205}\text{Pb} = 0.99969$, and $^{205}\text{Pb}/^{204}\text{Pb} = 10900$, and U decay constants recommended by Jaffey et al. (1971). $^{206}\text{Pb}/^{238}\text{U}$ ratios and dates were corrected for initial ^{230}Th disequilibrium using a $\text{Th}/\text{U}[\text{magma}] = 3$ using the algorithms of Crowley et al. (2007), resulting in an increase in the $^{206}\text{Pb}/^{238}\text{U}$ dates of ~ 0.09 Ma. All common Pb in analyses was

attributed to laboratory blank and subtracted based on the measured laboratory Pb isotopic composition and associated uncertainty. U blanks are difficult to precisely measure, but are estimated at 0.07 pg.

Over the course of the experiment, analyses of the 500 Ma EARTHTIME standard solution that varied in size from 7-77 pg of radiogenic Pb yielded a weighted mean $^{206}\text{Pb}/^{238}\text{U}$ date of 499.97 ± 0.09 Ma ($n = 9$, MSWD = 0.6).

The weighted mean $^{206}\text{Pb}/^{238}\text{U}$ date was calculated with Isoplot 3.0 (Ludwig, 2003). The error on the weighted mean $^{206}\text{Pb}/^{238}\text{U}$ date is the internal error based on analytical uncertainties only, including counting statistics, subtraction of tracer solution, and blank and initial common Pb subtraction. It is given at the 95% confidence limit. The error on single analyses is the 2s internal error based on analytical uncertainties only. These errors should be considered when comparing dates from Boise State laboratory with $^{206}\text{Pb}/^{238}\text{U}$ dates from other laboratories that used the same EARTHTIME tracer solution or a tracer solution that was cross-calibrated using EARTHTIME gravimetric standards. When comparing Boise State dates with those derived from other geochronological methods using the U-Pb decay scheme (e.g., laser ablation ICPMS), a systematic uncertainty in the tracer calibration should be added to the internal error in quadrature. When comparing Boise State dates with those derived from other decay schemes (e.g., $^{40}\text{Ar}/^{39}\text{Ar}$, ^{187}Re - ^{187}Os), systematic uncertainties in the tracer calibration and ^{238}U decay constant (Jaffey et al., 1971) should be added to the internal error in quadrature.

4.1.3 $^{40}\text{Ar}/^{39}\text{Ar}$

4.1.3.1 Pacific Centre for Isotope and Geochemical Research - UBC

$^{40}\text{Ar}/^{39}\text{Ar}$ data presented in Table 4.1 and Appendix II were generated using the following methodology. Each sample was crushed and sieved to obtain fragments ranging in the size range from 0.5 to 1 mm. A hand magnet was passed over the samples to remove magnetic minerals and metallic crusher

Area	Sample	Mineral	Age (Ma)
Squaw Creek	08-RC-024-1A	Muscovite	82.8 +/- 2.7
Squaw Creek	08-RC-024-1B	Muscovite	104.6 +/- 2.2
Squaw Creek	08-RC-028-1	Muscovite	90.1 +/- 4.3
Jessie Creek	09-RC-063-C1	Muscovite	104.1 +/- 3.7
Silver Creek	09-RC-044-A1	Whole Rock	121.0 +/- 2.8
Klutlan Glacier	08-RC-060-1B	Muscovite	267.5 +/- 6.4
Klutlan Glacier	08-RC-071-1	Muscovite	256.8 +/- 6.6

Table 4.1. $^{40}\text{Ar}/^{39}\text{Ar}$ plateau ages from rocks collected within the imbricate zone of the Duke River fault.

fragments/spall. The samples were washed in deionized water, rinsed and then air-dried at room temperature.

Mineral separates were hand-picked, wrapped in aluminum foil and stacked in an irradiation capsule with similar-aged samples and neutron flux monitors (Fish Canyon Tuff sanidine, 28.02 Ma (Renne et al., 1998); MAC-83 biotite, 24.36, (Sandeman et al., 1999).

The samples were irradiated at the McMaster Nuclear Reactor in Hamilton, Ontario, for 72 MWH, with a neutron flux of approximately 3×10^{16} neutrons/cm². Analyses (n=33) of 11 neutron flux monitors irradiated with the samples produced errors of <0.25% in the J value.

The samples were analyzed at the Noble Gas Laboratory at the Pacific Centre for Isotopic and Geochemical Research, University of British Columbia. The separates were step-heated at incrementally higher powers in the defocused beam of a 10W CO₂ laser (New Wave Research MIR10) until fused. The gas evolved from each step was analyzed by a VG5400 mass spectrometer equipped with an ion-counting electron multiplier. All measurements were corrected for total system blank, mass spectrometer sensitivity, mass discrimination, radioactive decay during and subsequent to irradiation, as well as interfering Ar from atmospheric contamination and the irradiation of Ca, Cl and K. The plateau and correlation ages were calculated using Isoplot ver.3.09 (Ludwig, 2003). Errors are quoted at the 2-sigma (95% confidence) level and are propagated from all sources except mass spectrometer sensitivity and age of the flux monitor.

4.1.3.2 Geological Survey of Canada - Ottawa

Selected samples were processed for ⁴⁰Ar/³⁹Ar analysis of whole rock by standard preparation techniques, including hand-picking of unaltered pieces in the size range 0.25 to 0.50 mm. Individual mineral separates were loaded into aluminum foil packets along with a single grain of Fish Canyon Tuff Sanidine (FCT-SAN) to act as flux monitor (apparent age = 28.03 Ma; Renne et al., 1998). The sample packets were arranged radially inside an aluminum can. The samples were

submitted for a 60 MWH irradiation at the research reactor of McMaster University in Hamilton, Ontario, Canada.

Laser $^{40}\text{Ar}/^{39}\text{Ar}$ step-heating analysis was carried out at the Geological Survey of Canada geochronology laboratories in Ottawa, Ontario. Upon return from the reactor, samples were split into two aliquots each and loaded into individual 1.5 mm-diameter holes in a copper planchet. The planchet was then placed in the extraction line and the system evacuated. Heating of individual sample aliquots in steps of increasing temperature was achieved using a Merchantek MIR10 10W CO_2 laser equipped with a 2 mm x 2 mm flat-field lens. The released Ar gas was cleaned over getters, and then analyzed isotopically using a Nu Instruments multicollector Noblesse mass spectrometer, equipped with a Faraday detector and three ion counters. For the analyses, a single ion counter peak-hopping mode was used for small signals, and in cases where the ^{40}Ar signal exceeded ion counting tolerance, a Faraday plus single ion counter peak-hopping routine was employed. Baselines were measured prior to each analysis. Blank measurements were made throughout the analytical sessions, the values for which are included in Appendix III. Mass fractionation and detector efficiencies were determined from repeated measurements of air aliquots, whereby ^{40}Ar and ^{36}Ar signals were measured on all collectors. $^{40}\text{Ar}/^{36}\text{Ar}$ ratios were then determined for each collector individually, and for each combination of collectors (ex. ^{40}Ar on the Faraday/ ^{36}Ar on each ion counter). Raw data from the mass spectrometer was imported and processed using a spreadsheet programmed with data handling macros written by M.E. Villeneuve that employ average, linear or non-linear regression protocols based on the equations of Koppers (2002).

Error analysis on individual steps follows numerical error analysis routines outlined in Scaillet (2000); error analysis on grouped data follows algebraic methods of Roddick (1988). Corrected argon isotopic data are listed in Appendix III, and presented (Figure 4.3) as spectra of gas release or on inverse-isochron plots (Roddick et al. 1980). Each gas-release spectrum plotted contains step-heating data from up to two aliquots, alternately shaded and normalized to the total volume of ^{39}Ar released for each aliquot. Such plots provide a visual image of replicated

heating profiles, evidence for Ar-loss in the low temperature steps, and the error and apparent age of each step.

Neutron flux gradients throughout the sample canister were evaluated by analyzing the sanidine flux monitors included with each sample packet and interpolating a linear fit against calculated J-factor and sample position. The error on individual J-factor values is conservatively estimated at $\pm 0.6\%$ (2s). Because the error associated with the J-factor is systematic and not related to individual analyses, correction for this uncertainty is not applied until calculation of dates from isotopic correlation diagrams (Roddick, 1988). Nucleogenic interference corrections were $(^{40}\text{Ar}/^{39}\text{Ar})_{\text{K}} = 0.025 \pm 0.005$, $(^{38}\text{Ar}/^{39}\text{Ar})_{\text{K}} = 0.011 \pm 0.010$, $(^{40}\text{Ar}/^{37}\text{Ar})_{\text{Ca}} = 0.002 \pm 0.002$, $(^{39}\text{Ar}/^{37}\text{Ar})_{\text{Ca}} = 0.00068 \pm 0.00004$, $(^{38}\text{Ar}/^{37}\text{Ar})_{\text{Ca}} = 0.00003 \pm 0.00003$, $(^{36}\text{Ar}/^{37}\text{Ar})_{\text{Ca}} = 0.00028 \pm 0.00016$. All errors are quoted at the 2s level of uncertainty.

4.2 U-Pb Results

Two U-Pb zircon samples help to constrain the timing of movement along the Duke River fault.

Sample 08-RC-176 is a fine-medium-grained granite body that crops out within the imbricate zone near the Klutlan Glacier area (Figure 4.1a). Single zircon grains from this sample were analyzed using the LA-ICPMS method at the PCIGR at UBC and yielded an interpreted age of 351 ± 2.8 Ma (Fig. 4.1b).

Sample 09-RC-151 is a medium-grained, biotite-hornblende-pyroxene diorite that crops out near Hoge Creek in the hanging wall of the Duke River fault (Fig. 3.22 & 4.1c). Single zircon grains from this sample were analyzed using the TIMS methods at the geochronology laboratory at Boise State University and yielded an age of 15.45 ± 0.01 Ma (Fig. 4.1d).

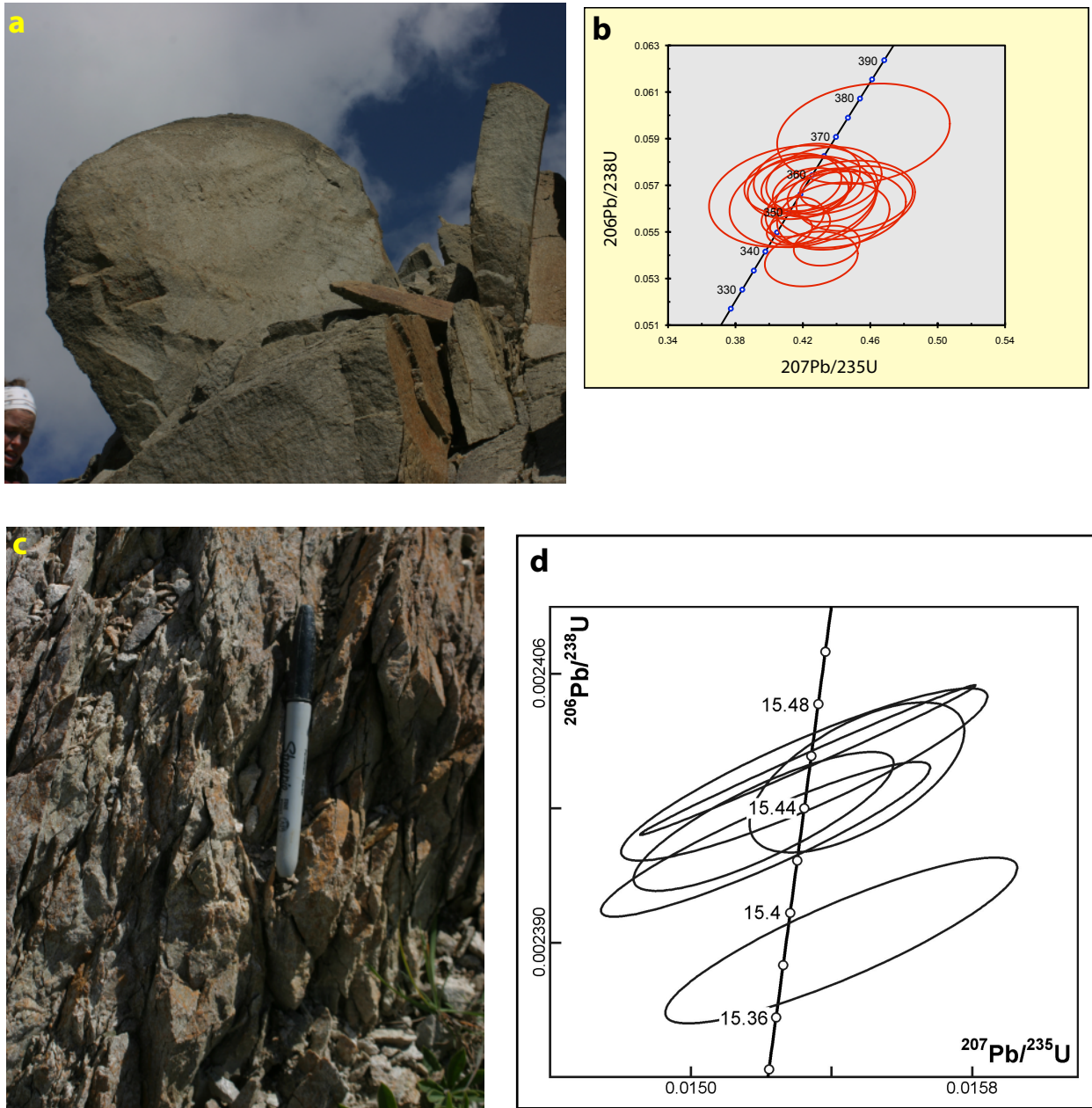


Figure 4.1. a) Concordia plot for sample 08-RC-076-1, a felsic intrusive body samples near Klutlan Glacier; analyzed using LA-ICPMS at PCIGR-UBC, ellipses are at the 95% confidence level. b) Concordia plot for sample 09-RC-151A01, a diorite collected near Hoge Creek; analyzed using TIMS at Boise State University, ellipses are at the 95% confidence interval.

4.3 $^{40}\text{Ar}/^{39}\text{Ar}$ Results

Samples 08-RC-024-1A and 08-RC-024-1B are fine-grained, calcareous, quartz-feldspar-muscovite schist from the Icefield Formation within the Duke River fault imbricate zone near Squaw Creek. Muscovite grains that define the main foliation in these samples were analyzed using $^{40}\text{Ar}/^{39}\text{Ar}$ methods at the PCIGR at UBC. The age of these two samples are 82.8 +/- 2.7 Ma and 104.6 +/- 2.2 Ma, respectively (Table 4.1; Fig. 4.2 a, b).

Sample 08-RC-028-1 is a fine-grained, calcareous, quartz-feldspar-muscovite schist from the Icefield Formation within the Duke River fault imbricate zone near Squaw Creek (Fig. 4.3a). The main foliation in this sample is made up of fine-grained muscovite that was analyzed using $^{40}\text{Ar}/^{39}\text{Ar}$ methods at the PCIGR at UBC. The age of this sample is 90.1 +/- 4.3 Ma (Table 4.1; Fig. 4.2c).

Sample 09-RC-044-A01 is a medium-grained hornblende gabbro that crops out near Silver Creek. The unit has been partially altered to actinolite, epidote, feldspar and calcite (Fig. 4.3b) and intrudes into the Icefield Formation within the Duke River fault imbricate zone. The whole rock $^{40}\text{Ar}/^{39}\text{Ar}$ age of 121.0 +/- 2.8 Ma was obtained at the Geological Survey of Canada (Table 4.1; Fig. 4.2d).

Sample 09-RC-063A01 is a foliated, muscovite-bearing gabbro that intrudes the Icefield Formation within the Duke River fault imbricate zone near Jessie Creek that has been significantly altered to calcite and clay (Fig. 4.3c). The main foliation in this sample is composed of bands of muscovite and clay and dynamically recrystallized feldspar. Muscovite from the sample yielded a $^{40}\text{Ar}/^{39}\text{Ar}$ age of 104.1 +/- 3.7 Ma at the Geological Survey of Canada (Table 4.1; Fig. 4.3e).

Sample 08-RC-060-1B is a carbonaceous, quartz-feldspar-muscovite schist that has been assigned to the Bullion formation that crops out within the Duke River fault imbricate zone near the Klutlan Glacier (Fig. 4.3d). The main foliation in this sample is made up muscovite that was analyzed at the PCIGR at UBC and yielded a $^{40}\text{Ar}/^{39}\text{Ar}$ age of 267.5 +/- 6.4 Ma (Table 4.1; Fig. 4.2f).

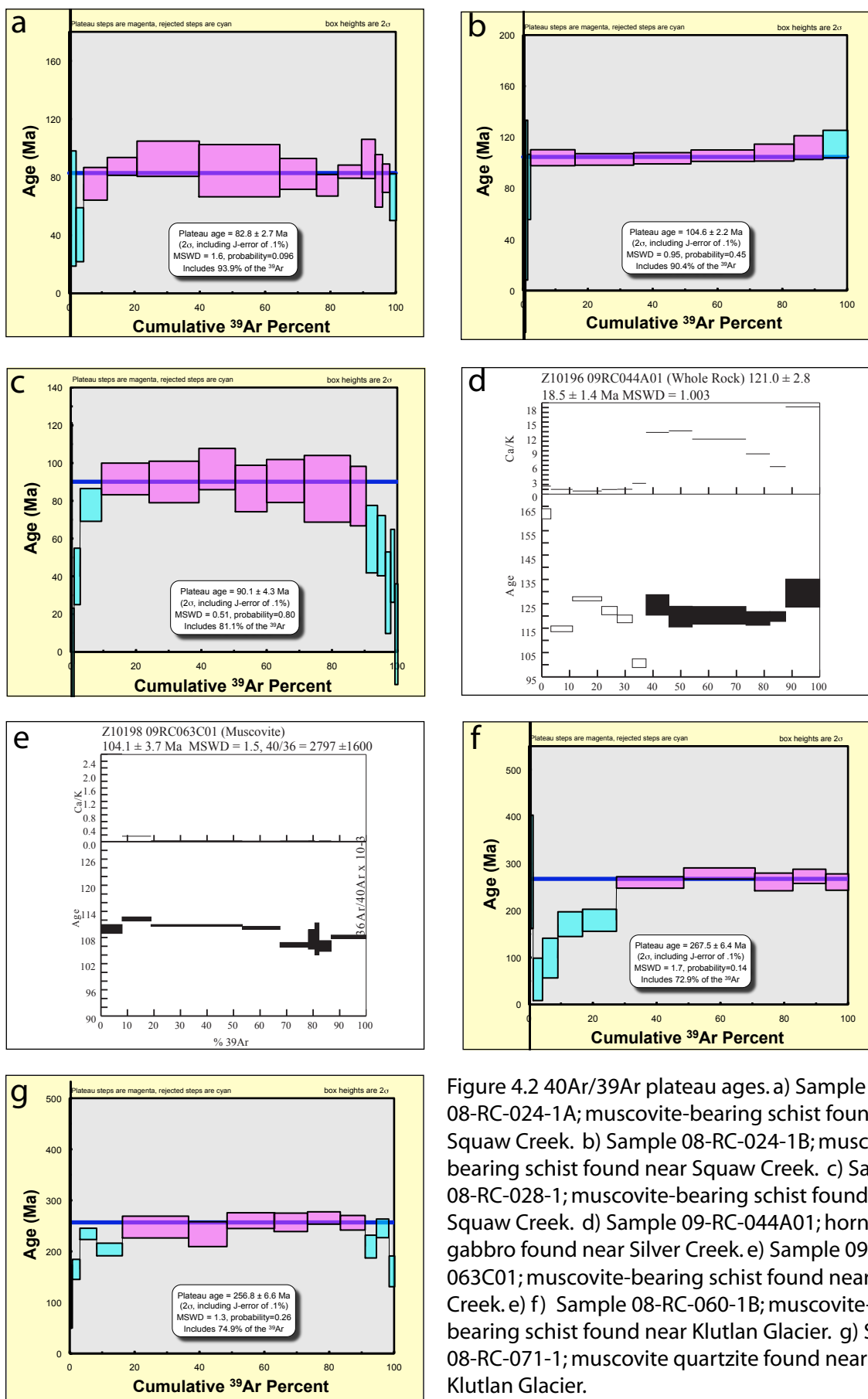


Figure 4.2 $^{40}\text{Ar}/^{39}\text{Ar}$ plateau ages. a) Sample 08-RC-024-1A; muscovite-bearing schist found near Squaw Creek. b) Sample 08-RC-024-1B; muscovite-bearing schist found near Squaw Creek. c) Sample 08-RC-028-1; muscovite-bearing schist found near Squaw Creek. d) Sample 09-RC-044A01; hornblende gabbro found near Silver Creek. e) Sample 09-RC-063C01; muscovite-bearing schist found near Jessie Creek. e) f) Sample 08-RC-060-1B; muscovite-bearing schist found near Klutlan Glacier. g) Sample 08-RC-071-1; muscovite quartzite found near Klutlan Glacier.

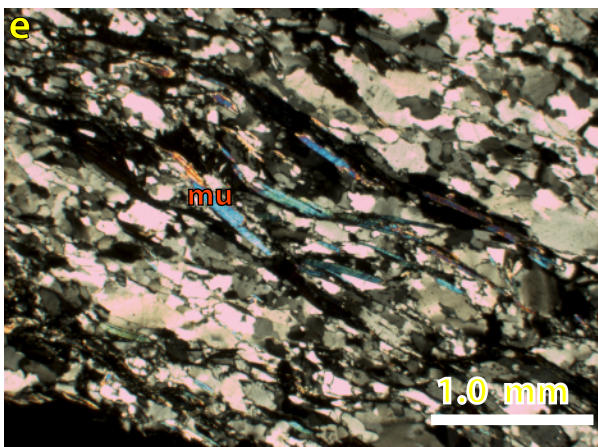
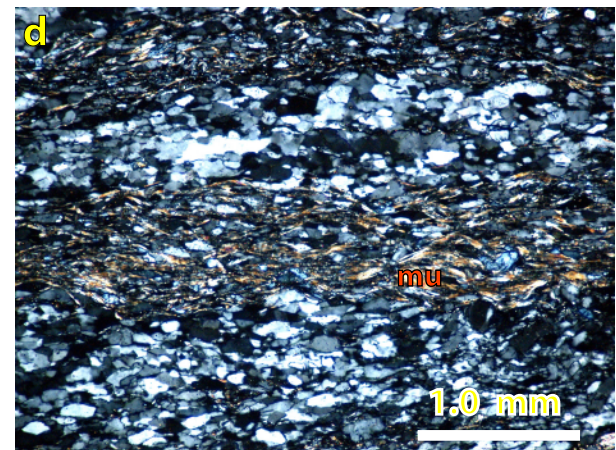
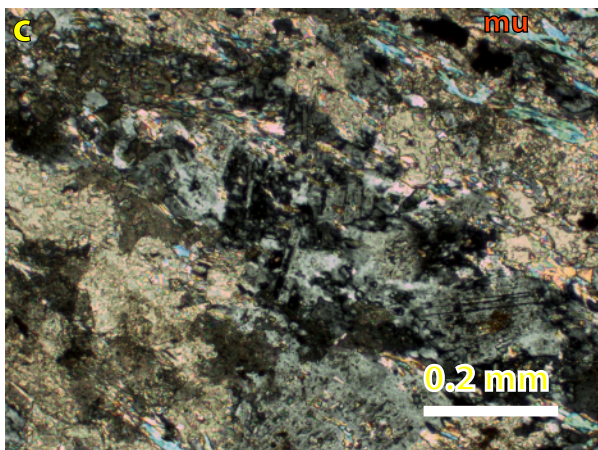
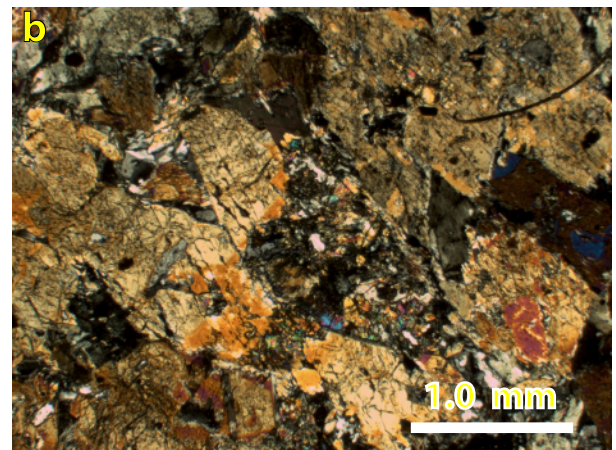
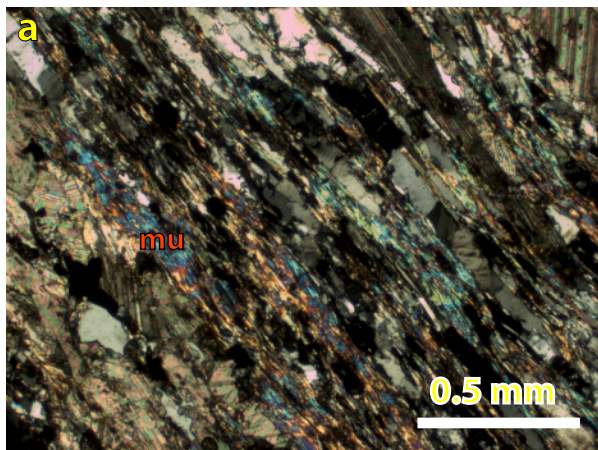


Figure 4.3 Photo-micrographs of muscovite (mu)-bearing samples that were collected for $^{40}\text{Ar}/^{39}\text{Ar}$ geochronology. a) Sample 08-RC-028-1; a calcareous, quartz-feldspar-muscovite schist found near Squaw Creek. b) Sample 09-RC-044-A01; hornblende within a gabbro that has been partially altered to actinolite found near Silver Creek. c) Sample 09-RC-063C01; a feldspar-muscovite schist with significant amounts of secondary clay and calcite found near Jessie Creek. d) Sample 08-RC-061-1B; a carbonaceous, quartz-feldspar-muscovite schist found near Klutlan Glacier. e) Sample 08-RC-071-1; a muscovite-bearing quartzite found near Klutlan Glacier.

Sample 08-RC-071-1 is a muscovite-bearing quartzite from the Bullion formation that crops out within the hanging wall of Duke River fault near the Klutlan Glacier (Fig. 4.3e). The main foliation in this sample is made up muscovite that was analyzed at the PCIGR at UBC and yielded an $^{40}\text{Ar}/^{39}\text{Ar}$ of 256.6 ± 6.6 Ma (Table 4.1; Fig. 4.2g).

4.4 Discussion

4.4.1 Significance of Permian Ages Along the Duke River Fault

The Permian ages presented above from metamorphic muscovite within Alexander terrane units adjacent to the Duke River fault are interpreted to record a regional metamorphic event within the Alexander terrane. There is evidence of an orogenic event and coeval plutonism that affected much of the Alexander terrane at approximately this time (Gardner et al., 1988; Berenak et al., 2011; Van Staal et al., 2010). Unlike the locations mapped further south along the Duke River fault trace, the muscovite in the rocks near Klutlan Glacier have not been reset by Cretaceous movements. This indicates that at most only a few kilometres of uplift has occurred along the fault in this area since the Permian. Several models explain this; 1) this portion of the Duke River fault has not undergone the same amount of uplift as in other areas; 2) this fault was not part of the Cretaceous Duke River fault and that structure is no longer present or exists somewhere else; 3) this structure is not the Duke River fault and what has been mapped here is a subsidiary fault in the Klutlan Glacier area.

4.4.2 Cretaceous Movements Along the Duke River Fault

The Cretaceous ages (82.8 to 104.6 Ma) from rocks collected within the Icefield Formation (and one gabbro that intrudes the Icefield Formation) within the Duke River fault imbricate zone are interpreted to record movement along the Duke River fault. The muscovite grains that yielded these ages have been recrystallized during the development of the main ductile foliation that developed during

movement along the Duke River fault and constrain the timing of early movements along the Duke River fault to the late Early Cretaceous to Late Cretaceous time. In sample 08-RC-028-1 the muscovite is very fine-grained and has been deformed into shear bands, however, in situ dating of the muscovite was not carried out on the thin section that the shear bands were observed in. It is not known whether the grains that make up the shear bands record the same $^{40}\text{Ar}/^{39}\text{Ar}$ age as muscovite grains that were hand picked from the crushed sample for dating.

The spread in ages of these samples is attributed to either, 1) argon loss related to fluids percolating through the deformation zone during movement along the Duke River fault (Kirschner et al., 1996; Hames and Cheney, 1997; Dunlap and Kronenberg, 2001); 2) (hydro)thermal resetting of fine-grained muscovite that may be related to episodes of high heat flow in and near the Duke River fault (e.g. associated with the Wrangell volcanic episode in Miocene time); and/or mica growth at various times during prolonged deformation within the Duke River fault imbricate zone. Secondary calcite and quartz is present in most samples collected along the fault and suggests that large amounts of fluids have moved through the Duke River fault imbricate zone.

The Early Cretaceous whole rock $^{40}\text{Ar}/^{39}\text{Ar}$ age for the hornblende gabbro body near Silver Creek, either dates the crystallization of the gabbro or possibly a metamorphic event that has altered the gabbro and reset the $^{40}\text{Ar}/^{39}\text{Ar}$ system. It is probable that heat generated during movement along the fault has metamorphosed the gabbro in the Early Cretaceous time during the initial movement of the fault. Another possibility is that the Duke River fault is a crustal-scale feature that may have localized emplacement of gabbroic intrusions in the Early Cretaceous. This would suggest that the $^{40}\text{Ar}/^{39}\text{Ar}$ age provides a crystallization age for the gabbro body. There are abundant of gabbroic intrusions all along the Duke River fault, suggesting a possible link between mafic intrusions and the fault.

4.4.3 Miocene to Pliocene Movement on the Duke River Fault

The Miocene U-Pb zircon age obtained for a diorite body near Hoge Creek provides direct evidence that the Duke River fault has been active since the Miocene or was reactivated sometime after the Miocene. The diorite that is deformed by the fault near Hoge Creek and is one of several lines of evidence for this reactivation. Near Squaw Creek a crystal tuff that has been interpreted to belong to the Miocene Wrangell volcanics is clearly deformed by the Duke River fault. Similarly, near Bullion Creek a quartz-feldspar porphyritic tuff considered to belong to the Miocene Wrangell volcanics is deformed along its contact with the Duke River fault. Northwest of Hoge Creek, the Wrangell volcanics are folded above the Duke River fault (Fig. 4.4), clearly indicating that the fault has been active since the deposition of the Wrangell Volcanics, which spanned 18-8 Ma.

4.4.4 Summary

With the exception of the Klutlan Glacier area, the Duke River fault was a deep, crustal scale structure that was deforming below the brittle ductile transition zone in the early Late Cretaceous time. Over time the fault moved up section such that it was deforming in a brittle regime in the Miocene time. Either the fault was progressively deforming from the Cretaceous to the Miocene time and gradually moved up section or there was a pulse of ductile deformation in the Cretaceous and then a period of erosion and rebound with a reactivation at higher level in the crust in the Miocene time.

Although no evidence of this found over the course of this study, regional studies suggest that the Duke River fault along with the Denali fault was active in the Oligocene. Pull-apart basins filled with Oligocene Amphitheatre conglomerates have been mapped along both of these faults in southwest Yukon (Ridgeway and Decelles, 2006).

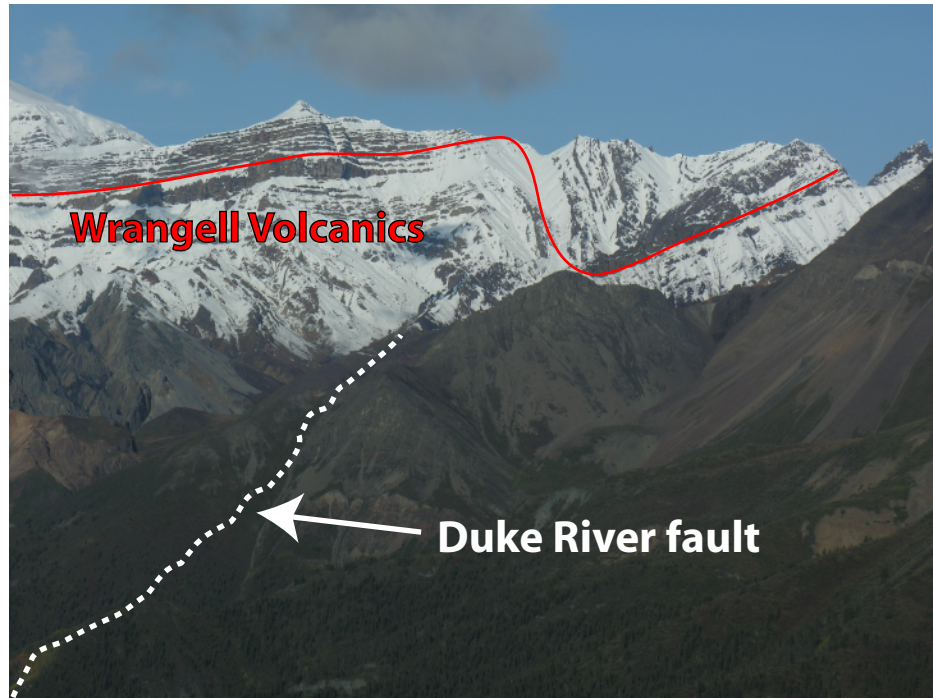


Figure 4.4 Photograph of the Kluane Range mountains northwest of Hoge Creek. The red line outlines bedding in a thick package or Wrangell Volcanics (8-18 Ma) that have been deposited on top of the Duke River fault. The volcanics have been folded by the recent movements along the fault.

5: DISCUSSION AND CONCLUSIONS

5.1 Timing and Kinematics of the Duke River Fault

As the six mapped areas described above show, the Duke River fault consistently separates two very distinct tectonic terranes from one another. These terranes differ in terms of their stratigraphic relationships, metamorphic grade and deformation histories. Each of these differences suggests that the Duke River fault has accommodated significant amounts of movement. For example based on the difference in metamorphic grade of Wrangellia (prehnite-pumpellyite) and Alexander terrane (greenschist) an estimated amount of vertical motion is 10 to 13 kilometres. From the data collected at each of the mapped areas the movement along the Duke River fault appears to have been episodic with the main phase of deformation likely occurring in the Cretaceous; with some significant reactivation occurring in the Pliocene.

5.1.1 Cretaceous Motion of the Duke River Fault

Within the imbricate zone of the Duke River fault, ductile deformation attributed to movement along the DRF has overprinted regional fabrics within the Alexander terrane. The presence of dynamically recrystallized feldspar indicates that parts of the Duke River fault zone were deformed under high heat conditions given that it has been shown to take temperatures greater than 450 degrees Celsius to recrystallize feldspar (Price and Cosgrove, 1990).

Shear bands in thin sections cut parallel to elongation lineations suggest the Alexander terrane has been thrust over Wrangellia. Cretaceous $\text{Ar}^{39}/\text{Ar}^{40}$ ages from muscovite that define the ductile foliation fabric suggest this thrust movement occurred during the Early Late Cretaceous time.

5.1.2 Miocene to Pliocene Reactivation of the Duke River Fault

There are several lines of evidence that indicate the Duke River fault was reactivated in the Miocene. Miocene to Pliocene crystal tuffs in the Squaw Creek area are deformed by brittle processes that have resulted in closely spaced fracture sets that sit at a 60° angle to each other. Middle to Late Miocene (?) crystal tuff northeast of the Bullion Creek area are deformed by brittle processes that have resulted in sections of clay gouge and brecciated tuff near the Duke River fault. Similarly, The middle Miocene (16 Ma) biotite-pyroxene-hornblende diorite body near Hoge Creek has been deformed into fault gouge along its base by the Duke River fault zone. Of note is the large scale 12 to 23 kilometre (considering an average dip of the fault to be 40 degrees and that the pluton was emplaced between 9 and 15 kilometres depth), thrust movements that the Duke River fault must have accommodated in order to put 16 million year old pluton at the top of a large mountain on top of Alexander terrane stratigraphy. Northwest of Hoge Creek, the Wrangell volcanics are folded above the Duke River fault. These features show that the Duke River fault was active after the Miocene and possibly the Pliocene.

Reactivation of the Duke River fault in the Miocene occurs at the time of the onset of subduction of the Yakutat block beneath the North American plate (Fig. 5.1a). The Yakutat block has been shown to have moved northwestwards with the Pacific Plate along margin parallel strike slip faults until it reached the Gulf of Alaska in the middle Miocene at which point it began to subduct beneath the North American Plate (Plafker et al., 1994; Bruhn et al., 2004). Global Positioning System (GPS) motion vectors show that some of the present day deformation related to the Yakutat block collision is causing the southwest corner of the Yukon to move towards the north-northeast (Fig. 5.1b) (Mazzotti and Hyndman, 2002). The Duke River fault is favourably oriented to accommodate northeast-southwest compression by reverse slip. Micro-seismicity recorded along the Duke River fault in the southwest Yukon suggests the fault accommodates part of the active uplift of the St. Elias Mountains (Power, 1988; Page et al., 1991).

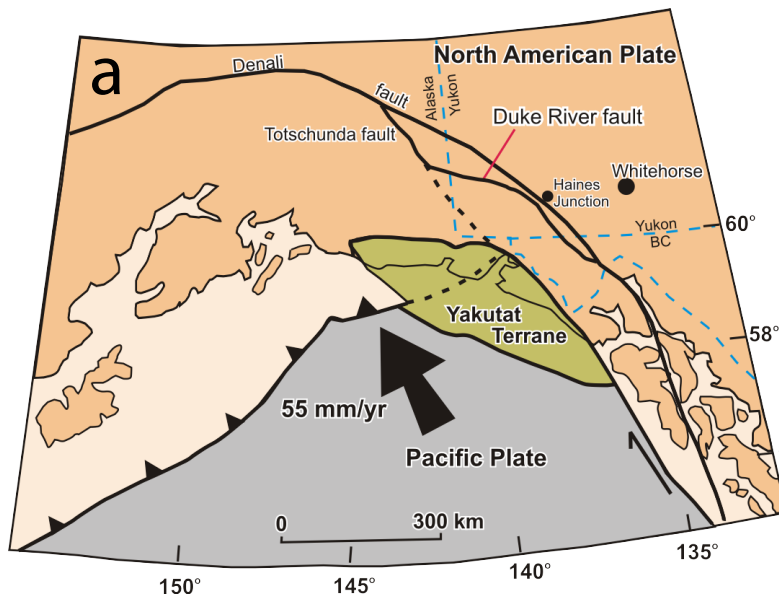
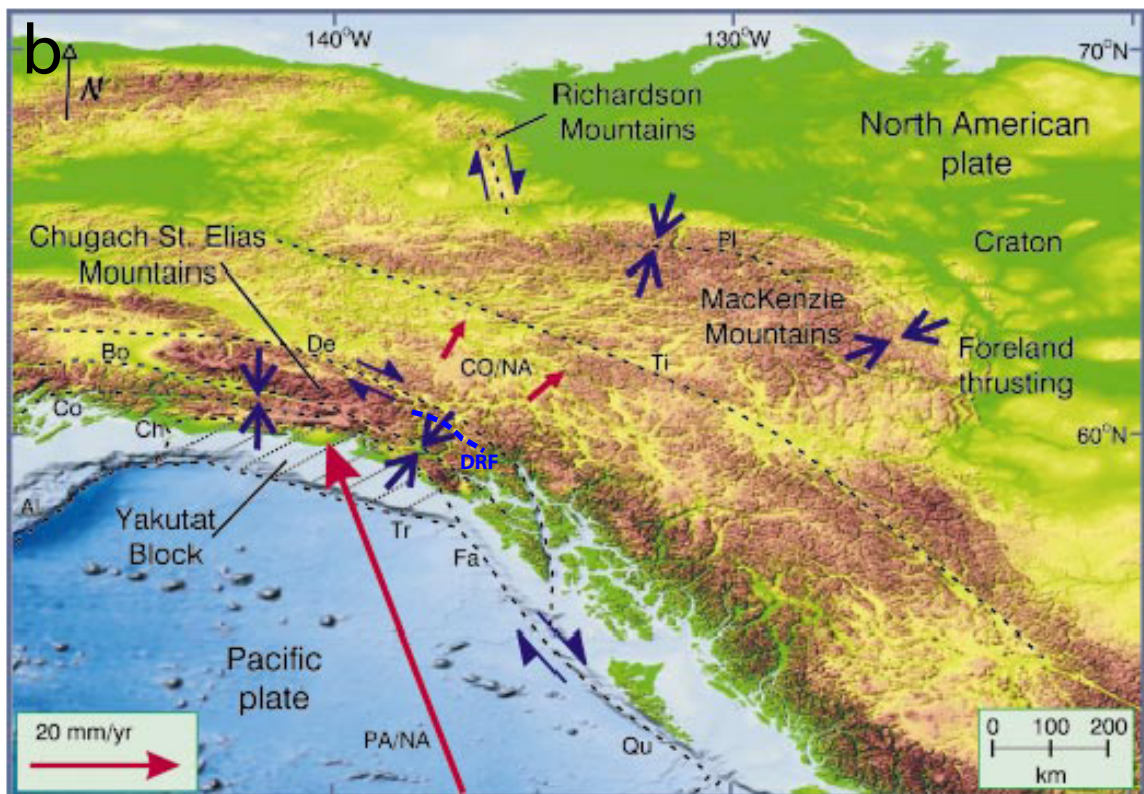


Figure 5.1. a) Diagram showing relative plate motion of the Pacific Plate, with respect to the North American Plate and the Yakutat terrane (*modified from Bruhn et al, 2004*). b) Map of northwestern Canada and eastern Alaska. Red arrows indicate Pacific- North America and northern Cordillera- North America plate motions. Dashed lines are main fault systems; Al-Aluetian trench, Bo- Border Ranges fault, Ch - Chugach-Saint Elias fault, Co-Contact Thrust, De- Denali fault, Fa - Fairweather fault, Pl -Plateau thrust, Qu - Queen Charlotte fault, Ti Tintina fault, Tr - Transition fault., DRF - Duke River fault. (*modified from Mazzotti and Hyndman, 2002*).



5.2 Pre-Tertiary Tectonic Framework of the Northern Cordillera

Based on the results of this study the Alexander terrane was situated further outboard (west in today's coordinates) than its current location. Compression and vertical stacking of the Icefield Formation within the Duke River fault imbricate zone suggest that the Alexander terrane has moved significant distance (at minimum 10's of kilometres) closer to Wrangellia prior to the Tertiary. Evidence of vertical movement on the scale of 13 kilometres is based on the difference in the degree of deformation between Wrangellia and the Alexander terrane. This vertical movement is interpreted to have been accommodated by thrust faulting along the Duke River fault and also suggests that the Alexander terrane was situated away from Wrangellia before movement along the Duke River fault.

5.3 The Role of the Duke River Fault in Northern Cordilleran Tectonics

In the northwestern Cordillera, from northern Washington to Juneau, Alaska, there is evidence of a regional mid-Cretaceous (110 -90 Ma) compressional event that affected a 1200 km long section of the Cordillera mainly along the western edge of the Coast Plutonic Complex (Crawford et al., 1987; Saleeby et al., 1990; McClelland and Mattinson, 2000; Rusmore et al., 2000). West-vergent thrust faults mapped at numerous locations along the western edge of the Coast Plutonic Complex, record deformation that began by at least 110 Ma and ceased by 90 Ma (Journeay and Friedman, 1993; Crawford et l., 1987; McClelland and Mattinson, 2000). Both east and northeast-verging thrust faults, coeval with the later phase of the west-vergent thrust systems, occur east of the Coast Plutonic Complex in British Columbia (Rusmore and Woodsworth, 1991). Similarities in the age of deformation along both the east and west verging thrust faults with the $^{40}\text{Ar}/^{39}\text{Ar}$ ages from the Duke River fault zone suggest the Duke River fault may form part of the northern extension of this penetrative phase of shortening. The northeast directed thrusting that was mapped in British Columbia is described as a series of back thrusts to an extensive west-verging thrust system (Rusmore and Woodsworth, 1991). In all

cases, as with the Duke River fault, the thrust faults emplaced rocks of relatively high metamorphic grade over rocks characterised by lower grade.

Most workers in the northern Cordillera agree that the thrust faulting that occurred all along the length of the Cordillera is related to final accretion of the Insular Superterrane to North America (Crawford et al., 1987; Saleeby et al., 1990; McClelland and Mattinson, 2000; Rusmore et al., 2000). Saleeby et al. (1990) suggest that the mid-Cretaceous thrust system that occurs between the Insular Superterrane and the Intermontane terrane either represent the closing of a marginal basin between the Insular Superterrane and the North American margin along an east dipping subduction zone or shortening and related magmatism that occurred in an intra-arc setting, above an east dipping subduction zone. McClelland and Mattison (2000) link this event to the closing of the Gravina basin that developed between the Alexander terrane the Intermontane terrane in the Late Jurassic. It seems likely that this subduction event was active all along the eastern margin of the Insular Superterrane and that the Duke River fault zone is evidence of deformation that occurred as a result of the final assembly of the Insular terrane with North America.

5.4 Conclusions and Future Work

The Duke River fault is a crustal scale structure that accommodated a pulse of thrust movement in the early Late Cretaceous. Within in an imbricate zone along the Duke River fault, development of a ductile foliation and folding of this fabric, overprints regional structures within the Icefield and Bullion formations. A later pulse of thrusting within the Duke River fault imbricate zone again accommodated significant vertical motion (8-15 kilometres) in the Miocene to Pliocene time. This crustal scale fault may be a suture zone between Wrangellia and Alexander terrane and may be linked to widespread compression that was affecting the entire Northern Cordillera from northern Washington to southwest Yukon.

To further understand the role the Duke River fault plays in the tectonic story of the Canadian and Alaskan Cordillera a detailed study of the metamorphic conditions on either side of the fault would be beneficial. Age dating of deformed plutonic rocks from within the imbricate zone at different localities along the fault would further constrain the timing of movement of the fault.

REFERENCE LIST

- Berenak, L.P., Van Staal, C., McClelland, W.C., Israel, S.A., Mihalynuk, M.G., Gordee, S.M., Joyce, N., 2010, Crustal affinity of Late Cambrian-Early Ordovician rocks in the northern Alexander terrane, northwestern Canada: Geological Society of America Abstracts with Programs, vol. 42, no. 5, p. 574.
- Beranek, L.P., van Staal, C.R., Gordee, S.M., McClelland, W.C., Israel, S. and Mihalynuk, M.G., In press. Geochemistry and stratigraphic architecture of Late Cambrian to Early Ordovician backarc rift volcanism on the Alexander terrane: implications for the origin of an Arctic realm element in the North American Cordillera. *Journal of Geology*,
- Berg, H.C., Jones, D.L., and Richter, D.H., 1972, Gravina-Nutzotin belt - Tectonic significance of an upper mesozoic sedimentary and volcanic sequence in souther and southeastern Alaska, in Survey, U.S.G., ed., U.S. Geological Survey Professional paper 800-D: College, p. 24.
- Bruhn, R.L., Pavlis, T.L., Plafker, G., and Serpa, L., 2004, Deformation during terrane accretion in the Saint Elias orogen, Alaska: Geological Society of America Bulletin, v. 116, p. 16.
- Colpron, M., Nelson, J.L., and Murphy, D.C., 2007, Northern Cordilleran terranes and their interactions through time: *GSA Today*, v. 17, p. 1-10.
- Condon, D., et al., 2007, EARTHTIME; isotopic tracers and optimized solutions for high-precision U-Pb ID-TIMS geochronology, EOS, Transactions, American Geophysical Union, 88 (52, Suppl.), Abstract V41E-06
- Coney, P.J., Jones, D.L., and Monger, J.W.H., 1980, Cordilleran suspect terranes: *Nature*, v. 288, p. 329-333.
- Crawford, M.L., Hollister, L.S., and Woodsworth, G.J., 1987, Crustal deformation and regional metamorphism across a terrane boundary, Coast Plutonic Complex, British Columbia: *Tectonics*, v. 6, p. 343-361.
- Crowley, J.L., Schoene, B., Boring, S.A., 2007. U-Pb dating of zircon in the Bishop Tuff at the millennial scale: *Geology* 35: p 1123-1126
- Dodds, C.J. and Campbell, R.B., 1992. Geology of Mount St. Elias map area (115B and C[E1/2]), Yukon Territory. Geological Survey of Canada, Open File, 2189.

- Dunlap, W., Kronenberg, A., 2001. Argon loss during deformation of micas: constraints from laboratory deformation experiments. *Contributions to Mineralogy and Petrology*. vol 141, no 2 p 174-185
- Gabrielse, H., Murphy, D.C., and Mortensen, In Press. Cretaceous and Cenozoic orogen-parallel displacements, magmatism and paleogeography in the northern Canadian Cordillera, in Haggart, J., Monger, J.W.H., and Enkin, R., eds., *Paleogeography of western North America: Constraints on latitudinal displacements*, Volume Special Paper, Geological Association of Canada.
- Gabrielse, H., Murphy, D.C. and Mortensen, J.K., 2011 Cretaceous and Cenozoic orogen-parallel displacements, magmatism and paleogeography in the northern Canadian Cordillera. In: *Paleogeography of western North America: Constraints on latitudinal displacements*, J. Haggart, J.W.H. Monger and R. Enkin (eds.), Geological Association of Canada, Special Paper,
- Gabrielse, H., and Yorath, C.J., 1991, Tectonic synthesis, Chapter 18, in Gabrielse, H., and Yorath, C.J., eds., *Geology of the Cordilleran Orogen in Canada*, Volume Geology of Canada, no. 4, Geological Survey of Canada, p. 677-705.
- Gardner, M.C., Bergman, S.C., Cushing, G.W., MacKevett, E.M., Plafker, G., Campbell, R.B., Dodds, C.J., McClelland, W.C., and Mueller, P.A., 1988, Pennsylvanian pluton stitching of Wrangellia and the the Alexander Terrane, Wrangell Mountains, Alaska: *Geology*, v. 16, p. 967-971.
- Gehrels, G. E., Saleeby, J. B., and Berg, H. C., 1983, Preliminary description of the Late Silurian–Early Devonian Klakas orogeny in the southern Alexander terrane, in Stevens, C. H., ed., *Pre-Jurassic rocks in western North American suspect terranes*: Los Angeles, Pacific Section, Society of Economic Paleontologists and Mineralogists, p. 131–141.
- Gehrels, G.E. and Saleeby, J.B., 1987. Geology of southern Prince of Wales Island, southeastern Alaska. *Geological Society of America Bulletin*, vol. 98, p. 123-137.
- Gordey, S.P., and Makepeace, A.J., 2001. Geological map of the Yukon Territory. Geological Survey of Canada Open File 3754
- Koppers, A.A.P. 2002. ArArCALC – software for $^{40}\text{Ar}/^{39}\text{Ar}$ age calculations. *Computers and Geosciences*, v. 28, 605-619.
- Gerstenberger, H., Haase, G., 1997, A highly effective emitter substance for mass spectrometric Pb isotope ratio determinations: *Chemical Geology* 136:309-312
- Greene, A.R., Scoates, J.S., Weis, D., 2008. Wrangellia flood basalts in Alaska: A record of plume-lithosphere interaction in a Late Triassic accreted oceanic plateau. *Geochemistry, Geophysics, Geosystems*, vol. 9, Q12004, doi:10.1029/2008GC002092.

- Greene, A.R., Scoates, J.S., Weis, D. and Israel, S., 2009. Geochemistry of Triassic flood basalts from the Yukon (Canada) segment of the accreted Wrangellia oceanic plateau. *Lithos*, vol. 110, p. 1-19.
- Hames, W.E., Cheney, J.T., 1997. On the loss of ^{40}Ar from muscovite during polymetamorphism. *Geochimica et Cosmochimica Acta*, vol 61, Issue 18 p 3863-3872.
- Hulbert, L.J., 1997. Geology and metallogeny of the Kluane mafic-ultramafic belt, Yukon Territory, Canada: Eastern Wrangellia - A new Ni-Cu-PGE metallogenic terrane. Geological Survey of Canada, Bulletin 506, p. 265.
- Israel, S., and Cobbett, R., 2008, Kluane Ranges bedrock geology, White River area (Parts of NTS 115F/9, 15 and 16; 115G/12 and 115K/1, 2), in Emond, D.S., Blackburn, L.R., and Weston, L.H., eds., Yukon Exploration and Geology 2007, Yukon Geological Survey, p. 16.
- Israel, S., Cobbett, R., and Fozard, C., 2007, Bedrock geology of the Miles Ridge area, Yukon (parts of NTS 115F/15, 16 and 115K/1, 2) (1:50,000 scale), Yukon Geological Survey, Open File 2007-7.
- Israel, S., Tizzard, A. and Major, J., 2006. Bedrock geology of the Duke River area, parts of NTS 115G/2, 3, 4, 6 and 7, southwestern Yukon. In: Yukon Exploration and Geology 2005, D.S. Emond, G.D. Bradshaw, L.L. Lewis and L.H. Weston (eds.), Yukon Geological Survey, p. 139-154.
- Israel, S., and van Zeyl, D., 2004, Preliminary geological map of the Quill Creek are, (parts of NTS 115G/5, 6, 12), southwest Yukon (1:50,000 scale). Yukon Geological Survey, Open File 2004-20.
- Israel, S. and Van Zeyl, D.P., 2005. Preliminary geology of the Quill Creek map area, southwest Yukon, parts of NTS 115G/5, 6, 12. In: Yukon Exploration and Geology 2004, D.S. Emond, L.L. Lewis and G.D. Bradshaw (eds.), Yukon Geological Survey, p. 129-146.
- Jaffey, A.H., Flynn, K.F., Glendenin, L.E., Bentley, W.C., and Essling, A.M., 1971, Precision measurements of half-lives and specific activities of ^{235}U and ^{238}U , *Physical Review C*, 4:1889-1906.
- Kapp, P.A., and Gehrels, G.E., 1998, Detrital zircon constraints on the tectonic evolution of the Gravina belt, southeastern Alaska: *Canadian Journal of Earth Sciences*, v. 35, p. 253-268.
- Kirchner, D.L., Cosca, M.A., Masson, H., Hunziker, J.C., 1996 Staircase $^{40}\text{Ar}/^{39}\text{Ar}$ spectra of fine-grained white mica: Timing and duration of deformation and empirical constraints on argon diffusion. *Journal of Geology*
- Krogh, T.E., 1973, A low contamination method for hydrothermal decomposition

of zircon and extraction of U and Pb for isotopic age determination: *Geochimica et Cosmochimica Acta* 37:485-494.

Ludwig, K.R., 2003. User's manual for Isoplot 3.00. Berkeley Geochronology Center: Berkeley, CA, 70 p.

MacIntyre, D.G. and Schroeter, T.G., 1984. Mineral occurrences in the Mount Henry Clay area (114P/7, 8); in *Geological Fieldwork 1984*, British Columbia Ministry of Energy Mines and Petroleum Resources, Paper 1985-1, pages 365-380.

MacKevett, E.M., 1971. Stratigraphy and general geology of the McCarthy C-5 quadrangle, Alaska. USGS, Bulletin, 1321, p. 35.

MacKevett, E.M., Jr. and Jones, D.L., 1975. Relations between Alexander and Taku-Skolai terranes in the McCarthy quadrangle. In: *Geological Survey Research 1975*, USGS, Professional Paper 975, 69 p.

Mazzotti, S., and Hyndman, R.D., 2002, Yakutat collision and strain transfer across the northwestern Canadian Cordillera: *Geological Society of America*, v. 30, p. 4.

McClelland, W.C., 1992, Permian and older rocks of the southwestern Iskut River map area, northwestern British Columbia, *Current Research, Part A, Volume Paper 92-1A*, Geological Survey of Canada, p. 303-307.

McClelland, W.C., Gehrels, G.E. and Saleeby, J.B., 1992. Upper Jurassic-Lower Cretaceous basinal strata along Cordilleran margin: Implications for the accretionary history of the Alexander-Wrangellia-Peninsular terrane. *Tectonics*, vol. 11, p. 823-835.

McClelland, W.C., and Mattinson, J.M., 2000, Cretaceous-Tertiary evolution of the western Coast Mountains, central southeastern Alaska, in Stowell, H.H., and McClelland, W.C., eds., *Tectonics of the Coast Mountains in southeast Alaska and British Columbia*, Volume Special Paper 343, Geological Society of America, p. 159-182.

Mihalynuk, M.G., Smith, M.T., MacIntyre, D.G., and Deshenes, M., 1993. Tatshenshini project, Northwestern British Columbia (114P/ 11, 12, 13, 14: 1140/9, 10, 14, 15 and 16); in *Geological Fieldwork 1992*, Grant, B. and Newell, J.M., Editors, British Columbia Ministry of Energy Mines and Petroleum Resources, Paper 1993-1, pages 189-229.

Monger, J.W.H., Price, R.A., and Templeman-Kluit, D.J., 1982, Tectonic accretion and the origin of two metamorphic and plutonic belts in the Canadian Cordillera: *Geology*, v. 10, p. 70-75.

Monger, J.W.H., and Price, R.A., 1979, Geodynamic evolution of the Canadian Cordillera - Progress and problems: *Canadian Journal of Earth Sciences*, v. 16, p. 770-791.

- Muller, J.E., 1967, Kluane Lake map-area, Yukon Territory, Geological Survey of Canada, Memoir 340, p. 137.
- Page, R.A., Biswas, N.N., Lahr, J.C., and Pulpan, H., 1991, Seismicity of continental Alaska, In Slemmons, D.B., Engdahl, E.R., Zoback, M.D., and Blackwell, D.D., eds., *Neotectonics of North America*: Boulder, Colorado: Geological Society of America, v. 1.
- Peter, J.M. and Scott, S.D., 1999. Windy Craggy, Northwestern British Columbia: The World's largest Besshi-Type deposit. In: *Volcanic-associated massive sulfide deposits: Processes and examples in modern and ancient settings*, C.T. Barrie and M.D. Hannington (eds.), Society of Economic Geologists inc., *Reviews in economic geology*, 8, p. 261-295.
- Plafker, G., Moore, J.C., and Winkler, G.R., 1994, Geology of the southern Alaska margin, in *The Geology of North America*, vol. G1, *The Geology of Alaska*, edited by G. Plafker and H.C. Berg: Geological Society of America, p. 14.
- Power, M.A., 1988, Microearthquake seismicity on the Duke River Fault, Denali Fault System: *Yukon Geology*, v. 2, p. 7.
- Price, N.J., and Cosgrove, J.W., 1990, *Analysis of Geological Structures*, Cambridge University Press
- Read, P.B., 1976, Lardeau map-area (82K west half), British Columbia, Report of Activities, Part A, Volume Paper 76-1A, Geological Survey of Canada, p. 95-96.
- Read, P.B., and Monger, J.W.H., 1976, Pre-Cenozoic volcanic assemblages of the Kluane and Alsek Ranges, southwestern Yukon Territory, Geological Survey of Canada, Open File 381, p. 96.
- Renne, P.R., Swisher, C.C., Deino, A.L., Karner, D.B., Owens, T.L., and DePaolo, D.J., 1998. Intercalibration of standards, absolute ages and uncertainties in $^{40}\text{Ar}/^{39}\text{Ar}$ dating. *Chemical Geology* 145 p 117-152
- Ridgeway, K., and Decelles, P.G., 2006, Stream dominated alluvial fan and lacustrine depositional systems in Cenozoic Strik-slip basins, Denali Fault Systems, Yukon Territory, Canada in *Sedimentology* v. 40 issue 4 p 645-666
- Ridgeway, K.D., Trop, J.M., Nokleberg, W.J., Davidson, C.M., and Eastham, K.R., 2002, Mesozoic and Cenozoic tectonics of the eastern and central Alaska Range: Progressive basin development and deformation in a suture zone, in *Geological Society of America Bulletin* v. 114 no. 12 p 1480-1504
- Roddick, J.C., 1988. The assessment of errors in $^{40}\text{Ar}/^{39}\text{Ar}$ dating. In: *Radiogenic Age and Isotopic Studies*, Report 2. Geological Survey of Canada, Paper 88-2, pp. 7–16.
- Roddick, J.C., Cliff, R.A., and Rex, D.C., 1980. The evolution of excess argon in alpine biotites — a $^{40}\text{Ar}/^{39}\text{Ar}$ analysis. *Earth and Planetary Science Letters* 48: 185–208.

- Rusmore, M.E., and Woodsworth, G.J., 1991, Coast Plutonic Complex: A mid-Cretaceous contractional orogen: *Geology*, v. 19, p. 4.
- Rusmore, M.E., Woodsworth, G.J., and Gehrels, G.E., 2000, Late Cretaceous evolution of the eastern Coast Mountains, Bella Coola, British Columbia, in Stowell, H.H., and McClelland, W.C., eds., *Tectonics of the Coast Mountains, southeastern Alaska and British Columbia*: Boulder, Colorado, Geological Society of America Special Paper 343, p. 89-105.
- Saleeby, J.B., Cowan, D.S., Brandon, M.T., and McGroder, M.F., 1990, Regionally extensive mid-Cretaceous west-vergent thrust fault system in the northwestern Cordillera: Implications for continental margin tectonism.: *Geology*, v. 18, p. 4
- Scaillet, S., 2000. Numerical error analysis in $^{40}\text{Ar}/^{39}\text{Ar}$ dating, *Chemical Geology* v.162, 269–298.
- Schmitz, M.D., Schoene, B., 2007, Derivation of isotope ratios, errors and error correlations for U-Pb geochronology using ^{205}Pb - ^{235}U -(^{233}U)-spiked isotope dilution thermal ionization mass spectrometric data: *Geochemistry, Geophysics, Geosystems* (G³) 8, Q08006, doi:10.1029/2006GC001492.
- Smith, J.G., and MacKevett, E.M., 1970, The Skolai Group in the McCarthy B-4, C-4 and C-5 quadrangles, Wrangell Mountains, Alaska, U.S. Geological Survey, Bulletin 1274-Q, 1-26 p.
- Stacey, J.S., Kramers, J.D., 1975, Approximation of terrestrial lead isotope evolution by a two-stage model: *Earth and Planetary Science Letters* 26:207-221.
- Trop, J.M., and Ridgeway, K.D., 2007, Mesozoic and Cenozoic tectonic growth of southern Alaska: A sedimentary basin perspective, in Ridgeway, K.D., Trop, J.M., Geln, J.M.G., and O'Neill, J.M., eds., *Tectonic Growth of a Collisional Continental Margin: Crustal Evolution of Southern Alaska*: Geological Society of America Special Paper 431, P. 55-94, doi : 10.1130/2007.2431(04).
- van der Heyden, P., 1992. A Middle Jurassic to early Tertiary Andean-Sierran arc model for the Coast Belt of British Columbia. *Tectonics*, vol. 11, p. 82-97.
- Van Staal, C., Berenak, L., Israel, S.A., McClelland, W.C., Mihalynuk, M.G., Nelson, J., Joyce, N., 2010, New data and ideas on the Paleozoic-Triassic evolution of the Insular Superterrane of the North American Cordillera: *Geological Society of America Abstracts with Programs*, vol. 42, no. 5, p.574
- Wheeler, J.O., 1963. Rogers Pass map-area, British Columbia and Alberta (82N W half). Geological Survey of Canada, 32 p.
- Wheeler, J.O., Brookfield, A.J., Gabrielse, H., Monger, J.W.H., Tipper, H.W. and Woodsworth, G.J., 1991. Terrane Map of the Canadian Cordillera, Geological Survey of Canada, 1713A.

Appendix I – U-Pb LA-ICPMS Data

Table . Laser ablation ICP-MS analytical data for sample 08-RC-076.

	Isotopic Ratios													
	207/235	% 1s	206/238	% 1s	rho	207/206	% 1s							
1	0.43702	0.00767	0.05684	0.00034	0.34	0.0545	0.00086							
2	0.4325	0.014	0.0572	0.00059	0.32	0.0532	0.00157							
3	0.41407	0.01177	0.05707	0.00053	0.33	0.05356	0.00139							
4	0.43709	0.01071	0.05658	0.00047	0.34	0.05501	0.00122							
5	0.42501	0.01127	0.05384	0.00048	0.34	0.05605	0.00135							
6	0.41204	0.0055	0.05508	0.00026	0.35	0.05428	0.00066							
7	0.41819	0.01264	0.05692	0.00056	0.33	0.05375	0.00148							
8	0.42215	0.01095	0.05699	0.00049	0.33	0.05304	0.00125							
9	0.43417	0.00799	0.05441	0.00035	0.35	0.05591	0.00093							
10	0.44485	0.01704	0.05637	0.00069	0.32	0.0541	0.00189							
11	0.45598	0.02094	0.05921	0.00088	0.32	0.05919	0.00249							
12	0.41393	0.00755	0.05564	0.00035	0.34	0.05319	0.00087							
13	0.4246	0.00919	0.05669	0.00043	0.35	0.05376	0.00105							
14	0.43808	0.01364	0.05568	0.00059	0.34	0.05666	0.00159							
15	0.42238	0.01289	0.05734	0.00059	0.34	0.054	0.00149							
16	0.4144	0.02046	0.05653	0.00089	0.32	0.05506	0.0025							
17	0.41999	0.01778	0.0563	0.0008	0.34	0.05232	0.00199							
18	0.41837	0.00728	0.05532	0.00034	0.35	0.05426	0.00085							
19	0.45064	0.01413	0.05643	0.00057	0.32	0.05745	0.00164							
20	0.43953	0.01701	0.05596	0.00067	0.31	0.05681	0.00202							
Isotopic Ages							Background corrected mean counts per second							
206/238	2s	207/235	2s	207/206	2s	202	204	206	207	208	232	235	238	
356.4	2.1	368.1	5.42	391.5	34.91	15	15	15326	845	1922	55988	1777	220969	
358.6	3.59	365	9.92	337.2	65.48	35	0	5026	270	529	14473	574	71980	
357.8	3.22	351.8	8.45	352.5	57.64	22	0	6032	327	674	17774	725	86568	
354.8	2.84	368.2	7.57	412.7	48.09	3	0	7000	389	645	17766	819	101293	
338.1	2.95	359.6	8.03	453.9	52.59	40	3	7263	412	990	28104	890	110376	
345.6	1.61	350.3	3.95	382.6	26.99	4	2	42062	2311	6854	183089	5153	624645	
356.9	3.43	354.8	9.05	360.3	60.87	3	0	6469	352	749	20009	773	92932	
357.3	2.99	357.6	7.82	330.3	52.36	16	0	7492	402	822	21053	875	107469	
341.6	2.15	366.1	5.66	448.5	36.1	0	0	20999	1188	3432	91937	2515	315261	
353.5	4.18	373.7	11.98	375.1	76.39	43	0	4417	241	423	10546	499	63995	
370.8	5.38	381.5	14.6	574.2	88.83	0	19	2991	179	323	7750	361	41244	
349	2.17	351.7	5.42	336.7	36.74	45	26	24687	1328	4191	117764	2950	362146	
355.4	2.59	359.3	6.55	360.8	43.41	0	0	22104	1202	3061	84402	2603	318061	
349.3	3.58	368.9	9.63	477.5	60.96	51	18	7529	431	906	25366	905	110270	
359.4	3.57	357.8	9.2	371.1	60.93	7	17	8378	457	982	24499	996	119102	
354.5	5.44	352	14.69	414.5	97.96	32	0	3679	204	375	8350	454	53044	
353.1	4.87	356	12.71	299.3	84.54	0	0	6952	367	887	23212	805	100582	
347.1	2.06	354.9	5.21	381.9	34.93	0	3	26662	1463	3817	102292	3217	392386	
353.9	3.51	377.7	9.89	508.3	62.04	0	12	5414	314	500	12671	642	78099	
351	4.1	369.9	12	483.3	77.35	2	3	3344	192	401	10495	402	48630	

Appendix II – U-Pb TIMS Data

U-Pb isotopic data.

Sample	Radiogenic Isotope Ratios														Isotopic Ages					
	Th	²⁰⁶ Pb*	mol %	Pb*	Pb _c	²⁰⁶ Pb	²⁰⁸ Pb	²⁰⁷ Pb	²⁰⁷ Pb	²⁰⁶ Pb	corr.	²⁰⁷ Pb	²⁰⁶ Pb	corr.	²⁰⁷ Pb	±	²⁰⁷ Pb	±	²⁰⁶ Pb	±
	U	x10 ⁻¹³ mol	²⁰⁶ Pb*	Pb _c	(pg)	²⁰⁴ Pb	²⁰⁶ Pb	²⁰⁶ Pb	% err	²³⁵ U	% err	²³⁸ U	% err	coef.	²⁰⁶ Pb	±	²³⁵ U	±	²³⁸ U	±
(a)	(b)	(c)	(c)	(c)	(c)	(d)	(e)	(e)	(f)	(e)	(f)	(e)	(f)		(g)	(f)	(g)	(f)	(g)	(f)
09RC151A01																				
z1*	0.420	0.1063	96.17%	7	0.35	485	0.137	0.046767	1.513	0.015475	1.602	0.002400	0.154	0.609	37.37	36.12	15.59	0.25	15.45	0.02
z2*	0.450	0.1434	91.47%	3	1.10	218	0.145	0.046314	2.604	0.015325	2.758	0.002400	0.176	0.881	14.02	62.44	15.44	0.42	15.45	0.03
z3	0.435	0.0915	93.14%	4	0.55	271	0.142	0.046824	2.490	0.015431	2.634	0.002390	0.170	0.856	40.26	59.40	15.55	0.41	15.39	0.03
z4*	0.364	0.1097	94.52%	5	0.52	340	0.117	0.046019	1.860	0.015211	1.974	0.002397	0.142	0.814	-1.37	44.72	15.33	0.30	15.43	0.02
z5*	0.348	0.1459	91.68%	3	1.09	224	0.112	0.046329	2.377	0.015335	2.525	0.002401	0.152	0.969	14.75	56.98	15.45	0.39	15.46	0.02
z6*	0.341	0.1305	92.81%	4	0.83	259	0.109	0.046058	2.357	0.015217	2.499	0.002396	0.158	0.900	0.67	56.66	15.33	0.38	15.43	0.02

(a) z1, z2, etc. are labels for analyses composed of single zircon grains that were annealed and chemically abraded (Mattinson, 2005). Fraction labels with * denote analyses used in the weighted mean calculation.

(b) Model Th/U ratio calculated from radiogenic 208Pb/206Pb ratio and 207Pb/235U date.

(c) Pb* and Pb_c are radiogenic and common Pb, respectively. mol % ²⁰⁶Pb* is with respect to radiogenic and blank Pb.

(d) Measured ratio corrected for spike and fractionation only. Fractionation correction is 0.15 ± 0.03 (1 sigma) %/amu (atomic mass unit) for single-collector Daly analyses, based on analysis of EARTHTIME 202Pb-205Pb tracer solution.

(e) Corrected for fractionation, spike, common Pb, and initial disequilibrium in 230Th/238U. Common Pb is assigned to procedural blank with composition of 206Pb/204Pb = 18.60 ± 0.80%; 207Pb/204Pb = 15.69 ± 0.32%; 208Pb/204Pb = 38.51 ± 0.74% (1 sigma). 206Pb/238U and 207Pb/206Pb ratios corrected for initial disequilibrium in 230Th/238U using Th/U [magma] = 3.

(f) Errors are 2 sigma, propagated using algorithms of Schmitz and Schoene (2007) and Crowley et al. (2007).

(g) Calculations based on the decay constants of Jaffey et al. (1971). 206Pb/238U and 207Pb/206Pb dates corrected for initial disequilibrium in 230Th/238U using Th/U [magma] = 3.

Appendix III – $^{40}\text{Ar}/^{39}\text{Ar}$ Data

Information on Analysis

08RC-024-1A muscovite

Total Fusion Age 83.00 ± 5.44
 $\pm 6.55\%$

Volumes are $1\text{E-}13\text{ cm}^3\text{ NPT}$

Neutron flux monitors: 28.02 Ma FCs (Renne et al., 1998)

Isotope production ratios: $(40\text{Ar}/39\text{Ar})\text{K}=0.0302$, $(37\text{Ar}/39\text{Ar})\text{Ca}=1416.4306$, $(36\text{Ar}/39\text{Ar})\text{Ca}=0.3952$, $\text{Ca}/\text{K}=1.83(37\text{ArCa}/39\text{ArK})$.

$J = 0.0048978 \pm 0.0000245$

25-Jul-09

Plateau Age

Plateau age = $82.8 \pm 2.7\text{ Ma}$
(2σ , including J-error of .1%)
MSWD = 1.6, probability=0.096
Includes 93.9% of the ^{39}Ar

Normal Isochron

Age = $99 \pm 63\text{ Ma}$
Initial $^{40}\text{Ar}/^{36}\text{Ar} = 217 \pm 180$
MSWD = 0.033

Reverse isochron

Age = $88 \pm 22\text{ Ma}$
Initial $^{40}\text{Ar}/^{36}\text{Ar} = 270 \pm 59$
MSWD = 3.5E+8

Incremental Heating	$^{39}\text{Ar}(\text{k})$ (cum %)	Age $\pm 2\sigma$ (Ma)	$^{40}\text{Ar}(\text{r})$ (%)	$^{39}\text{Ar}(\text{k})$ (%)	$\text{K}/\text{Ca} \pm 2\sigma$
2.00 W	0.25	152.42 ± 116.17	37.26	0.25	0.542 ± 0.215
2.20 W	1.76	58.26 ± 39.60	19.55	1.51	1.975 ± 0.585
2.40 W	4.13	40.44 ± 18.59	18.68	2.37	0.646 ± 0.060
2.70 W	11.41	75.38 ± 11.24	49.44	7.28	0.103 ± 0.004
3.00 W	20.54	87.23 ± 6.19	55.99	9.12	0.050 ± 0.002
3.30 W	39.72	92.47 ± 12.01	59.38	19.19	0.563 ± 0.026
3.60 W	64.43	84.29 ± 17.91	49.27	24.71	8.845 ± 1.132
3.90 W	75.64	82.09 ± 10.54	52.74	11.21	6.231 ± 0.485
4.20 W	82.29	74.27 ± 7.43	49.61	6.64	9.212 ± 2.307
4.50 W	89.46	83.58 ± 4.48	63.60	7.18	10.275 ± 2.441
4.80 W	93.63	92.46 ± 13.44	62.26	4.17	7.632 ± 1.867
5.10 W	95.84	77.34 ± 18.06	37.32	2.21	7.066 ± 2.666
5.50 W	98.03	79.10 ± 9.71	55.33	2.19	7.401 ± 3.047
6.00 W	100.00	66.13 ± 16.09	33.70	1.97	6.083 ± 1.448

Normal Isochron	$^{39}\text{K}/^{36}\text{Ar} \pm 2\sigma$	$^{40}\text{Ar}/^{36}\text{Ar} \pm 2\sigma$	r.i.	Inverse Isochro	$^{39}\text{K}/^{40}\text{Ar} \pm 2\sigma$	$^{36}\text{Ar}/^{40}\text{Ar} \pm 2\sigma$	r.i.
2.00 W	9.8 ± 4.2	471.2 ± 208.2	0.9455	2.00 W	0.020765 ± 0.002993	0.002122 ± 0.000938	0.2717
2.20 W	10.8 ± 1.6	367.4 ± 58.7	0.8914	2.20 W	0.029273 ± 0.002122	0.002722 ± 0.000435	0.4214
2.40 W	14.7 ± 1.5	363.5 ± 37.9	0.9382	2.40 W	0.040505 ± 0.001464	0.002751 ± 0.000287	0.2917
2.70 W	33.4 ± 3.7	585.5 ± 71.3	0.9052	2.70 W	0.056989 ± 0.002953	0.001708 ± 0.000208	0.3937
3.00 W	37.4 ± 2.8	672.9 ± 51.2	0.9294	3.00 W	0.055587 ± 0.001570	0.001486 ± 0.000113	0.2770
3.30 W	40.5 ± 5.8	729.2 ± 110.8	0.9300	3.30 W	0.055521 ± 0.003101	0.001371 ± 0.000208	0.3394
3.60 W	29.5 ± 4.6	583.4 ± 99.2	0.8947	3.60 W	0.050651 ± 0.003849	0.001714 ± 0.000291	0.4168
3.90 W	34.9 ± 4.3	626.5 ± 79.7	0.9473	3.90 W	0.055717 ± 0.002271	0.001596 ± 0.000203	0.2909
4.20 W	34.1 ± 2.8	587.4 ± 50.2	0.9223	4.20 W	0.058051 ± 0.001922	0.001702 ± 0.000146	0.3233
4.50 W	53.7 ± 4.6	814.6 ± 69.3	0.9711	4.50 W	0.065977 ± 0.001350	0.001228 ± 0.000104	0.1225
4.80 W	45.7 ± 6.5	785.2 ± 126.3	0.8782	4.80 W	0.058226 ± 0.004480	0.001274 ± 0.000205	0.4614
5.10 W	19.8 ± 2.4	471.8 ± 61.6	0.9298	5.10 W	0.041887 ± 0.002015	0.002120 ± 0.000277	0.3204
5.50 W	40.3 ± 6.2	663.0 ± 101.8	0.9921	5.50 W	0.060715 ± 0.001179	0.001508 ± 0.000232	0.0239
6.00 W	19.8 ± 1.9	446.0 ± 48.7	0.8477	6.00 W	0.044379 ± 0.002574	0.002242 ± 0.000245	0.4850

Isotope Ratios	$^{40}\text{R}/^{39}\text{K}$	1σ	$^{40}\text{R}/^{39}\text{Ar}$	1σ	$^{40}\text{Ar}/^{39}\text{Ar}$	1σ	$^{37}\text{Ar}/^{39}\text{Ar}$	1σ	$^{36}\text{Ar}/^{39}\text{Ar}$	1σ
2.00 W	17.955215	7.13500	0.03116	0.00205	48.15426	3.46790	1.00626	0.19966	0.10242	0.02176
2.20 W	6.685288	2.30851	0.13516	0.00472	34.18430	1.23791	0.27647	0.04097	0.09304	0.00674
2.40 W	4.617614	1.07340	0.15301	0.00254	24.70368	0.44602	0.84484	0.03943	0.06812	0.00339
2.70 W	8.690519	0.66146	0.33390	0.00832	17.51149	0.45282	5.30276	0.09978	0.03134	0.00167
3.00 W	10.089846	0.36680	0.42882	0.00523	17.88094	0.25168	10.93866	0.22634	0.02958	0.00098
3.30 W	10.712692	0.71359	0.90313	0.02423	18.02891	0.50266	0.96860	0.02204	0.02495	0.00176
3.60 W	9.742796	1.05915	1.27506	0.04678	19.77248	0.75016	0.06173	0.00395	0.03386	0.00262
3.90 W	9.482436	0.62278	0.52574	0.01021	17.97702	0.36579	0.08762	0.00341	0.02867	0.00174
4.20 W	8.560573	0.43727	0.29906	0.00452	17.25581	0.28521	0.05927	0.00742	0.02934	0.00119
4.50 W	9.658213	0.26488	0.28429	0.00208	15.18631	0.15521	0.05314	0.00631	0.01862	0.00079
4.80 W	10.711017	0.79844	0.18701	0.00707	17.20379	0.66069	0.07154	0.00875	0.02189	0.00156
5.10 W	8.921241	1.06435	0.13790	0.00309	23.90270	0.57434	0.07727	0.01458	0.05062	0.00313
5.50 W	9.129075	0.57276	0.09430	0.00040	16.49962	0.16011	0.07377	0.01519	0.02487	0.00192
6.00 W	7.604726	0.94191	0.11595	0.00321	22.56200	0.65344	0.08975	0.01068	0.05054	0.00242

Information on Analysis

08RC-060-1B muscovite

Total Fusion Age 238.06 ± 6.67
 $\pm 2.80\%$

Volumes are 1E-13 cm³ NPT

Neutron flux monitors: 28.02 Ma FCs (Renne et al., 1998)

Isotope production ratios: (40Ar/39Ar)K=0.0302, (37Ar/39Ar)Ca=1416.4306, (36Ar/39Ar)Ca=0.3952, Ca/K=1.83(37ArCa/39ArK).

J = 0.0048988 \pm 0.0000245

22-Jul-09

Plateau Age

Plateau age = 267.5 ± 6.4 Ma
(2 σ , including J-error of .1%)
MSWD = 1.7, probability=0.14
Includes 72.9% of the ³⁹Ar

Normal Isochron

Age = 382 ± 380 Ma
Initial ⁴⁰Ar/³⁶Ar = -43 ± 540
MSWD = 0.067

Reverse isochron

Age = 307 ± 450 Ma
Initial ⁴⁰Ar/³⁶Ar = 111 ± 690
MSWD = 0.00020

Incremental Heating	39Ar(k) (cum %)	Age \pm 2 σ (Ma)	40Ar(r) (%)	39Ar(k) (%)	K/Ca \pm 2 σ
2.00 W	0.02	225.30 \pm 3050.09	72.72	0.02	0.187 \pm 0.770
2.20 W	0.34	506.62 \pm 203.09	97.95	0.31	16.411 \pm 378.968
2.40 W	1.00	281.56 \pm 120.37	58.28	0.67	2.641 \pm 3.684
2.70 W	3.87	53.61 \pm 44.86	15.79	2.87	0.713 \pm 0.087
3.00 W	8.78	98.83 \pm 42.22	27.05	4.90	0.216 \pm 0.017
3.30 W	16.62	170.90 \pm 25.98	41.28	7.84	0.200 \pm 0.016
3.60 W	27.08	179.43 \pm 23.55	44.72	10.46	0.795 \pm 0.073
3.90 W	48.29	259.44 \pm 12.01	75.99	21.21	16.380 \pm 8.776
4.20 W	70.71	278.58 \pm 11.93	82.54	22.42	7.244 \pm 0.960
4.60 W	82.64	260.54 \pm 18.83	75.38	11.93	2.118 \pm 0.328
5.10 W	92.94	272.60 \pm 15.26	80.45	10.30	6.808 \pm 2.843
2.00 W	100.00	260.14 \pm 17.25	74.91	7.06	2.788 \pm 0.434

Normal Isochron	$^{39}\text{K}/^{36}\text{Ar} \pm 2\sigma$	$^{40}\text{Ar}/^{36}\text{Ar} \pm 2\sigma$	r.i.	Inverse Isochron	$^{39}\text{K}/^{40}\text{Ar} (\pm 2\sigma + r)$	$^{36}\text{Ar}/^{40}\text{Ar} (\pm 2\sigma + r)$	r.i.
2.00 W	29.2 ± 1112.1	1085.7 ± 41405.4	0.9991	2.00 W	0.026872 ± 0.042317	0.000921 ± 0.035125	0.0329
2.20 W	218.7 ± 4734.6	14730.8 ± 318900.7	1.0000	2.20 W	0.014847 ± 0.001790	0.000068 ± 0.001470	0.0033
2.40 W	12.0 ± 7.3	708.8 ± 435.0	0.9874	2.40 W	0.016954 ± 0.001647	0.001411 ± 0.000866	0.1300
2.70 W	9.0 ± 1.4	350.9 ± 54.7	0.9279	2.70 W	0.025716 ± 0.001502	0.002849 ± 0.000444	0.2784
3.00 W	9.6 ± 1.4	405.2 ± 62.5	0.9222	3.00 W	0.023610 ± 0.001410	0.002468 ± 0.000381	0.3340
3.30 W	10.3 ± 1.0	503.5 ± 51.3	0.9338	3.30 W	0.020418 ± 0.000746	0.001986 ± 0.000202	0.2955
3.60 W	11.2 ± 0.9	534.8 ± 45.9	0.8039	3.60 W	0.021013 ± 0.001083	0.001870 ± 0.000160	0.4704
3.90 W	29.8 ± 3.7	1233.6 ± 153.7	0.9786	3.90 W	0.024148 ± 0.000621	0.000811 ± 0.000101	0.1326
4.20 W	41.2 ± 7.4	1698.0 ± 305.6	0.9917	4.20 W	0.024294 ± 0.000564	0.000589 ± 0.000106	0.0884
4.60 W	28.7 ± 6.0	1203.1 ± 252.5	0.9894	4.60 W	0.023846 ± 0.000728	0.000831 ± 0.000174	0.1011
5.10 W	36.8 ± 7.1	1516.1 ± 294.7	0.9857	5.10 W	0.024241 ± 0.000797	0.000660 ± 0.000128	0.1107
2.00 W	28.0 ± 4.8	1180.1 ± 203.9	0.9807	2.00 W	0.023735 ± 0.000802	0.000847 ± 0.000146	0.1531

Isotope Ratios		$^{40}\text{Ar}/^{39}\text{Ar}$	1 σ	$^{40}\text{Ar}/^{39}\text{Ar}$	1 σ	$^{40}\text{Ar}/^{39}\text{Ar}$	1 σ	$^{37}\text{Ar}/^{39}\text{Ar}$	1 σ	$^{36}\text{Ar}/^{39}\text{Ar}$	1 σ
22JUL201	2.00 W	27.084838	194.99662	0.00061	0.00043	37.16644	29.23257	2.92136	6.03090	0.03514	0.65188
22JUL202	2.20 W	66.004035	15.16941	0.01577	0.00073	67.38379	4.06074	0.03327	0.38415	0.00462	0.04949
22JUL203	2.40 W	34.391915	7.93838	0.02940	0.00129	59.00499	2.86471	0.20674	0.14420	0.08330	0.02533
22JUL204	2.70 W	6.142882	2.60795	0.08333	0.00210	38.89473	1.13487	0.76541	0.04690	0.11097	0.00833
22JUL205	3.00 W	11.466330	2.51715	0.15515	0.00430	42.30906	1.26235	2.52622	0.10230	0.10505	0.00760
22JUL206	3.30 W	20.232544	1.61198	0.28689	0.00476	48.91283	0.89248	2.72513	0.11165	0.09785	0.00473
22JUL207	3.60 W	21.293285	1.46784	0.37180	0.00848	47.59582	1.22634	0.68619	0.03163	0.08914	0.00340
22JUL208	3.90 W	31.491815	0.78222	0.65612	0.00676	41.44098	0.53223	0.03333	0.00893	0.03358	0.00208
22JUL209	4.20 W	33.999435	0.78524	0.68917	0.00662	41.19109	0.47815	0.07537	0.00499	0.02426	0.00218
22JUL210	4.60 W	31.635722	1.22746	0.37367	0.00475	41.95883	0.63978	0.25776	0.01998	0.03493	0.00364
22JUL211	5.10 W	33.212635	1.00143	0.31744	0.00422	41.28086	0.67801	0.08020	0.01674	0.02723	0.00263
22JUL212	2.00 W	31.582843	1.12431	0.22219	0.00332	42.15713	0.71187	0.19579	0.01525	0.03576	0.00305

Information on Analysis

08RC-028-1 muscovite

Total Fusion Age 83.02 ± 4.18
 $\pm 5.04\%$

Volumes are 1E-13 cm³ NPT

Neutron flux monitors: 28.02 Ma FCs (Renne et al., 1998)

Isotope production ratios: (40Ar/39Ar)K=0.0302, (37Ar/39Ar)Ca=1416.4306, (36Ar/39Ar)Ca=0.3952, Ca/K=1.83(37ArCa/39ArK).

J = 0.0048978 \pm 0.0000245

02-Aug-09

Plateau Age

Plateau age = 90.1 ± 4.3 Ma
(2 σ , including J-error of .1%)
MSWD = 0.51, probability=0.80
Includes 81.1% of the ³⁹Ar

Normal Isochron

Age = 99 ± 130 Ma
Initial ⁴⁰Ar/³⁶Ar = 75 ± 470
MSWD = 0.034

Reverse isochron

Age = 95 ± 55 Ma
Initial ⁴⁰Ar/³⁶Ar = 166 ± 110
MSWD = 5.9E+6

Incremental Heating	39Ar(k) (cum %)	Age $\pm 2\sigma$ (Ma)	40Ar(r) (%)	39Ar(k) (%)	K/Ca $\pm 2\sigma$
2.00 W	0.10	-157.87 \pm 76.32	3936.22	0.10	3.149 \pm 4.312
2.20 W	0.79	-6.36 \pm 27.40	7.67	0.69	4.004 \pm 1.830
2.40 W	2.57	39.89 \pm 14.89	44.12	1.78	10.433 \pm 2.886
2.70 W	9.28	77.62 \pm 8.69	80.57	6.70	9.576 \pm 1.941
3.00 W	23.71	91.36 \pm 8.38	81.71	14.43	12.504 \pm 2.631
3.20 W	39.14	89.79 \pm 10.92	74.42	15.44	12.120 \pm 1.906
3.30 W	50.25	96.55 \pm 10.90	80.42	11.11	19.294 \pm 2.077
3.40 W	59.90	86.22 \pm 12.18	68.60	9.65	10.877 \pm 1.379
3.60 W	71.38	90.23 \pm 11.25	74.27	11.48	13.681 \pm 3.074
3.80 W	85.56	86.15 \pm 17.56	63.09	14.18	6.730 \pm 0.618
3.90 W	90.37	82.32 \pm 15.76	66.47	4.81	5.634 \pm 0.828
4.10 W	93.89	59.59 \pm 17.78	45.57	3.52	1.993 \pm 0.282
4.40 W	96.26	56.12 \pm 15.92	44.94	2.37	1.140 \pm 0.068
4.80 W	97.80	31.37 \pm 21.48	23.81	1.54	0.591 \pm 0.044
5.30 W	99.09	45.48 \pm 19.34	34.10	1.29	0.292 \pm 0.013
6.00 W	100.00	9.50 \pm 26.57	7.93	0.91	0.144 \pm 0.010

Normal Isochron	39(k)/36(a) ± 2σ		λ(a+r)/36(a) ± 2σ		r.i.	Inverse Isochron	39(k)/40(a ± 2σ +r)		36(a)/40(a ± 2σ +r)		r.i.
2.00 W	16.9 ± 7.1		6.8 ± 50.0		0.0564	2.00 W	2.478737 ± 18.151637		0.146561 ± 1.074964		0.9984
2.20 W	29.5 ± 8.0		274.4 ± 85.8		0.8600	2.20 W	0.107334 ± 0.017129		0.003645 ± 0.001140		0.4927
2.40 W	51.5 ± 11.2		530.0 ± 129.0		0.8678	2.40 W	0.097153 ± 0.011763		0.001887 ± 0.000459		0.4530
2.70 W	138.8 ± 42.9		1538.4 ± 487.5		0.9744	2.70 W	0.090227 ± 0.006429		0.000650 ± 0.000206		0.2184
3.00 W	126.4 ± 39.4		1632.7 ± 515.8		0.9859	3.00 W	0.077411 ± 0.004091		0.000612 ± 0.000194		0.1603
3.20 W	83.4 ± 21.8		1162.4 ± 312.6		0.9694	3.20 W	0.071750 ± 0.004740		0.000860 ± 0.000231		0.2294
3.30 W	109.6 ± 35.8		1522.8 ± 507.0		0.9780	3.30 W	0.071974 ± 0.005001		0.000657 ± 0.000219		0.1969
3.40 W	65.2 ± 14.7		945.5 ± 222.2		0.9527	3.40 W	0.068950 ± 0.004926		0.001058 ± 0.000249		0.2886
3.60 W	82.4 ± 21.6		1155.8 ± 312.3		0.9674	3.60 W	0.071255 ± 0.004877		0.000865 ± 0.000234		0.2395
3.80 W	51.0 ± 13.1		803.3 ± 218.5		0.9391	3.80 W	0.063450 ± 0.005934		0.001245 ± 0.000339		0.3294
3.90 W	62.0 ± 17.7		885.0 ± 263.8		0.9526	3.90 W	0.070049 ± 0.006356		0.001130 ± 0.000337		0.2874
4.10 W	36.3 ± 6.7		543.9 ± 112.7		0.8828	4.10 W	0.066755 ± 0.006499		0.001839 ± 0.000381		0.4531
4.40 W	37.6 ± 6.1		537.6 ± 100.0		0.8531	4.40 W	0.069979 ± 0.006794		0.001860 ± 0.000346		0.4997
4.80 W	25.9 ± 4.6		388.1 ± 77.4		0.8621	4.80 W	0.066775 ± 0.006756		0.002577 ± 0.000514		0.4754
5.30 W	29.5 ± 4.1		448.9 ± 80.9		0.7587	5.30 W	0.065695 ± 0.007717		0.002228 ± 0.000402		0.6254
6.00 W	23.7 ± 5.0		321.0 ± 76.2		0.8771	6.00 W	0.073867 ± 0.008433		0.003115 ± 0.000740		0.4441
Additional Parameters	40(r)/39(k)	1σ	40(r+a)	1σ	40Ar/39Ar	1σ	37Ar/39Ar	1σ	36Ar/39Ar	1σ	
2.00 W	17.068666	3.94818	0.00023	0.00086	0.43368	1.47734	0.17338	0.11870	0.05910	0.01240	
2.20 W	0.717161	1.54132	0.03859	0.00303	9.34598	0.74342	0.13633	0.03115	0.03400	0.00462	
2.40 W	4.554195	0.85922	0.10964	0.00633	10.32289	0.62328	0.05233	0.00724	0.01944	0.00211	
2.70 W	8.954204	0.51238	0.44373	0.01558	11.11288	0.39484	0.05702	0.00578	0.00722	0.00111	
3.00 W	10.580080	0.49765	1.11363	0.02880	12.94793	0.34136	0.04366	0.00459	0.00792	0.00123	
3.20 W	10.394326	0.64799	1.28515	0.04103	13.96711	0.46042	0.04505	0.00354	0.01200	0.00157	
3.30 W	11.197707	0.64927	0.92222	0.03112	13.92374	0.48278	0.02830	0.00152	0.00913	0.00149	
3.40 W	9.970518	0.72114	0.83595	0.02909	14.53288	0.51814	0.05019	0.00318	0.01535	0.00173	
3.60 W	10.446101	0.66759	0.96260	0.03203	14.06381	0.48035	0.03991	0.00448	0.01215	0.00159	
3.80 W	9.962577	1.03959	1.33504	0.06110	15.78963	0.73693	0.08113	0.00373	0.01964	0.00252	
3.90 W	9.509086	0.93114	0.41019	0.01808	14.30504	0.64770	0.09691	0.00712	0.01616	0.00230	
4.10 W	6.840806	1.03753	0.31494	0.01505	15.00745	0.72914	0.27391	0.01939	0.02762	0.00254	
4.40 W	6.435496	0.92711	0.20245	0.00962	14.31543	0.69351	0.47896	0.01436	0.02671	0.00214	
4.80 W	3.573281	1.23373	0.13771	0.00674	14.99611	0.75718	0.92379	0.03454	0.03882	0.00339	
5.30 W	5.200644	1.11969	0.11736	0.00675	15.23202	0.89288	1.86496	0.04236	0.03439	0.00238	
6.00 W	1.075465	1.50793	0.07335	0.00402	13.53189	0.77071	3.78311	0.12526	0.04312	0.00448	

Information on Analysis

08RC024-1B muscovite

Total Fusion Age 104.89 ± 2.45
 $\pm 2.34\%$

Volumes are 1E-13 cm³ NPT

Neutron flux monitors: 28.02 Ma FCs (Renne et al., 1998)

Isotope production ratios: (40Ar/39Ar)K=0.0302, (37Ar/39Ar)Ca=1416.4306, (36Ar/39Ar)Ca=0.3952, Ca/K=1.83(37ArCa/39ArK).

J = 0.0048990 \pm 0.0000245

21-Jul-09

Plateau Age

Plateau age = 104.6 ± 2.2 Ma
(2 σ , including J-error of .1%)
MSWD = 0.95, probability=0.45
Includes 90.4% of the ³⁹Ar

Normal Isochron

Age = 125 ± 140 Ma
Initial ⁴⁰Ar/³⁶Ar = 191 ± 96
MSWD = 0.017

Reverse isochron

Age = 107.8 ± 7.5 Ma
Initial ⁴⁰Ar/³⁶Ar = 221 ± 21
MSWD = 2.2E+8

Incremental Heating	³⁹ Ar(k) (cum %)	Age $\pm 2\sigma$ (Ma)	⁴⁰ Ar(r) (%)	³⁹ Ar(k) (%)	K/Ca $\pm 2\sigma$
2.00 W	0.00	99.93 \pm 879.43	5.20	0.00	0.422 \pm 1.000
2.20 W	0.01	-188.79 \pm 127.10	27.12	0.01	1.590 \pm 1.647
2.40 W	0.06	-129.74 \pm 102.71	21.17	0.05	0.735 \pm 0.072
2.60 W	0.16	-5.03 \pm 122.18	1.09	0.10	0.457 \pm 0.028
2.90 W	0.33	33.11 \pm 60.07	10.92	0.17	0.091 \pm 0.003
3.20 W	0.56	39.07 \pm 71.48	13.29	0.23	0.094 \pm 0.003
3.50 W	1.11	70.64 \pm 62.44	28.90	0.55	9.572 \pm 1.260
3.80 W	2.04	80.93 \pm 25.36	38.56	0.93	27.880 \pm 3.723
4.00 W	15.92	103.72 \pm 6.18	97.97	13.88	19.842 \pm 17.076
4.30 W	33.92	102.40 \pm 4.47	96.76	18.00	22.915 \pm 10.041
4.60 W	51.65	103.39 \pm 4.37	96.13	17.73	11.349 \pm 3.437
5.00 W	71.25	105.44 \pm 4.45	96.11	19.60	17.709 \pm 6.596
5.40 W	83.61	107.77 \pm 6.62	94.83	12.36	20.709 \pm 11.166
5.80 W	92.45	111.66 \pm 9.27	93.30	8.84	9.742 \pm 4.312
6.20 W	100.00	114.41 \pm 10.69	91.68	7.55	6.842 \pm 2.948

Normal Isochron	$^{39}\text{K}/^{36}\text{Ar} \pm 2\sigma$	$^{40}\text{Ar}/^{36}\text{Ar} \pm 2\sigma$	r.i.	Inverse Isochron	$^{39}\text{K}/^{40}\text{Ar} (\pm 2\sigma + r)$	$^{36}\text{Ar}/^{40}\text{Ar} (\pm 2\sigma + r)$	r.i.
2.00 W	1.4 ± 0.8	311.7 ± 151.9	0.6078	2.00 W	0.004487 ± 0.002067	0.003208 ± 0.001564	0.3376
2.20 W	3.1 ± 0.3	232.4 ± 36.2	0.5174	2.20 W	0.013406 ± 0.001832	0.004302 ± 0.000671	0.7243
2.40 W	3.7 ± 0.3	243.9 ± 37.7	0.3589	2.40 W	0.014986 ± 0.002202	0.004101 ± 0.000634	0.8483
2.60 W	5.6 ± 1.1	292.3 ± 77.2	0.7322	2.60 W	0.019320 ± 0.003476	0.003421 ± 0.000904	0.6745
2.90 W	9.6 ± 1.6	331.8 ± 71.0	0.7772	2.90 W	0.028971 ± 0.003902	0.003014 ± 0.000645	0.6210
3.20 W	10.2 ± 2.1	340.8 ± 91.1	0.7829	3.20 W	0.029839 ± 0.004963	0.002934 ± 0.000784	0.6168
3.50 W	14.8 ± 3.8	415.8 ± 131.3	0.8000	3.50 W	0.035578 ± 0.006739	0.002405 ± 0.000759	0.5951
3.80 W	19.9 ± 3.1	481.3 ± 83.1	0.8792	3.80 W	0.041324 ± 0.003398	0.002078 ± 0.000358	0.4583
4.00 W	1347.3 ± 4224.7	16531.7 ± 51836.7	1.0000	4.00 W	0.081500 ± 0.001808	0.000060 ± 0.000190	0.0041
4.30 W	803.3 ± 974.4	9848.7 ± 11945.9	0.9998	4.30 W	0.081562 ± 0.001992	0.000102 ± 0.000123	0.0084
4.60 W	651.3 ± 667.2	8118.2 ± 8316.7	0.9998	4.60 W	0.080226 ± 0.001561	0.000123 ± 0.000126	0.0092
5.00 W	634.3 ± 644.9	8068.8 ± 8203.6	0.9998	5.00 W	0.078607 ± 0.001530	0.000124 ± 0.000126	0.0089
5.40 W	452.6 ± 499.5	5969.4 ± 6587.4	0.9997	5.40 W	0.075827 ± 0.001944	0.000168 ± 0.000185	0.0158
5.80 W	327.3 ± 366.2	4550.9 ± 5091.0	0.9995	5.80 W	0.071918 ± 0.002512	0.000220 ± 0.000246	0.0133
6.20 W	250.6 ± 255.9	3637.2 ± 3715.2	0.9995	6.20 W	0.068911 ± 0.002185	0.000275 ± 0.000281	0.0246

Isotope Ratios	$^{40}\text{Ar}/^{39}\text{Ar}$	1 σ	$^{40}\text{Ar}/^{39}\text{Ar}$	1 σ	$^{40}\text{Ar}/^{39}\text{Ar}$	1 σ	$^{37}\text{Ar}/^{39}\text{Ar}$	1 σ	$^{36}\text{Ar}/^{39}\text{Ar}$	1 σ
2.00 W	11.598167	52.45509	0.00013	0.00002	222.70982	51.26268	1.29392	1.53452	0.71476	0.19500
2.20 W	20.235601	6.46240	0.00039	0.00002	74.60428	5.09472	0.34327	0.17773	0.32094	0.01766
2.40 W	14.132536	5.39582	0.00275	0.00019	66.72379	4.89922	0.74255	0.03617	0.27372	0.01140
2.60 W	0.566753	6.87650	0.00450	0.00040	51.74575	4.65182	1.19423	0.03596	0.17727	0.01725
2.90 W	3.772046	3.45302	0.00511	0.00034	34.40205	2.31436	5.97926	0.10797	0.10528	0.00869
3.20 W	4.458471	4.12268	0.00654	0.00054	33.40629	2.77577	5.76841	0.10668	0.09954	0.01030
3.50 W	8.131218	3.66434	0.01305	0.00123	28.13594	2.66199	0.05704	0.00375	0.06762	0.00858
3.80 W	9.342852	1.49712	0.01898	0.00077	24.22883	0.99489	0.01958	0.00131	0.05028	0.00386
4.00 W	12.050635	0.36942	0.14427	0.00121	12.29992	0.13621	0.02752	0.01184	0.00075	0.00116
4.30 W	11.892787	0.26723	0.18684	0.00147	12.29065	0.14994	0.02383	0.00522	0.00125	0.00076
4.60 W	12.011091	0.26107	0.18715	0.00127	12.49458	0.12138	0.04811	0.00728	0.00155	0.00079
5.00 W	12.255629	0.26612	0.21117	0.00140	12.75145	0.12395	0.03083	0.00574	0.00159	0.00080
5.40 W	12.535098	0.39676	0.13806	0.00146	13.21789	0.16920	0.02637	0.00711	0.00222	0.00122
5.80 W	13.001915	0.55645	0.10407	0.00118	13.93444	0.24311	0.05604	0.01240	0.00307	0.00171
6.20 W	13.332448	0.64301	0.09282	0.00131	14.54080	0.23009	0.07980	0.01719	0.00401	0.00204

Information on Analysis

08RC-071-1 muscovite

Total Fusion Age 241.40 ± 6.81
 $\pm 2.82\%$

Volumes are 1E-13 cm³ NPT

Neutron flux monitors: 28.02 Ma FCs (Renne et al., 1998)

Isotope production ratios: (40Ar/39Ar)K=0.0302, (37Ar/39Ar)Ca=1416.4306, (36Ar/39Ar)Ca=0.3952, Ca/K=1.83(37ArCa/39ArK).

J = 0.0048964 \pm 0.0000245

01-Aug-09

Plateau Age

Plateau age = 256.8 ± 6.6 Ma
(2 σ , including J-error of .1%)
MSWD = 1.3, probability=0.26
Includes 74.9% of the ³⁹Ar

Normal Isochron

Age = 259 ± 300 Ma
Initial ⁴⁰Ar/³⁶Ar = 40 ± 750
MSWD = 0.0042

Reverse isochron

Age = 257 ± 76 Ma
Initial ⁴⁰Ar/³⁶Ar = 113 ± 76
MSWD = 1.5E+8

Incremental Heating	39Ar(k) (cum %)	Age $\pm 2\sigma$ (Ma)	40Ar(r) (%)	39Ar(k) (%)	K/Ca $\pm 2\sigma$
2.00 W	0.01	-608.14 \pm 3795.71	109.10	0.01	0.058 \pm 0.126
2.20 W	0.11	332.26 \pm 198.85	72.77	0.10	0.440 \pm 0.591
2.40 W	0.51	111.57 \pm 61.67	39.96	0.40	5.822 \pm 12.252
2.70 W	2.85	164.61 \pm 19.81	64.14	2.34	4.936 \pm 2.359
3.00 W	8.14	233.76 \pm 11.19	88.11	5.29	7.123 \pm 3.520
3.40 W	16.07	203.37 \pm 12.23	79.35	7.94	5.643 \pm 2.338
3.70 W	36.48	247.02 \pm 21.37	82.39	20.41	18.357 \pm 7.425
3.80 W	48.33	233.52 \pm 24.10	75.78	11.84	8.595 \pm 3.240
4.00 W	63.01	259.63 \pm 15.23	84.97	14.68	15.694 \pm 9.007
4.20 W	73.27	256.66 \pm 18.09	83.59	10.26	17.122 \pm 10.588
4.50 W	83.38	264.90 \pm 12.10	86.45	10.11	17.291 \pm 4.383
4.90 W	90.98	255.54 \pm 14.20	83.64	7.60	13.466 \pm 7.003
5.30 W	94.41	209.28 \pm 22.23	70.12	3.43	5.866 \pm 1.635
5.80 W	98.29	244.48 \pm 18.37	82.48	3.88	9.036 \pm 6.478
6.30 W	100.00	160.63 \pm 29.93	55.77	1.71	2.572 \pm 1.003

Normal Isochron	39(k)/36(a) ± 2σ)(a+r)/36(a) ± 2σ		r.i.	Inverse Isochron	39(k)/40(a ± 2σ +r)		36(a)/40(a ± 2σ +r)		r.i.
2.00 W	2.6 ± 6.8		141.3 ± 561.2		0.4105	2.00 W	0.018716 ± 0.070070		0.007078 ± 0.028120		0.7788
2.20 W	19.2 ± 21.2		1086.9 ± 1247.2		0.9409	2.20 W	0.017676 ± 0.006882		0.000920 ± 0.001056		0.2819
2.40 W	15.2 ± 5.2		492.5 ± 173.8		0.9487	2.40 W	0.030775 ± 0.003437		0.002030 ± 0.000717		0.2729
2.70 W	27.2 ± 5.0		825.6 ± 155.7		0.9650	2.70 W	0.032989 ± 0.001632		0.001211 ± 0.000228		0.2267
3.00 W	78.3 ± 20.9		2503.2 ± 669.3		0.9923	3.00 W	0.031293 ± 0.001035		0.000399 ± 0.000107		0.0973
3.40 W	46.9 ± 8.9		1436.6 ± 275.3		0.9851	3.40 W	0.032675 ± 0.001076		0.000696 ± 0.000133		0.1526
3.70 W	46.5 ± 13.7		1684.5 ± 502.3		0.9811	3.70 W	0.027584 ± 0.001593		0.000594 ± 0.000177		0.1648
3.80 W	32.9 ± 8.2		1223.0 ± 309.2		0.9704	3.80 W	0.026938 ± 0.001646		0.000818 ± 0.000207		0.1907
4.00 W	53.3 ± 12.5		1974.7 ± 468.7		0.9844	4.00 W	0.026968 ± 0.001127		0.000506 ± 0.000120		0.1357
4.20 W	48.6 ± 13.4		1808.4 ± 502.8		0.9861	4.20 W	0.026861 ± 0.001242		0.000553 ± 0.000154		0.1250
4.50 W	58.9 ± 11.9		2192.2 ± 447.3		0.9861	4.50 W	0.026853 ± 0.000912		0.000456 ± 0.000093		0.1159
4.90 W	49.0 ± 11.8		1813.5 ± 435.4		0.9902	4.90 W	0.027002 ± 0.000908		0.000551 ± 0.000132		0.0746
5.30 W	27.8 ± 5.9		991.0 ± 213.7		0.9727	5.30 W	0.028008 ± 0.001403		0.001009 ± 0.000218		0.1917
5.80 W	47.3 ± 14.2		1693.2 ± 509.4		0.9894	5.80 W	0.027920 ± 0.001220		0.000591 ± 0.000178		0.0897
6.30 W	19.7 ± 4.1		668.8 ± 145.0		0.9615	6.30 W	0.029420 ± 0.001754		0.001495 ± 0.000324		0.2380

Isotope Ratios	40(r)/39(k)		1σ	40(r+a)		1σ	40Ar/39Ar		1σ	37Ar/39Ar		1σ	36Ar/39Ar		1σ
2.00 W	58.326817		153.12925	0.00097		0.00165	53.10535		99.24669	9.38109		10.20033	0.37831		0.48383
2.20 W	41.193715		13.49387	0.00987		0.00175	56.55560		11.00305	1.24080		0.83447	0.05240		0.02868
2.40 W	12.997383		3.70432	0.02353		0.00122	32.52165		1.81433	0.09377		0.09867	0.06616		0.01121
2.70 W	19.463575		1.22557	0.12754		0.00293	30.34106		0.75001	0.11062		0.02643	0.03682		0.00337
3.00 W	28.183506		0.71938	0.30389		0.00446	31.98432		0.52873	0.07665		0.01894	0.01279		0.00170
3.40 W	24.309562		0.77305	0.43683		0.00678	30.63272		0.50379	0.09675		0.02004	0.02134		0.00202
3.70 W	29.893673		1.38364	1.33110		0.03546	36.28263		1.04720	0.02974		0.00602	0.02153		0.00317
3.80 W	28.152908		1.54834	0.79075		0.02146	37.15132		1.13442	0.06352		0.01197	0.03037		0.00377
4.00 W	31.532705		0.99282	0.97949		0.01797	37.11096		0.77511	0.03479		0.00998	0.01879		0.00221
4.20 W	31.145297		1.17724	0.68724		0.01377	37.25790		0.86085	0.03189		0.00986	0.02060		0.00284
4.50 W	32.219808		0.79132	0.67705		0.00959	37.26905		0.63218	0.03158		0.00400	0.01700		0.00172
4.90 W	30.999568		0.92368	0.50643		0.00622	37.06336		0.62315	0.04055		0.01054	0.02044		0.00245
5.30 W	25.058070		1.40963	0.21999		0.00501	35.73218		0.89427	0.09307		0.01297	0.03606		0.00381
5.80 W	29.565651		1.18768	0.24978		0.00429	35.84504		0.78298	0.06043		0.02166	0.02118		0.00317
6.30 W	18.971801		1.84691	0.10481		0.00291	34.01566		1.01338	0.21223		0.04138	0.05090		0.00536

CO₂ laser step-heating ⁴⁰Ar/³⁹Ar data^e. All uncertainties quoted at 2s level.

Power ^a	Volume ³⁹ Ar x10 ⁻¹¹ cc	³⁶ Ar/ ³⁹ Ar	±	³⁷ Ar/ ³⁹ Ar	±	³⁸ Ar/ ³⁹ Ar	±	⁴⁰ Ar/ ³⁹ Ar	±	% ⁴⁰ Ar ATM	⁴⁰ Ar/ ³⁹ Ar	±	f ₃₉ ^b (%)	Apparent Age Ma ^c	±
09RC044A01 Whole Rock; J=.00733140 ^d (Z10196; 0.0000-N 0.0000-E)															
Aliquot: A															
2.6*	0.0319	0.0328	0.0005	0.8640	0.0110	0.1540	0.0110	22.570	0.108	42.9	12.885	0.174	3.3	162.9	2.1
3.2	0.0762	0.0040	0.0003	0.5150	0.0060	0.0140	0.0110	10.168	0.052	11.7	8.978	0.094	7.8	115.0	1.2
3.8	0.1021	0.0033	0.0002	0.3450	0.0040	-0.0110	-0.0110	10.950	0.051	8.8	9.989	0.069	10.5	127.5	0.9
4.2*	0.0543	0.0028	0.0003	0.5080	0.0070	-0.0110	-0.0110	10.416	0.095	7.9	9.590	0.140	5.6	122.6	1.7
4.6*	0.0528	0.0014	0.0004	0.5310	0.0070	0.0070	0.0110	9.711	0.072	4.1	9.310	0.127	5.4	119.1	1.6
5.0	0.0483	0.0050	0.0004	1.1690	0.0120	0.0120	0.0110	9.314	0.075	15.9	7.830	0.145	5.0	100.7	1.8
5.5*	0.0799	0.0034	0.0011	6.6830	0.0630	-0.0120	-0.0110	10.788	0.064	9.3	9.780	0.346	8.2	124.9	4.3
5.8*	0.0818	0.0021	0.0012	6.8400	0.0660	-0.0110	-0.0110	10.017	0.052	6.3	9.386	0.350	8.4	120.1	4.3
6.2*	0.1883	0.0009	0.0010	5.9590	0.0550	-0.0110	-0.0110	9.690	0.027	2.7	9.430	0.298	19.3	120.6	3.7
6.5*	0.0837	0.0007	0.0008	4.3570	0.0460	-0.0110	-0.0110	9.531	0.050	2.1	9.326	0.230	8.6	119.3	2.8
7.0*	0.0554	0.0006	0.0005	2.9810	0.0310	-0.0110	-0.0110	9.570	0.051	1.9	9.390	0.165	5.7	120.1	2.0
15.0*	0.1196	0.0021	0.0016	9.4470	0.0970	-0.0110	-0.0110	10.807	0.048	5.8	10.178	0.473	12.3	129.8	5.8
09RC063A01 Muscovite; J=.00732810 ^d (Z10197; 0.0000-N 0.0000-E)															
Aliquot: A															
2.6	0.0214	0.0209	0.0006	1.1650	0.0150	0.0150	0.0110	11.768	0.075	52.6	5.579	0.193	1.3	72.3	2.5
3.2	0.0244	0.0069	0.0010	5.4090	0.0590	0.0040	0.0110	8.579	0.064	23.7	6.544	0.304	1.5	84.5	3.8
3.8	0.0942	0.0042	0.0034	19.9750	0.2110	-0.0120	-0.0110	8.889	0.060	14.1	7.639	0.994	5.9	98.3	12.5
4.2	0.1641	0.0007	0.0003	1.9380	0.0210	-0.0110	-0.0110	9.495	0.034	2.2	9.285	0.107	10.3	118.8	1.3
4.6*	0.2702	0.0003	0.0001	0.1590	0.0020	-0.0110	-0.0110	10.153	0.024	0.9	10.066	0.032	16.9	128.4	0.4
5.0*	0.3109	0.0002	0.0001	0.1060	0.0020	-0.0110	-0.0110	10.214	0.021	0.7	10.146	0.027	19.4	129.4	0.3
5.4*	0.1613	0.0003	0.0001	0.0900	0.0020	-0.0110	-0.0110	9.998	0.030	0.8	9.921	0.043	10.1	126.6	0.5
5.8*	0.1478	0.0002	0.0001	0.1290	0.0020	-0.0110	-0.0110	10.234	0.034	0.6	10.176	0.045	9.2	129.8	0.6
6.5*	0.0697	0.0003	0.0002	0.1540	0.0040	-0.0110	-0.0110	10.546	0.075	0.8	10.462	0.094	4.4	133.3	1.2
15.0*	0.3350	0.0007	0.0001	0.3840	0.0040	-0.0110	-0.0110	10.924	0.022	1.8	10.724	0.032	21.0	136.5	0.4
Aliquot: B															
2.8	0.0096	0.0144	0.0013	3.5240	0.0700	-0.0140	-0.0110	10.483	0.251	40.6	6.228	0.447	1.4	80.5	5.7
3.5	0.0273	0.0050	0.0005	1.6700	0.0310	-0.0120	-0.0110	9.610	0.092	15.3	8.143	0.167	4.0	104.6	2.1
4.2	0.0473	0.0027	0.0003	0.6770	0.0140	-0.0110	-0.0110	7.522	0.054	10.6	6.724	0.094	7.0	86.8	1.2
4.6	0.0396	0.0022	0.0003	1.2740	0.0230	-0.0110	-0.0110	6.427	0.066	10.3	5.767	0.122	5.9	74.7	1.6
5	0.0361	0.0026	0.0006	3.0090	0.0500	-0.0110	-0.0110	8.625	0.074	9.0	7.847	0.191	5.3	100.9	2.4
5.5	0.0422	0.0012	0.0011	6.3620	0.1010	-0.0110	-0.0110	9.613	0.087	3.7	9.260	0.340	6.2	118.4	4.2
6.5*	0.0755	0.0003	0.0002	0.5910	0.0110	-0.0110	-0.0110	10.414	0.043	0.8	10.328	0.067	11.2	131.6	0.8

CO₂ laser step-heating ⁴⁰Ar/³⁹Ar data^e. All uncertainties quoted at 2s level.

Power ^a	Volume ³⁹ Ar x10 ⁻¹¹ cc	³⁶ Ar/ ³⁹ Ar	±	³⁷ Ar/ ³⁹ Ar	±	³⁸ Ar/ ³⁹ Ar	±	⁴⁰ Ar/ ³⁹ Ar	±	% ⁴⁰ Ar ATM	⁴⁰ Ar/ ³⁹ Ar	±	f ₃₉ ^b (%)	Apparent Age Ma ^c	±
7.0	0.2041	0.0002	0.0001	0.1500	0.0030	-0.0110	-0.0110	10.449	0.021	0.5	10.394	0.027	30.2	132.4	0.3
7.5*	0.0734	0.0004	0.0001	0.1320	0.0050	-0.0110	-0.0110	10.727	0.043	1.2	10.599	0.061	10.9	135.0	0.8
8.5*	0.0414	0.0005	0.0003	0.1450	0.0070	-0.0110	-0.0110	10.791	0.065	1.4	10.640	0.100	6.1	135.5	1.2
15.0*	0.0794	0.0006	0.0001	0.2630	0.0060	-0.0110	-0.0110	11.091	0.043	1.7	10.900	0.060	11.8	138.6	0.7
09RC063C01 Muscovite; J=.00732480 ^d (Z10198; 0.0000-N 0.0000-E)															
Aliquot: A															
2.6	0.1231	0.0024	0.0002	1.3640	0.0150	-0.0110	-0.0110	9.289	0.040	7.6	8.580	0.081	8.0	110.0	1.0
3.0*	0.1684	0.0003	0.0001	0.0850	0.0020	-0.0110	-0.0110	8.859	0.030	1.1	8.765	0.038	10.9	112.3	0.5
3.4	0.5315	0.0001	0.0000	0.0140	0.0000	-0.0110	-0.0110	8.683	0.014	0.4	8.646	0.016	34.4	110.8	0.2
3.8*	0.2191	0.0002	0.0001	0.0080	0.0000	-0.0110	-0.0110	8.646	0.024	0.5	8.600	0.029	14.2	110.2	0.4
4.2*	0.1653	0.0001	0.0001	0.0120	0.0010	0.0020	0.0110	8.322	0.031	0.4	8.288	0.043	10.7	106.3	0.5
4.6*	0.0382	0.0000	-0.0004	0.0140	0.0030	0.0030	0.0110	8.386	0.138	0.0	8.387	0.179	2.5	107.6	2.2
5.2*	0.0233	0.0000	-0.0006	0.0000	0.0000	0.0030	0.0110	8.397	0.226	0.0	8.397	0.294	1.5	107.7	3.7
6.0*	0.0710	0.0003	0.0002	0.0130	0.0020	0.0000	0.0110	8.348	0.075	1.0	8.266	0.098	4.6	106.1	1.2
15.0*	0.2038	0.0001	0.0001	0.0050	0.0000	-0.0110	-0.0110	8.469	0.026	0.4	8.436	0.033	13.2	108.2	0.4
09RC066A01 Biotite; J=.00732150 ^d (Z10199; 0.0000-N 0.0000-E)															
Aliquot: A															
2.6	0.1264	0.0092	0.0001	0.0840	0.0010	-0.0120	-0.0110	7.536	0.025	36.0	4.825	0.048	3.5	62.6	0.6
3.0	0.1494	0.0015	0.0001	0.2250	0.0030	-0.0110	-0.0110	8.782	0.024	5.2	8.327	0.038	4.2	106.8	0.5
3.5	0.3133	0.0005	0.0000	0.0470	0.0010	-0.0110	-0.0110	12.459	0.015	1.2	12.312	0.020	8.8	155.7	0.2
4.1	0.3427	0.0003	0.0000	0.0230	0.0000	-0.0110	-0.0110	12.841	0.016	0.7	12.754	0.020	9.6	161.1	0.2
4.5	0.2544	0.0002	0.0000	0.0170	0.0000	-0.0110	-0.0110	13.585	0.020	0.4	13.533	0.024	7.1	170.4	0.3
5.0	0.7439	0.0002	0.0000	0.0110	0.0000	-0.0110	-0.0110	14.945	0.015	0.5	14.873	0.016	20.8	186.5	0.2
5.5	0.5532	0.0002	0.0000	0.0090	0.0000	-0.0110	-0.0110	15.143	0.016	0.4	15.088	0.017	15.5	189.0	0.2
6.0	0.5092	0.0002	0.0000	0.0190	0.0000	-0.0110	-0.0110	15.664	0.018	0.3	15.613	0.019	14.3	195.3	0.2
6.5	0.2720	0.0002	0.0000	0.0230	0.0000	-0.0110	-0.0110	15.915	0.022	0.4	15.855	0.026	7.6	198.1	0.3
7.0	0.2079	0	-0.0001	0.0400	0.0010	-0.0110	-0.0110	15.681	0.023	0.0	15.684	0.028	5.8	196.1	0.3
8.0	0.0475	0.0002	0.0002	0.1150	0.0020	-0.0110	-0.0110	15.261	0.061	0.4	15.199	0.084	1.3	190.4	1.0
15.0	0.0494	0.0004	0.0003	0.9160	0.0100	-0.0110	-0.0110	14.485	0.070	0.9	14.355	0.111	1.4	180.3	1.3
Aliquot: B															
2.6	0.1073	0.0169	0.0002	0.0790	0.0030	-0.0140	-0.0110	10.318	0.035	48.3	5.335	0.073	2.5	69.1	0.9
3.0	0.1894	0.002	0.0001	0.2260	0.0040	-0.0110	-0.0110	5.661	0.020	10.4	5.075	0.032	4.4	65.8	0.4
3.5	0.2309	0.001	0.0001	0.1100	0.0020	-0.0110	-0.0110	10.971	0.021	2.7	10.673	0.028	5.3	135.7	0.3
4.0	0.4038	0.0005	0.0000	0.0250	0.0010	-0.0110	-0.0110	12.263	0.017	1.3	12.106	0.020	9.3	153.2	0.2

CO₂ laser step-heating ⁴⁰Ar/³⁹Ar data^e. All uncertainties quoted at 2s level.

Power ^a	Volume ³⁹ Ar x10 ⁻¹¹ cc	³⁶ Ar/ ³⁹ Ar	±	³⁷ Ar/ ³⁹ Ar	±	³⁸ Ar/ ³⁹ Ar	±	⁴⁰ Ar/ ³⁹ Ar	±	% ⁴⁰ Ar ATM	⁴⁰ Ar/ ³⁹ Ar	±	f ₃₉ ^b (%)	Apparent Age Ma ^c	±
4.5	0.4086	0.0003	0.0000	0.0180	0.0010	-0.0110	-0.0110	12.487	0.017	0.7	12.396	0.019	9.4	156.7	0.2
5.0	0.6789	0.0003	0.0000	0.0110	0.0010	-0.0110	-0.0110	13.471	0.016	0.7	13.377	0.017	15.6	168.6	0.2
5.5	0.5462	0.0003	0.0000	0.0090	0.0010	-0.0110	-0.0110	13.751	0.017	0.6	13.670	0.018	12.6	172.1	0.2
6.0	0.3681	0.0002	0.0000	0.0080	0.0010	-0.0110	-0.0110	13.738	0.019	0.5	13.664	0.021	8.5	172.0	0.3
6.5	0.3067	0.0002	0.0000	0.0140	0.0010	-0.0110	-0.0110	14.192	0.021	0.5	14.126	0.024	7.1	177.6	0.3
7.0	0.9798	0.0002	0.0000	0.0310	0.0010	-0.0110	-0.0110	14.327	0.016	0.3	14.277	0.016	22.6	179.4	0.2
15.0	0.1235	0.0005	0.0002	0.6890	0.0120	-0.0110	-0.0110	13.923	0.034	1.0	13.788	0.056	2.8	173.5	0.7
09RC096B01 Muscovite; J=.00751790 ^d (Z10200; 0.0000-N 0.0000-E)															
Aliquot: A															
2.8	0.1814	0.0034	0.0001	0.0070	0.0000	-0.0110	-0.0110	11.619	0.022	8.6	10.617	0.033	1.8	138.5	0.4
3.4	0.7114	0.0007	0.0000	0.0050	0.0000	-0.0110	-0.0110	12.785	0.014	1.7	12.567	0.016	6.8	162.9	0.2
3.8	0.6974	0.0007	0.0000	0.0050	0.0000	-0.0110	-0.0110	12.872	0.014	1.5	12.679	0.016	6.7	164.3	0.2
4.2	1.4051	0.0003	0.0000	0.0050	0.0000	-0.0110	-0.0110	13.764	0.014	0.7	13.664	0.014	13.5	176.4	0.2
4.5	1.3174	0.0004	0.0000	0.0040	0.0000	-0.0110	-0.0110	15.397	0.016	0.7	15.290	0.016	12.7	196.3	0.2
4.8	1.0400	0.0002	0.0000	0.0050	0.0000	-0.0110	-0.0110	16.251	0.017	0.3	16.196	0.017	10.0	207.3	0.2
5.2	1.6591	0.0003	0.0000	0.0060	0.0000	-0.0110	-0.0110	16.205	0.016	0.6	16.116	0.017	16.0	206.3	0.2
5.5	1.2570	0.0003	0.0000	0.0100	0.0000	-0.0110	-0.0110	15.758	0.016	0.5	15.673	0.016	12.1	201.0	0.2
6.2	0.4656	0.0003	0.0000	0.0180	0.0000	-0.0110	-0.0110	16.596	0.019	0.5	16.510	0.021	4.5	211.1	0.3
6.5	0.3595	0.0001	0.0000	0.0230	0.0000	-0.0110	-0.0110	16.356	0.020	0.2	16.320	0.022	3.5	208.8	0.3
6.8	0.3255	0.0005	0.0000	0.0290	0.0000	-0.0110	-0.0110	15.978	0.021	1.0	15.825	0.023	3.1	202.8	0.3
7.2	0.1960	0.0002	0.0001	0.0460	0.0010	-0.0110	-0.0110	15.268	0.024	0.3	15.219	0.028	1.9	195.4	0.3
7.5	0.1019	0.0002	0.0001	0.0540	0.0010	-0.0110	-0.0110	15.407	0.037	0.4	15.345	0.046	1.0	197.0	0.6
8.0	0.1936	0	0.0001	0.0680	0.0010	-0.0110	-0.0110	15.688	0.026	0.1	15.676	0.034	1.9	201.0	0.4
15.0	0.4831	0.0003	0.0000	0.2250	0.0020	-0.0110	-0.0110	15.558	0.018	0.6	15.464	0.022	4.7	198.4	0.3
Aliquot: B															
3.9	0.6831	0.0002	0.0000	0.0070	0.0000	-0.0110	-0.0110	15.214	0.017	0.3	15.169	0.018	12.1	194.8	0.2
4.2	1.5848	0.0002	0.0000	0.0060	0.0000	-0.0110	-0.0110	14.632	0.017	0.3	14.587	0.017	28.1	187.7	0.2
4.5	1.1542	0.0001	0.0000	0.0100	0.0000	-0.0110	-0.0110	14.575	0.015	0.3	14.537	0.016	20.5	187.1	0.2
5.0	1.1372	0.0001	0.0000	0.0220	0.0010	-0.0110	-0.0110	16.523	0.017	0.2	16.486	0.018	20.2	210.8	0.2
5.5	0.3799	0.0001	0.0000	0.0280	0.0010	-0.0110	-0.0110	15.081	0.019	0.3	15.038	0.021	6.7	193.2	0.3
7.0	0.4469	0.0001	0.0000	0.0960	0.0020	-0.0110	-0.0110	14.758	0.019	0.3	14.720	0.020	7.9	189.4	0.3
15.0	0.2539	0.0002	0.0001	0.2770	0.0050	-0.0110	-0.0110	14.109	0.022	0.3	14.065	0.028	4.5	181.3	0.4

09RC101A01 Biotite; J=.00751370^d (Z10201; 0.0000-N 0.0000-E)

Aliquot: A

CO₂ laser step-heating ⁴⁰Ar/³⁹Ar data^e. All uncertainties quoted at 2s level.

Power ^a	Volume ³⁹ Ar x10 ⁻¹¹ cc	³⁶ Ar/ ³⁹ Ar	±	³⁷ Ar/ ³⁹ Ar	±	³⁸ Ar/ ³⁹ Ar	±	⁴⁰ Ar/ ³⁹ Ar	±	% ⁴⁰ Ar ATM	⁴⁰ Ar/ ³⁹ Ar	±	f ₃₉ ^b (%)	Apparent Age Ma ^c	±
2.6	0.1267	0.0035	0.0001	0.0070	0.0010	-0.0110	-0.0110	8.734	0.032	11.9	7.697	0.044	4.6	101.4	0.6
3.0	0.1677	0.0001	0.0001	0.0020	0.0000	-0.0110	-0.0110	12.043	0.028	0.3	12.003	0.034	6.1	155.8	0.4
3.5	0.2300	0.0001	0.0000	0.0020	0.0000	-0.0110	-0.0110	13.025	0.024	0.2	12.996	0.028	8.4	168.1	0.3
4.0	0.2999	0	0.0000	0.0020	0.0000	-0.0110	-0.0110	14.226	0.021	0.1	14.214	0.024	10.9	183.1	0.3
4.5	0.5938	0.0002	0.0000	0.0020	0.0000	-0.0110	-0.0110	15.826	0.017	0.4	15.757	0.019	21.6	201.9	0.2
5.0	0.8626	0.0002	0.0000	0.0020	0.0000	-0.0110	-0.0110	15.193	0.016	0.3	15.146	0.017	31.4	194.4	0.2
5.4	0.1871	0.0001	0.0001	0.0040	0.0000	-0.0110	-0.0110	14.831	0.029	0.1	14.813	0.034	6.8	190.4	0.4
6.0	0.0918	0.0001	0.0001	0.0050	0.0010	-0.0110	-0.0110	15.123	0.049	0.3	15.085	0.057	3.3	193.7	0.7
7.0	0.1170	0	-0.0001	0.0140	0.0010	-0.0110	-0.0110	16.016	0.040	0.0	16.017	0.049	4.3	205.0	0.6
15.0	0.0730	0.0001	0.0002	0.3180	0.0040	-0.0110	-0.0110	16.170	0.056	0.1	16.149	0.072	2.7	206.6	0.9
Aliquot: B															
2.6	0.3292	0.0038	0.0001	0.0940	0.0020	-0.0110	-0.0110	6.594	0.020	16.8	5.486	0.027	9.4	72.9	0.4
3.0	0.3505	0.0005	0.0000	0.0050	0.0010	-0.0110	-0.0110	15.407	0.022	1.0	15.253	0.024	10.1	195.7	0.3
3.5	0.7909	0.0002	0.0000	0.0040	0.0000	-0.0110	-0.0110	16.867	0.018	0.4	16.799	0.019	22.7	214.4	0.2
4.0	0.6443	0.0002	0.0000	0.0040	0.0000	-0.0110	-0.0110	18.285	0.021	0.4	18.217	0.022	18.5	231.4	0.3
4.5	0.4494	0.0003	0.0000	0.0040	0.0010	-0.0110	-0.0110	18.890	0.023	0.4	18.807	0.024	12.9	238.5	0.3
5.0	0.6827	0.0002	0.0000	0.0160	0.0000	-0.0110	-0.0110	18.589	0.021	0.4	18.516	0.021	19.6	235.0	0.3
5.5	0.1548	0.0003	0.0001	0.0370	0.0020	-0.0110	-0.0110	18.605	0.034	0.5	18.521	0.040	4.4	235.1	0.5
7.0	0.0818	0.0003	0.0001	0.2660	0.0060	-0.0110	-0.0110	17.624	0.051	0.6	17.522	0.065	2.3	223.1	0.8
15.0	0.0050	0.0027	0.0023	6.7030	0.1340	-0.0110	-0.0110	16.604	0.597	4.8	15.815	0.911	0.1	202.6	11.0

a: As measured by laser in % of full nominal power (10W)

b: Fraction ³⁹Ar as percent of total run

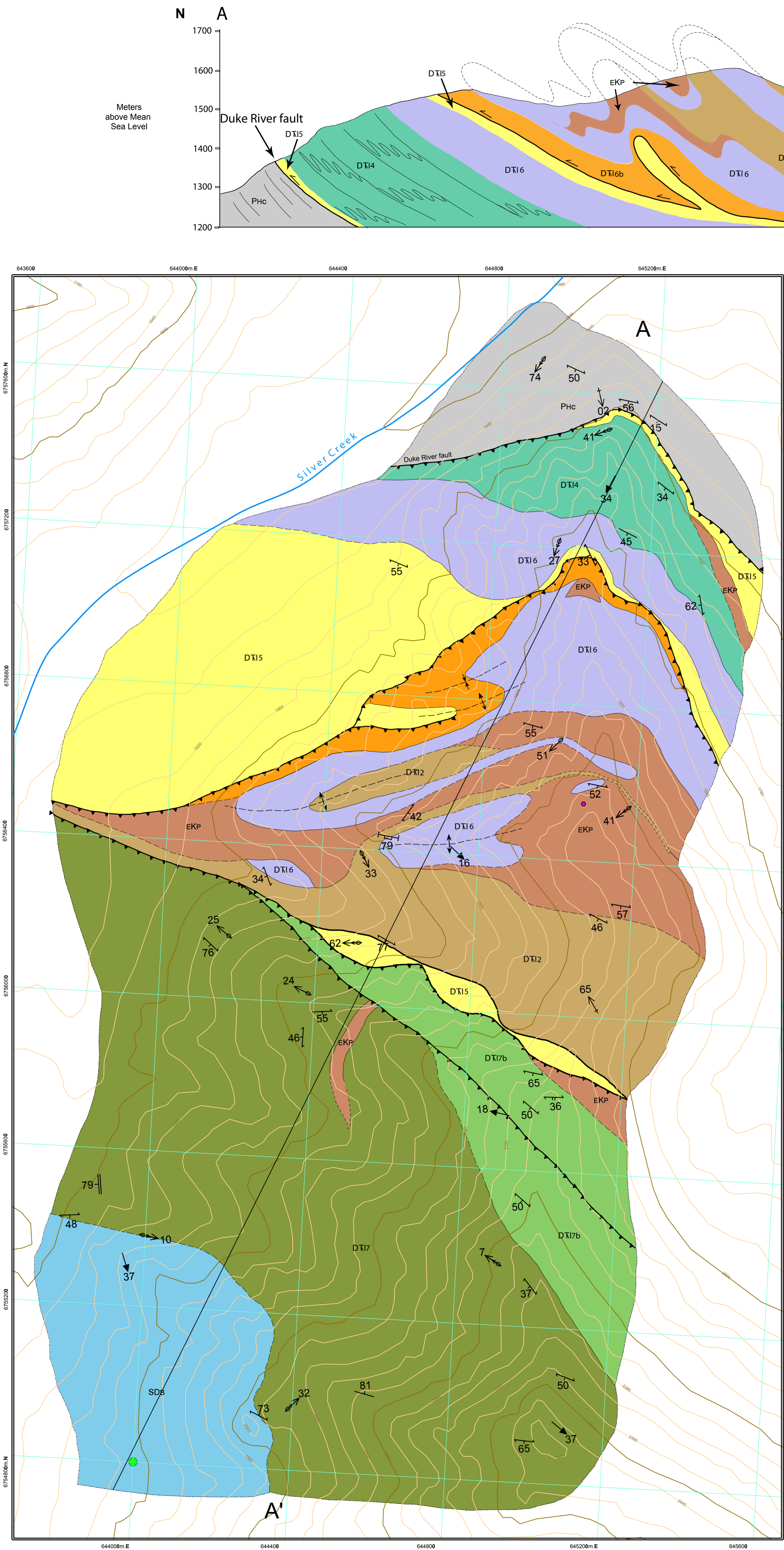
c: Errors are analytical only and do not reflect error in irradiation parameter J

d: Nominal J, from GSC Irradiation Batch #61, referenced to Fish Canyon Tuff Sanidine = 28.03 Ma (Renne et al., 1998a). The mass discrimination values used were 308.9 ± 1.0

³⁷Ar = 3.4*10⁻¹¹ to 7.3*10⁻¹¹ nmol, ³⁶Ar = 2.9*10⁻¹¹ to 3.4*10⁻¹¹ nmol, all at ±10 % uncertainty. Nucleogenic interference corrections are (⁴⁰Ar/³⁹Ar)_K = 0.025±0.005, (³⁸Ar/³⁹Ar)_K = 0.011±0.010,

*: Denotes a step that was used in the plateau or inverse isochron age calculation

Appendix III – Geologic Maps



LEGEND

INTRUSIVE ROCKS

EARLY CRETACEOUS

Pyroxenite Creek Ultramafic

EKP medium to coarse-grained, hornblende gabbro

LAYERED ROCKS

PERMIAN

Hasen Creek Formation

PHc black, thin-bedded chert to mudstone; grey, thin bedded limestone

ALEXANDER TERRANE

DEVONIAN TO TRIASSIC

Icefield formation

DTI2 dark grey to black, fine-grained, carbonaceous siltstone to shale; dark grey, thin-bedded chert

DTI4 grey, banded limestone to calcareous siltstone

DTI5 white, foliated gypsum

DTI6 white to light grey, massive to banded marble

DTI6b orange to beige, breccia dominated by marble clasts and cemented by calcite.

Icefield formation: Silver Creek member

DTI7 green and maroon, foliated pebble conglomerate; green, fine-grained, banded tuffs, green, fine to medium-grained volcanoclastic sandstone

DTI7b grey to brown, coarse-grained lithic sandstone to pebble conglomerate dominated by chert and siltstone clasts.

SILLURIAN TO DEVONIAN

Bullion Creek Limestone

SDB1 massive to thin-bedded light grey limestone or marble; thin-bedded dark grey limestone or marble; minor dark blue-grey calcareous argillites or phyllite

SYMBOLS

geologic contacts (defined, approximate).....

thrust fault (known, approximate, inferred, covered).....

fold axial trace (upright - anticline, syncline).....

mapping limit.....

bedding (tops known, inclined, vertical).....

foliation (dominant, late).....

stretching lineation.....

fold axis (dominant phase).....

crenulation lineation.....

dyke, vein.....

fault plane.....

isotopic age locations (Ar-Ar).....

fossil location (Wheeler, 1953).....

cross-section lines.....

Isotopic Age Determinations						
Type	Station #	Age	Mineral	Interpretation	Reference	
1	Ar-Ar	09-RC-044	120.6 ± 1.5	hornblende	crystallization	Cobbett, R. 2011

Fossil Age Determinations					
Type	Station #	Age	Fossil	Reference	
Macro	123-CAB-77	indeterminate	digitate organisms	Dodds & Campbell, 1993	

RECOMMENDED CITATION

Cobbett, R., 2011. Bedrock geology along the Duke River fault near Silver Creek, Yukon (NTS 115B/16) (1:5 000 scale). Yukon Geological Survey, Open File 2008-21.

Digital cartography and drafting by Rosie Cobbett, Yukon Geological Survey.

Any revisions or additional geological information known to the user would be welcomed by the Yukon Geological Survey.

Paper copies of this map, the accompanying report and Yukon MINFILE may be purchased from Geoscience Information and Sales, c/o Whitehorse Mining Recorder, Energy, Mines and Resources, Yukon Government, Room 102 - 300 Main St., Whitehorse, Yukon, Y1A 2B5. Ph. 867-667-5200. Fax. 867-667-5150, Email geosales@gov.yk.ca.

A digital PDF (portable document file) of this map may be downloaded free of charge from the Yukon Geological Survey website: <http://www.geology.gov.yk.ca>.

Yukon Geological Survey
Energy, Mines and Resources
Government of Yukon

Open File 2010-XX

Bedrock geology along the Duke River fault near Silver Creek, Yukon (NTS 115B/16) (1:5 000 scale)

by

Rosie Cobbett

1:5 000-scale topographic base data produced by CENTRE FOR TOPOGRAPHIC INFORMATION, NATURAL RESOURCES CANADA

FOUR HUNDRED METRE GRID
Universal Transverse Mercator Projection
North American Datum 1983
Zone 7

CONTOUR INTERVAL 40 m
Elevations in meters above Mean Sea Level

BEDROCK GEOLOGY
**THE DUKE RIVER FAULT
NEAR SILVER CREEK
YUKON**

SCALE 1:5 000

0 50 100 150 200
Meters

ALASKA NWT Yukon
Inuvik
Dawson City
Faro
Tungsten
Watson Lake
Whitehorse
Haines Junction
Beaver Creek
Alaska
British Columbia

115G/02 115G/01 115H/04
CONGDON CREEK CULTUS CREEK MCKINLEY CREEK

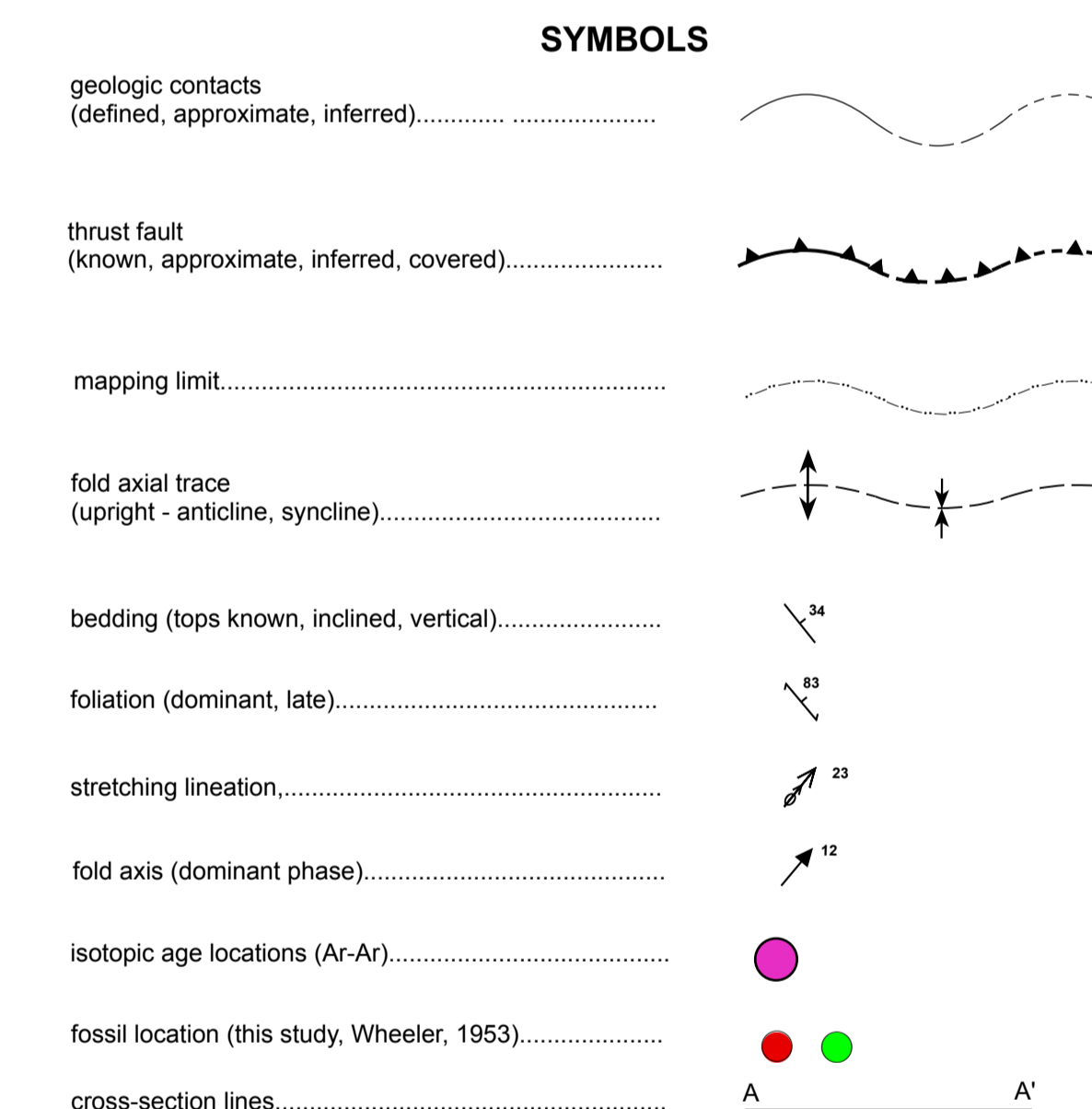
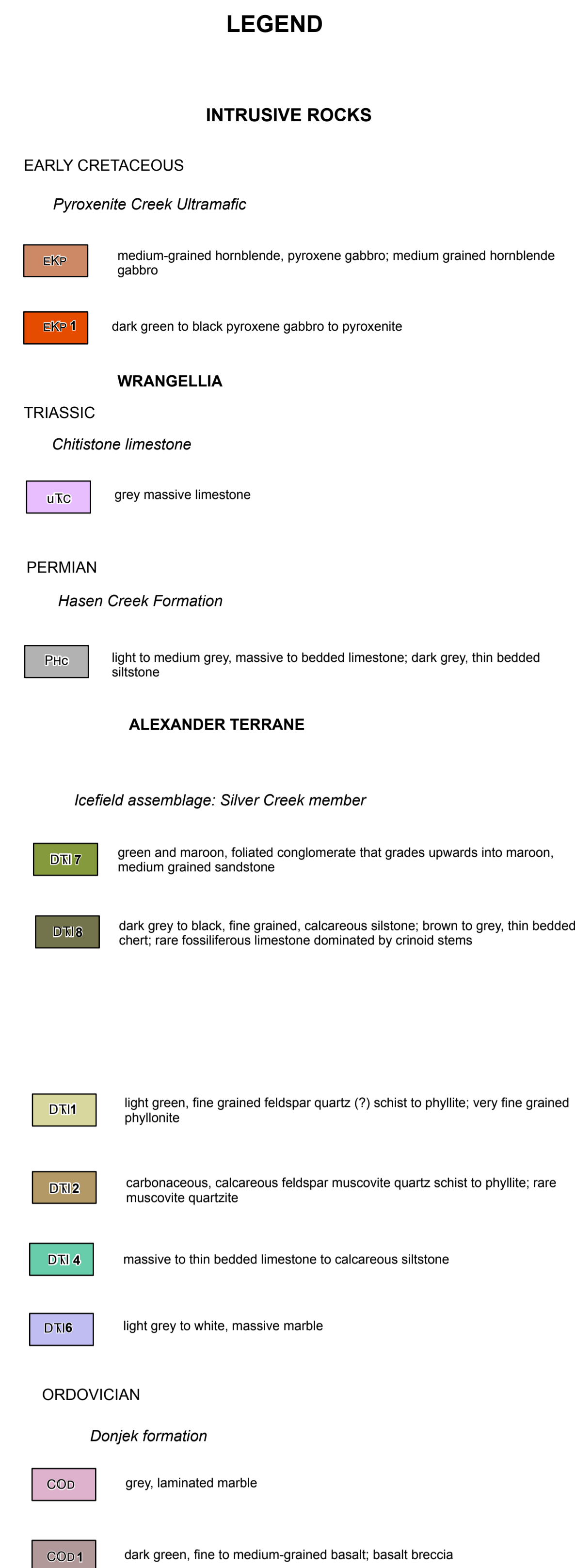
115B/15 115B/16 115A/13
SLIMS RIVER THIS MAP KLOO LAKE

115B/10 115B/09 115A/12
MOUNT LEACOCK AIRDROP LAKE AURIOL RANGE

True North
Grid North
Magnetic North
2.2°
22°43'

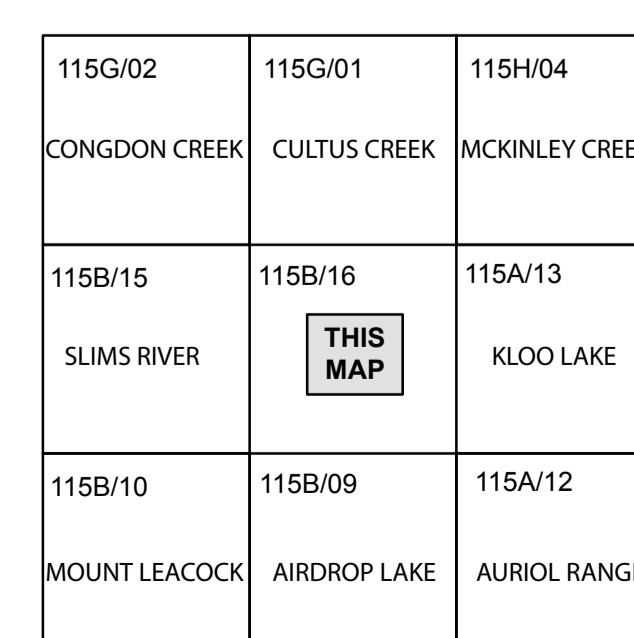
Use diagram only to obtain numerical values
APPROXIMATE MEAN DECLINATION 2008
FOR CENTRE OF MAP

127

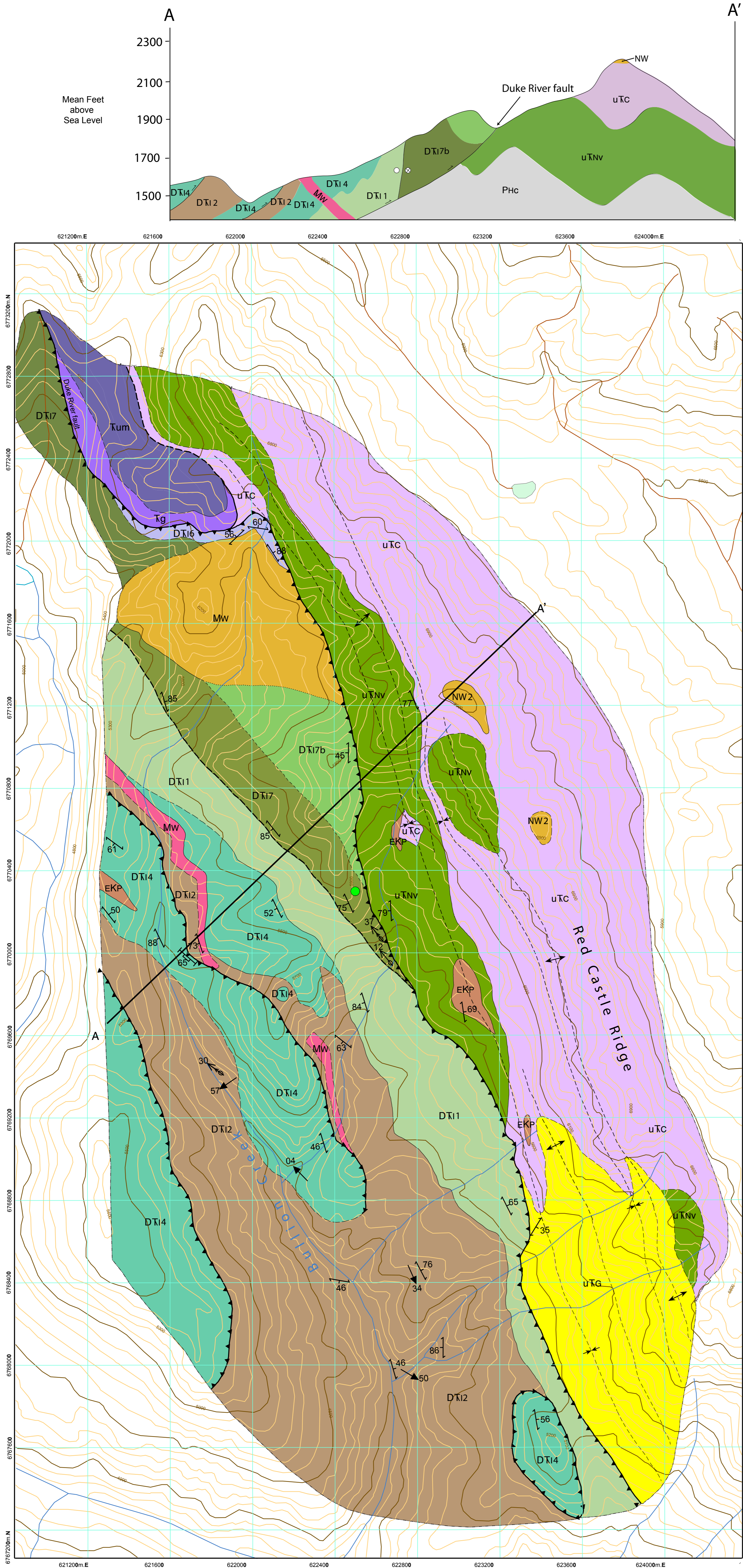


Fossil Age Determinations				
Type	Station #	Age	Fossil	Reference
1 Macro	F9-J0W-53	prob. Late Carboniferous	Lithostrotian	Dodds & Campbell, 1993
2 Macro	MV-74-185	Middle Triassic	Daonella	Dodds & Campbell, 1993
3 Micro	09-RC-091A01	Ordovician	Conodont	Cobbett et al. 2011

A digital PDF (portable document file) of this map may be downloaded free of charge from the Yukon Geological Survey website: <http://www.geology.gov.yk.ca>.



by
Rosie Cobbett



INTRUSIVE ROCKS

MIOCENE

Wrangell Suite

Mw fine to medium-grained, feldspar-quartz porphyritic granite

EARLY CRETACEOUS

Pyroxenite Creek Ultramafic

EKP medium-grained hornblende, pyroxene gabbro

Tum dark green to black medium-grained, ultramafic rock

Tg dark green, medium-grained, gabbro

MIOCENE

Wrangell Volcanics rocks

NW2 fine-grained, dark grey to black basalt; biege, fine to medium-grained crystal tuff with porphyritic feldspar.

WRANGELLIA

TRIASSIC

Chitstone Limestone

uTc light to medium grey, massive to bedded limestone

Chitstone Gypsum

uTg light grey to white, massive to laminated gypsum

Nikolai formation

uTnv dark green/maroon weathered and fresh, massive to locally foliated, amygdaloidal and vesicular basalt flows; rare pillows

Hasen Creek Formation

PHc grey to brown, fine-grained sandstone interbedded with medium to coarse-grained sandstone; locally beds of conglomerate

ALEXANDER TERRANE

DEVONIAN TO TRIASSIC

Icefield assemblage

DTi1 fine to very fine-grained, calcareous, feldspar-quartz-muscovite schist to phyllite

DTi2 fine-grained, carbonaceous, calcareous, quartz-muscovite schist to phyllite

DTi4 dark grey to black, fine-grained, thin-bedded calcareous silstone to banded silty limestone or marble

DTi6 light grey to white, massive marble

Icefield assemblage: Silver Creek member

DTi7 green and maroon, foliated pebble conglomerate, green, fine-grained banded tuffs and fine to medium-grained volcanoclastic sandstone; pyroxene-bearing basalt breccia; rare fossiliferous marble

DTi7b grey to brown, coarse-grained, lithic sandstone; grey-brown, fossiliferous limestone

LEGEND

SYMBOLS

geologic contacts (defined, approximate, inferred).....

fault; movement not known (defined, approximate, inferred).....

fault; dextral (defined, approximate, inferred).....

mapping limit.....

thrust fault (known, approximate, inferred).....

fold axial trace (upright - anticline, syncline).....

foliation (dominant, late).....

stretching lineation.....

mineral lineation.....

fold axis (dominant phase).....

fault plane.....

cross-section lines.....

macro fossil location.....

Isotopic Age Determinations					
Type	Station #	Age	Mineral	Interpretation	Reference
Ar-Ar	08-RC-060-1B	267.5 ± 6.4	muscovite	crystallization	Cobbett et al., 2011

Fossil Age Determinations			
Type	Station #	Age	Fossil
Macro	113-CAB-77-3	Late Permian	Parafusulina

RECOMMENDED CITATION

Cobbett, R., 2011. Bedrock geology along the Duke River fault near Bullion Creek, Yukon (NTS 115A/3 and parts of 115A/6) (1:10 000 scale). Yukon Geological Survey, Open File 2008-21.

Any revisions or additional geological information known to the user would be welcomed by the Yukon Geological Survey.

Paper copies of this map, the accompanying report and Yukon MINFILE may be purchased from Geoscience Information and Sales, c/o Whitehorse Mining Recorder, Energy, Mines and Resources, Yukon Government, Room 102 - 300 Main St., Whitehorse, Yukon, Y1A 2B5. Ph. 867-667-5200, Fx. 867-667-5150, Email geosales@gov.yk.ca.

A digital PDF (portable document file) of this map may be downloaded free of charge from the Yukon Geological Survey website: <http://www.geology.gov.yk.ca>.

Yukon Geological Survey
Energy, Mines and Resources
Government of Yukon

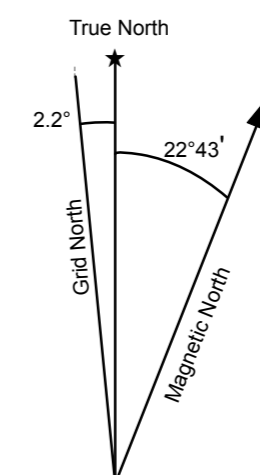
Open File 2011-XX Bedrock geology along the Duke River fault near Bullion Creek, Yukon (parts of 115G/02) (1:10 000 scale)

by
Rosie Cobbett

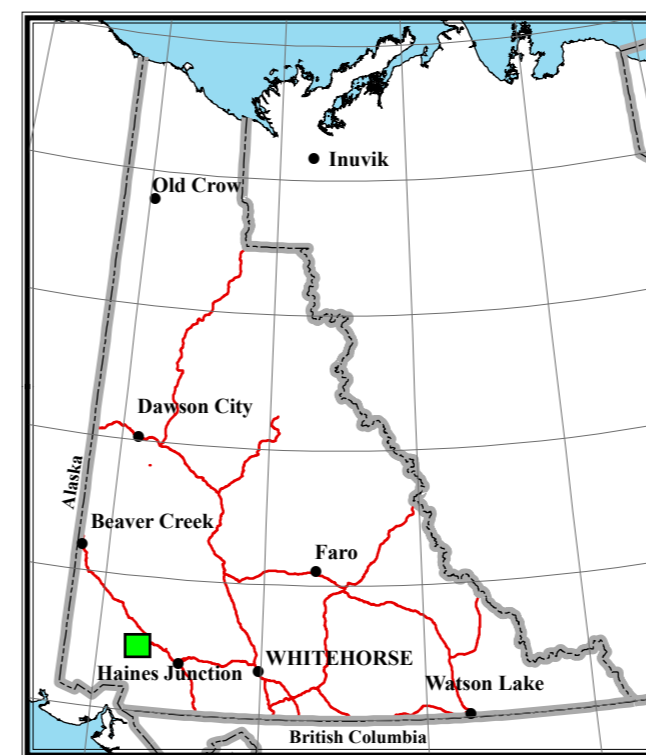
1:10 000-scale topographic base data
produced by
CENTRE FOR TOPOGRAPHIC
INFORMATION,
NATURAL RESOURCES CANADA

FOUR HUNDRED METER GRID
Universal Transverse Mercator Projection
North American Datum 1983
Zone 7

CONTOUR INTERVAL 100 Feet
Elevations in feet above Mean Sea Level

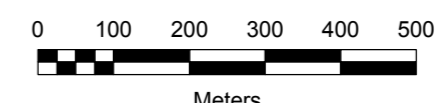


Use diagram only to obtain numerical values
APPROXIMATE MEAN DECLINATION 2008
FOR CENTRE OF MAP

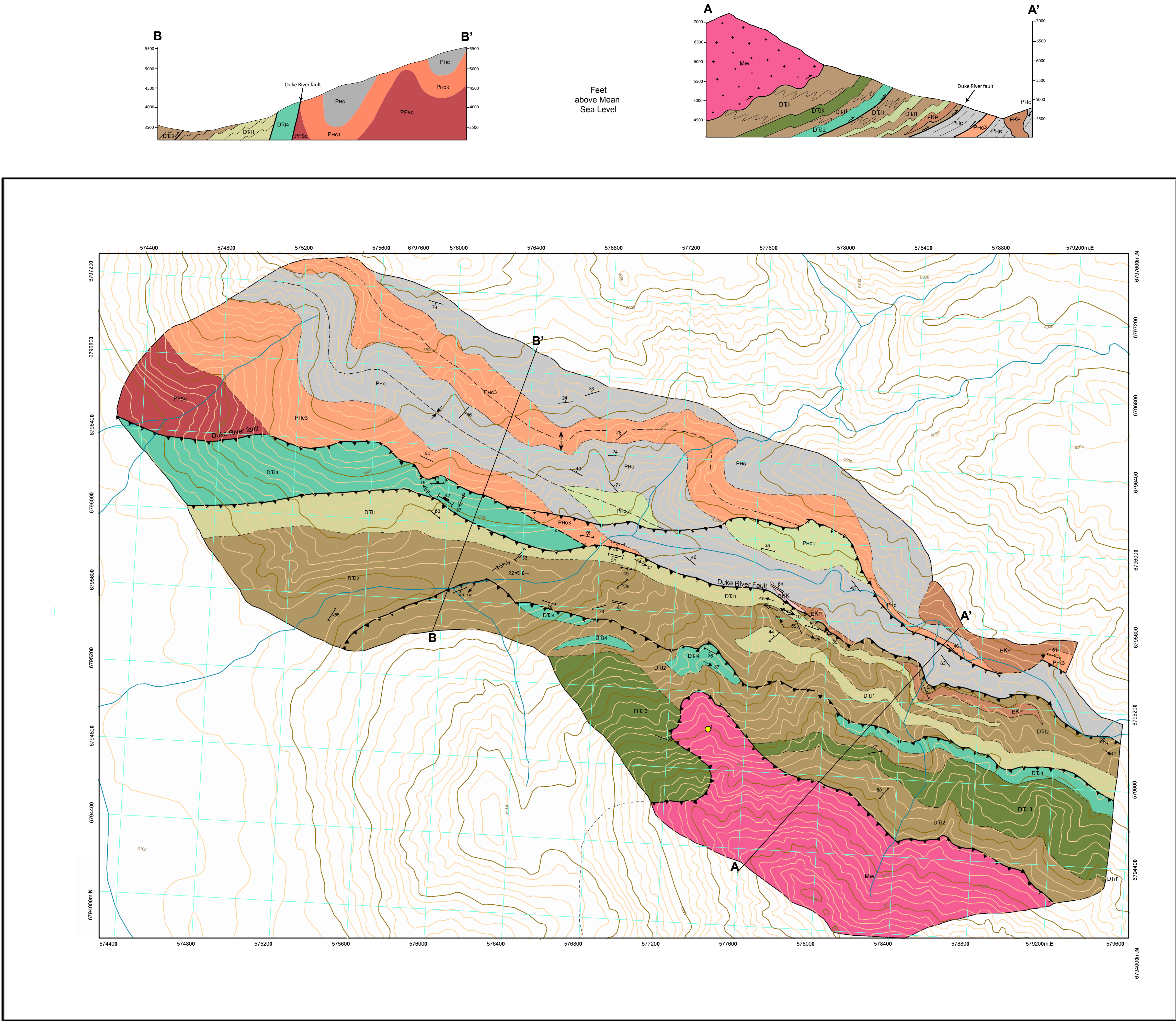


BEDROCK GEOLOGY THE DUKE RIVER FAULT NEAR BULLION CREEK YUKON

SCALE 1:10 000



115G/06 DUKE RIVER	115G/07 BURWASH LANDING	115G/08 GLADSTONE CREEK
115G/03 BIGHORN CREEK	115G/02 THIS MAP	115G/01 CULTUS CREEK
115B/14 KLUANE GLACIER	115B/15 SLIMS RIVER	115B/16 JARVIS RIVER



INTRUSIVE ROCKS

MIOCENE

Wrangell Suite

Mw fine to medium-grained, hornblende-biotite-pyroxene diorite

EARLY CRETACEOUS

Kluane Ranges Suite

EKK fine to medium-grained hornblende-biotite granodiorite to quartz monzonite

Pyroxenite Creek Ultramafic

EKP medium-grained pyroxene +/- hornblende gabbro, and biotite-hornblende diorite

DEVONIAN

PPSc green to purple medium to coarse-grained hornblende-pyroxene gabbro that is highly altered

LAYERED ROCKS

WRANGELLIA

PENNSYLVANIAN - PERMIAN

Skolai Group

Hasen Creek Formation

PHc light grey to brown, calcareous, fossiliferous packstone; medium-grained litharenite sandstone; grades into a poorly bedded pebble conglomerate with coarse-grained sandstone interbeds.

PHc2 light grey, laminated to massive limestone

PHc3 green and maroon boulder conglomerate dominated by well-rounded clasts of gabbro and diorite; locally maroon volcanic breccia with a sandy matrix

ALEXANDER TERRANE

DEVONIAN TO TRIASSIC

Icefield assemblage

DT11 fine-grained, calcareous, muscovite-feldspar +/- quartz schist to phyllite; very fine-grained phyllonite (feldspar and clay)

DT12 dark grey, carbonaceous and calcareous, thin-bedded siltstone

DT13 dark grey, fine-grained, locally amygdaloidal, plagioclase-phyric basalt; green, volcanic breccia made up of basalt clasts; rarely, blege, crystal tuffs

DT14 grey, thin-bedded limestone to marble

LEGEND

SYMBOLS

geologic contacts (defined, approximate, inferred, covered).....

fault: movement not known (defined, approximate, inferred, covered).....

mapping limit.....

thrust fault (known, approximate, inferred, covered).....

fold axial trace (upright - anticline, syncline).....

bedding (tops known).....

foliation (dominant, late).....

stretching lineation.....

intersection lineation.....

fold axis (dominant phase).....

dyke.....

fault plane.....

isotopic age locations (U-Pb).....

cross-section lines.....

Isotopic Age Determinations

Type	Station #	Age	Mineral	Interpretation	Reference
1	U-Pb 09-RC-151A01	15.44±0.03	zircon	crystallization	Cobbett et al., 2011

Cobbett, R., 2008. Bedrock geology along the Duke River fault near Hoge Creek, Yukon (NTS 115G/5) (1:50 000 scale). Yukon Geological Survey, Open File 2008-21.

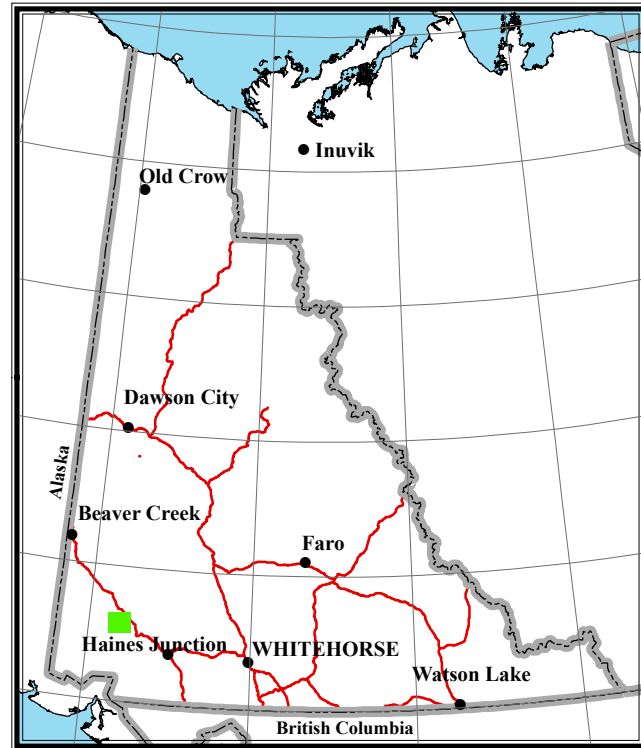
Digital cartography and drafting by Rosie Cobbett, Yukon Geological Survey.

Any revisions or additional geological information known to the user would be welcomed by the Yukon Geological Survey.

Paper copies of this map, the accompanying report and Yukon MINFILE may be purchased from Geoscience Information and Sales, c/o Whitehorse Mining Recorder, Energy, Mines and Resources, Yukon Government, Room 102 - 300 Main St., Whitehorse, Yukon, Y1A 2B5. Ph. 867-667-5200. Fx. 867-667-5150, Email geosales@gov.yk.ca.

A digital PDF (portable document file) of this map may be downloaded free of charge from the Yukon Geological Survey website: <http://www.geology.gov.yk.ca>.

Yukon Geological Survey
Energy, Mines and Resources
Government of Yukon



1:10 000-scale topographic base data
produced by
CENTRE FOR TOPOGRAPHIC
INFORMATION,
NATURAL RESOURCES CANADA

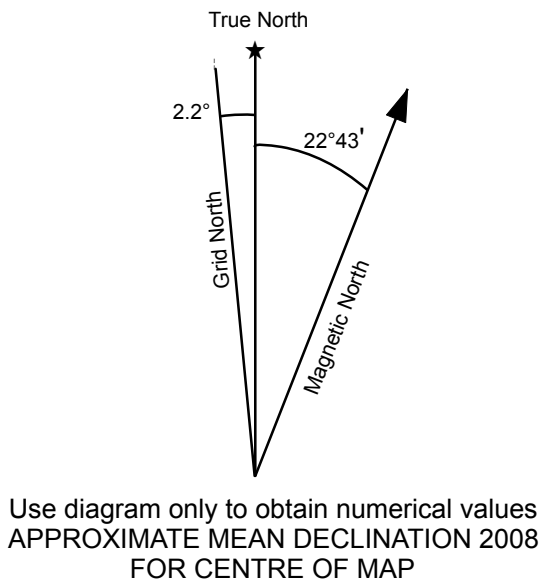
FOUR HUNDRED METRE GRID
Universal Transverse Mercator Projection
North American Datum 1983
Zone 7

CONTOUR INTERVAL 100 Feet
Elevations in feet above Mean Sea Level

BEDROCK GEOLOGY
THE DUKE RIVER FAULT
NEAR HOGE CREEK
YUKON

SCALE 1:10 000

0 200 400
Meters

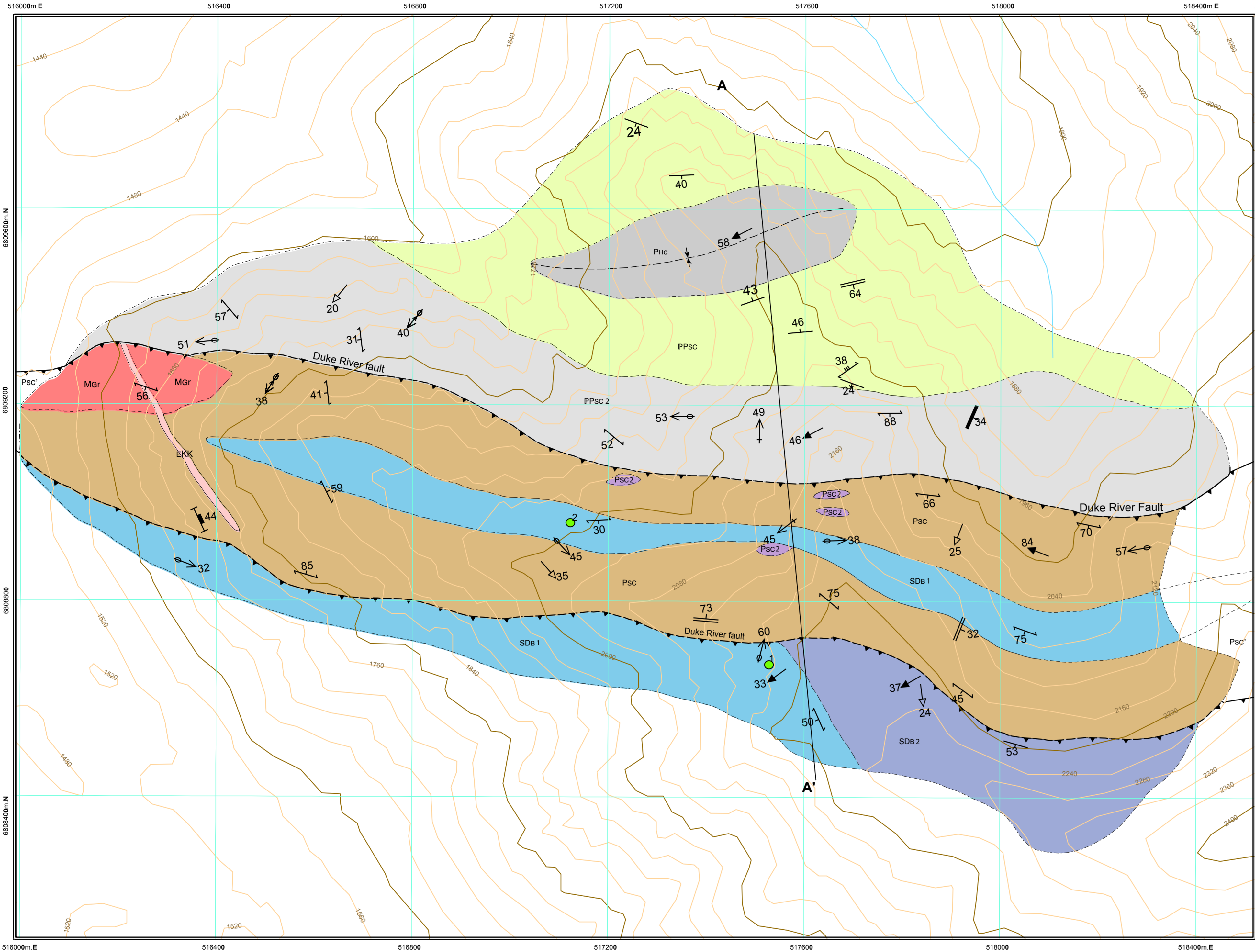


115F/09 TEEPEE LAKE	115G/12 LYNX CREEK	115G/11 NUNTAEA CREEK
115F/08 TEMPEST MOUNTAIN	115G/05 THIS MAP	115G/06 DUKE RIVER
115F/01 MOUNT STEELE	115G/04 DONJIK GLACIER	115G/03 BIGHORN CREEK

Open File 2008-21

Bedrock geology along the Duke River fault near Hoge Creek,
Yukon (NTS 115G/5) (1:10 000 scale)

by
Rosie Cobbett



EOCENE

INTRUSIVE ROCKS

Kluane Ranges suite

EKK

purple, fine to medium grained, felsic intrusive rock

DEVONIAN

Steele Creek Gabbro Complex

PSC

massive, locally foliated, grey-green hornblende pyroxene gabbro; minor medium-grained gabbro diabase; locally lueocratic gabbro

PSC

dark green to black, serpentinized ultramafic

MISSISSIPPIAN

MGr

fine to medium-grained granite

LAYERED ROCKS

WRANGELLIA

MISSISSIPPIAN - PERMIAN

Skolai Group

Hasen Creek Formation

Phc

grey to brown, fine-grained sandstone interbedded with medium to coarse-grained sandstone; locally beds of conglomerate

Station Creek Formation

PPsc

dark grey to green, very fine-grained tuffaceous siltstones, vitric tuffs and banded tuffs

PPsc2

dark green, fine-grained basalt; rare pillow basalts

ALEXANDER TERRANE

SILLURIAN TO DEVONIAN

Bullion Creek Limestone

SDb1

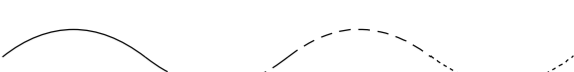
biege to grey fresh, orange weathered, thin-bedded to brecciated marble

SDb2

fine-grained, carbonaceous mica schist; fine to medium-grained greenschist; rare muscovite quartzite

SYMBOLS

geologic contacts
(defined, approximate, inferred, covered).....



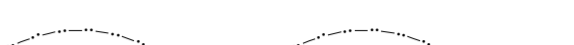
thrust fault
(known, approximate, inferred, covered).....



fold axial trace
(upright - anticline, syncline; overturned - anticline, syncline)



mapping limit.....



bedding (tops known, inclined, vertical).....



foliation (dominant, late).....



stretching lineation, mineral lineation.....



intersection lineation.....



fold axis (dominant phase).....



dyke, vein.....



crenulation lineation.....



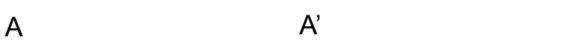
shear plane.....



isotopic age locations (Ar-Ar, U-Pb).....



cross-section lines.....



ice.....



Isotopic Age Determinations

Type	Station #	Age	Mineral	Interpretation	Reference
1	Ar-Ar 08-RC-060-1B	267.5 ± 6.4	muscovite	crystallization	Cobbett et al., 2011
2	Ar-Ar 08-RC-071-1	256.8 ± 6.6	muscovite	crystallization	Cobbett et al., 2011
3	U-Pb 08-RC-076-1	351 ±	zircon	crystallization	Cobbett et al., 2011

RECOMMENDED CITATION

Cobbett, R., 2011. Bedrock geology along the Duke River fault near Klutlan Glacier, Yukon (parts of NTS 115F/07) (1:5 000 scale). Yukon Geological Survey, Open File 2011-XX.

Digital cartography and drafting by Rosie Cobbett, Yukon Geological Survey.

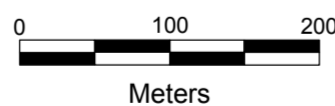
Any revisions or additional geological information known to the user would be welcomed by the Yukon Geological Survey.

Paper copies of this map, the accompanying report and Yukon MINFILE may be purchased from Geoscience Information and Sales, c/o Whitehorse Mining Recorder, Energy, Mines and Resources, Yukon Government, Room 102 - 300 Main St., Whitehorse, Yukon, Y1A 2B5. Ph. 867-667-5200. Fx. 867-667-5150, Email geosales@gov.yk.ca.

A digital PDF (portable document file) of this map may be downloaded free of charge from the Yukon Geological Survey website: <http://www.geology.gov.yk.ca>.

DUKE RIVER FAULT NEAR KLUTLAN GLACIER YUKON

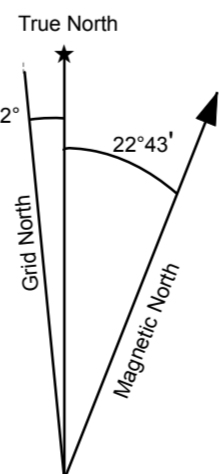
SCALE 1:5 000



Open File 2008-21

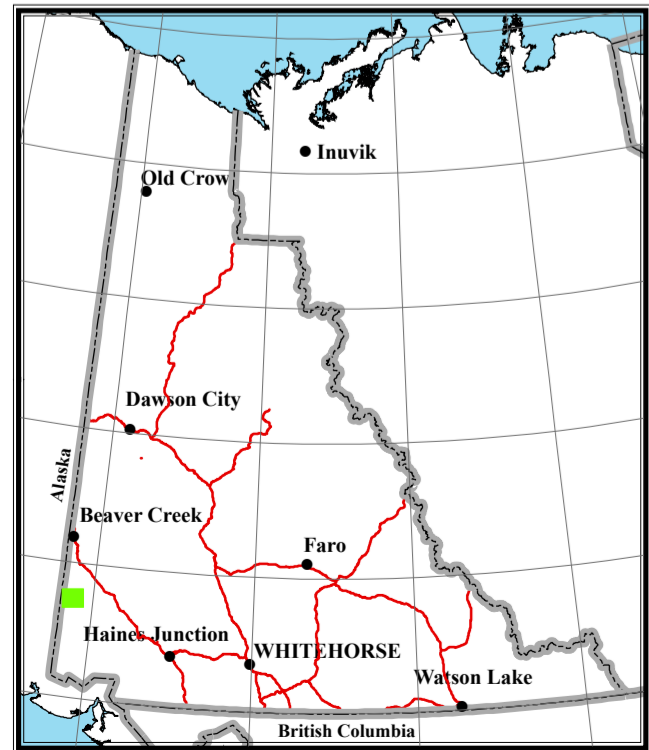
Bedrock geology along the Duke River fault near Klutlan Glacier, Yukon (NTS 115F/07) (1:5 000 scale)

by
Rosie Cobbett



Use diagram only to obtain numerical values
APPROXIMATE MEAN DECLINATION 2008
FOR CENTRE OF MAP

ALASKA	115F/10	115F/09
	BROOKE CREEK	TEEPEE LAKE
ALASKA	115F/07	115F/08
	THIS MAP	TEMPEST MOUNTAIN
ALASKA	115F/02	115F/01
	MOUNT MCAULAY	MOUNT MCBRIDE



FOUR HUNDRED METRE GRID
Universal Transverse Mercator Projection
North American Datum 1983
Zone 7

CONTOUR INTERVAL 20 Metre
Elevations in feet above Mean Sea Level

Yukon Geological Survey
Energy, Mines and Resources
Government of Yukon

N

A

Metres above
mean
Sea Level

2200

2000

1800

Duke River fault

A'

S

2200

2000

1800